2020

Aggregated DER Management in Advanced Distribution Grids

Mohsen Mahoor
University of Denver

Aggregated DER Management in Advanced Distribution Grids

Abstract

Evolution of modern power systems are more distinct in distribution grids, where the growing integration of microgrids as well as distributed energy resources (DERs), including renewable energy resources, electric vehicles (EVs), and energy storage, poses new challenges and opportunities to grid management and operation. Rapid growth of distribution automation as well as equipment monitoring technologies in the distribution grids further offer new opportunities for distribution asset management. The idea of aggregated DERs is proposed as a remedy to streamline management and operation of advanced distribution grids, as discussed under three subjects in this dissertation. The first subject matter focuses on DER aggregation in microgrid for distribution transformer asset management, while the second one stresses on aggregated DER for developing a spinning reserve-based optimal scheduling model of integrated microgrids. The aggregation of EV batteries in a battery swapping stations (BSS) for enhancing grid operation is investigated in the third subject.

Distribution transformer, as the most critical component in the distribution grids, is selected as the component of the choice for asset management practices, where three asset management studies are proposed. First, an approach in estimating transformer lifetime is presented based on the IEEE Std. C57.91-2011 and using sensory data. Second, a methodology to obtain a low-error estimate of transformer loss-of-life is investigated, leveraging an integrated machine learning and data fusion technique. Finally, a microgrid-based distribution transformer asset management model is developed to prolong the transformer lifetime. The resulting model aims at reshaping the distribution transformer loading via aggregating microgrid DERs in an efficient and asset management-aware manner.

The increasing penetration of microgrids in distribution grids sets the stage for the formation of multiple microgrids in an integrated fashion. Accordingly, a spinning reserved based optimal scheduling model for integrated microgrids is proposed to minimize not only the operation cost associated with all microgrids in the grid-connected operation, but also the costs of power deficiency and spinning reserve in the islanded operation mode. The resulting model aims at determining an optimal configuration of the system in the islanded operation, i.e., optimal super-holons combination, which plays a key role in minimizing the system-aggregated operation cost and improving the overall system reliability.

The evolving distribution grids introduce the concept of the BSS, which is emerging as a viable means for fast energy refill of EVs, to offer energy and ancillary services to the distribution grids through DER aggregation. Using a mixed-integer linear programming method, an uncertainty-constrained BSS optimal operation model is presented that not only covers the random customer demands of fully charged batteries, but also focuses on aggregating the available distributed batteries in the BSS to reduce its operation cost. Furthermore, the BSS is introduced as an energy storage for mitigating solar photovoltaic (PV) output fluctuations, where the distributed batteries in the BSS are modeled as an aggregated energy storage to capture solar generation variability.

Numerical simulations demonstrate the effectiveness of the proposed models as well as their respective viability in achieving the predefined operational objectives.

Document Type

Dissertation

Degree Name

Ph.D.

AGGREGATED DER MANAGEMENT IN ADVANCED DISTRIBUTION GRIDS

_____

A Dissertation

Presented to

the Faculty of the Daniel Felix Ritchie School of Engineering and Computer Science

University of Denver

_____

In Partial Fulfillment

of the Requirements for the Degree

Doctor of Philosophy

_____

by

Mohsen Mahoor

March 2020

Advisor: Dr. Amin Khodaei

Author: Mohsen Mahoor
Title: AGGREGATED DER MANAGEMENT IN ADVANCED DISTRIBUTION GRIDS
Advisor: Dr. Amin Khodaei
Degree Date: March 2020

Abstract

Evolution of modern power systems are more distinct in distribution grids, where the growing integration of microgrids as well as distributed energy resources (DERs), including renewable energy resources, electric vehicles (EVs), and energy storage, poses new challenges and opportunities to grid management and operation. Rapid growth of distribution automation as well as equipment monitoring technologies in the distribution grids further offer new opportunities for distribution asset management. The idea of aggregated DERs is proposed as a remedy to streamline management and operation of advanced distribution grids, as discussed under three subjects in this dissertation. The first subject matter focuses on DER aggregation in microgrid for distribution transformer asset management, while the second one stresses on aggregated DER for developing a spinning reserve-based optimal scheduling model of integrated microgrids. The aggregation of EV batteries in a battery swapping stations (BSS) for enhancing grid operation is investigated in the third subject.

Distribution transformer, as the most critical component in the distribution grids, is selected as the component of the choice for asset management practices, where three asset management studies are proposed. First, an approach in estimating transformer lifetime is presented based on the IEEE Std. C57.91-2011 and using sensory data. Second, a

methodology to obtain a low-error estimate of transformer loss-of-life is investigated, leveraging an integrated machine learning and data fusion technique. Finally, a microgrid-based distribution transformer asset management model is developed to prolong the transformer lifetime. The resulting model aims at reshaping the distribution transformer loading via aggregating microgrid DERs in an efficient and asset management-aware manner.

The increasing penetration of microgrids in distribution grids sets the stage for the formation of multiple microgrids in an integrated fashion. Accordingly, a spinning reserved based optimal scheduling model for integrated microgrids is proposed to minimize not only the operation cost associated with all microgrids in the grid-connected operation, but also the costs of power deficiency and spinning reserve in the islanded operation mode. The resulting model aims at determining an optimal configuration of the system in the islanded operation, i.e., optimal super-holons combination, which plays a key role in minimizing the system-aggregated operation cost and improving the overall system reliability.

The evolving distribution grids introduce the concept of the BSS, which is emerging as a viable means for fast energy refill of EVs, to offer energy and ancillary services to the distribution grids through DER aggregation. Using a mixed-integer linear programming method, an uncertainty-constrained BSS optimal operation model is presented that not only covers the random customer demands of fully charged batteries, but also focuses on aggregating the available distributed batteries in the BSS to reduce its operation cost. Furthermore, the BSS is introduced as an energy storage for mitigating solar photovoltaic

(PV) output fluctuations, where the distributed batteries in the BSS are modeled as an aggregated energy storage to capture solar generation variability.

Numerical simulations demonstrate the effectiveness of the proposed models as well as their respective viability in achieving the predefined operational objectives.

Acknowledgment

I would like first to express my heartfelt thanks to my advisor, Dr. Amin Khodaei, for his beneficial academic supervision, technical guidance, and unconditional supports during my PhD program. It has been a privilege to work with him, and I am deeply grateful for his various endless supports.

I thank my PhD defense committee members, Dr. Yun-Bo Yi, Dr. David Gao, and Dr. Mohammad Matin for taking the time to review my dissertation and making constructive comments.

I deeply express my eternal appreciation to my caring, wise, and strong mother and my beloved deceased father, I miss him every day. I also express my sincere gratitude to my siblings for their continued supports and abundant encouragements.

A very special thanks to my patient, smart, beautiful and lovely wife, Zohreh. She truly made the PhD journey sweet and delightful for me. Words cannot express how grateful I am for her absolute love, technical assistances, and endless supports.

Finally, I would like to thank all my wonderful colleagues and friends at the University of Denver, and also all my friends in Denver.

Table of Contents

List of Figures

List of Tables

Nomenclature

For Chapter Two:

Indices

d	Index for loads.
h	Index for day.
i	Index for DERs.
t	Index for hour.

Superscripts

ch	Distributed Energy Storage (DES) charge
dch	Distributed Energy Storage (DES) discharge.
H	Winding hottest-spot.
I	Initial value of variables and parameters.
R	Rated value.
TO	Transformer top oil.
U	Ultimate value of variables and parameters.
W	Transformer winding.
^	Superscript for calculated/given variables.
s	Index for training datasets.

Sets

D	Set of adjustable loads.
G	Set of dispatchable units.
S	Set of energy storage units.

Parameters

A	Transition matrix.
B	Control matrix.
C_1 / C_2	Weight factors.
H	Observation matrix.
I	Identity matrix.
K	Kalman gain.
P	Error covariance
Q	Process noise covariance.
E	Measurement noise covariance.
S	Number of train datasets.
u	Exogenous control input.
Z	A new value estimated either from the ANFIS or the RBF method.
Y	Target values for transformer loss of life.
$\hat{Y}$	ANFIS estimated values for transformer loss of life.
$\hat{O}$	RBF estimated values for transformer loss of life.
$\hat{x}$	State estimate.
DR	Ramp down rate.
DT	Minimum down time.
E	Load total required energy.
$F(.)$	Generation cost.
F_{AA}	Aging acceleration factor of insulation.

$F_{AA,n}$ Aging acceleration factor for the temperature which exist during the time interval Δt_n.

F_{EQA} Equivalent aging factor for the total time period.

M Large positive constant.

MC Minimum charging time.

MD Minimum discharging time.

MU Minimum operating time.

m/n An empirically derived exponent to calculate the variation of $\Delta\theta^H/\Delta\theta^{TO}$ with changes in load.

R Ratio of full-load loss to no-load loss.

Δt Time interval.

UR Ramp up rate.

UT Minimum up time.

w Binary islanding indicator (1 if grid-connected, 0 if islanded).

α, β Specified start and end times of adjustable loads.

ρ Market price.

η Energy storage efficiency.

ψ Transformer investment cost.

τ Time period.

θ Temperature (^{o}C).

Variables

C Energy storage available (stored) energy.

D Load demand.

I Commitment state of dispatchable units.

K Transformer loading ratio.

P DER output power.

P^M Utility grid power exchange with the microgrid.

P^{M1},P^{M2} Slack variable for utility grid power.

Q The cost of transformer loss of life.

T^{ch} Number of successive charging hours.

T^{dch} Number of successive discharging hours.

T^{on} Number of successive ON hours.

T^{off} Number of successive OFF hours.

u Energy storage discharging state (1 when discharging, 0 otherwise).

v Energy storage charging state (1 when charging, 0 otherwise).

x,y Binary variables for selecting slack variables associated with utility grid exchange.

z Adjustable load state (1 when operating, 0 otherwise).

λ,μ Dual variables.

Λ Reflected cost for transformer loss of life in the master problem.

For Chapter Three:

Indices

ch Superscript for energy storage charging mode.

d Index for loads.

dch Superscript for energy storage discharging mode.

h Index for super-holon.

i Index for DERs.

m Index for microgrids.

s Index for scenarios.

t Index for hour.

Sets

DA Set of adjustable loads.

G Set of dispatchable units.

H Set of super-holons.

K Set of islanded operation scenarios.

M Set of microgrids.

R Set of DERs.

S Set of energy storage systems.

Parameters

B Large positive number.

DR Ramp down rate.

DT Minimum down time.

E Adjustable load total required energy.

F(.) Generation cost of dispatchable units.

MC Minimum charging time.

MD Minimum discharging time.

MU Minimum operating time.

N_m Number of microgrids.

N_h Number of super-holons.

U Islanding state (0 when islanded, 1 otherwise).

UR Ramp up rate.

UT Minimum up time.

ρ Market price.

α,β Specified start and end times of adjustable loads.

π Value of net spinning-reserve.

η Energy storage efficiency.

υ Value of lost load.

$10MSR$ 10-minute maximum sustained rate.

Variables

C Energy storage stored energy.

D Load demand.

I Commitment state of dispatchable units (1 when committed, 0 otherwise).

P DER output power.

PD Power deficiency.

P^M Imported/exported power from/to the utility grid.

sr^{DG} *Spinning reserve of dispatchable DGs.*

sr^{ES} Spinning reserve of energy storage system.

sr^{net} Net spinning reserve of holon (microgrid).

SR^{Net} Net spinning reserve of super-holon.

T^{ch} Number of successive charging hours.

T^{dch} Number of successive discharging hours.

T^{on} Number of successive ON hours.

T^{off} Number of successive OFF hours.

τ Time period.

u Energy storage discharging state (1 when discharging, 0 otherwise).

v Energy storage charging state (1 when charging, 0 otherwise).

w Microgrid belonging to super-holon (1 when belonging, 0 otherwise).

z Adjustable load state (1 when operating, 0 otherwise).

ϕ, κ Auxiliary variables for linearization.

For Chapter Four:

Indices and Sets

B Index for battery.

t Index for time.

ch/dch Superscript for battery charging/discharging mode.

N Set of consumers and prosumers.

P Set of primal variables.

U Set of uncertain parameters.

Parameters

CB Capital cost of battery.

MC/MD Minimum charging/discharging time.

k Linear approximation slope of battery life as a function of number of cycles.

D Battery swapping demand.

ρ Electricity price.

τ Time duration.

$\eta^{ch/dch}$ Charging/discharging efficiency.

N Number of stations' chargers/dischargers in BSS.

M Large positive constant.

ε Small positive constant.

Δ^u The variability limit provided by the utility grid.

P^c Aggregated prosumers net load.

Variables

CD Battery degradation cost.

C Battery stored energy.

$P^{ch/dch}$ Battery charging/discharging power.

P_M Imported/exported power from/to the utility grid.

P^u Distribution feeder net load supplied by the utility grid.

$T^{ch/dch}$ Number of successive charging/discharging periods.

x Inside-station state (1 if inside, 0 otherwise).

x^F Battery fully-charged state (1 when fully-charged, 0 otherwise).

y Outside-station state (1 if outside, 0 otherwise).

u Outgoing swap state (1 when battery is going out)

v Incoming swap state (1 when battery is coming in).

$z^{ch/dch}$	Battery charging/discharging state (1 when charging/discharging, 0 otherwise).

1 Chapter One: Introduction

Modern power systems continue to evolve across the globe, affected by various reasons such as technology innovations, environmental issues, regulatory policies, and aging infrastructure. The power system changes are more apparent in distribution grids due to the nature of changes that compromise the integration of renewable energy resources and EV, energy storage, and microgrid development. Utilities are focusing on utilizing smart grid technologies including advanced metering infrastructure (AMI), new distribution automation as well as equipment monitoring in distribution grids in order to make better-informed decisions in terms of distribution asset management and system reliability. The increasing penetration of microgrids in distribution grids sets the stage for the formation of multiple microgrids in an integrated fashion. The integrated microgrids can reap the benefits of their available capacity to support other connected microgrids that experience power deficiency. Moreover, in the transition to transportation electrification, providing a fast energy refill approach for EV plays a pivotal role in its adoption. In this regard, BSS has been initially proposed as a viable method to pave the way for EVs fast energy refill. Nevertheless, the evolving distribution grid introduces a wide variety of challenges and opportunities in operation and maintenance of advanced distribution grids. As shown in Fig. 1.1, three subjects in the advanced distribution grids, which are casted

based on aggregated DER, will be discussed from asset management, integrated microgrids topology control, and optimal operation perspectives.

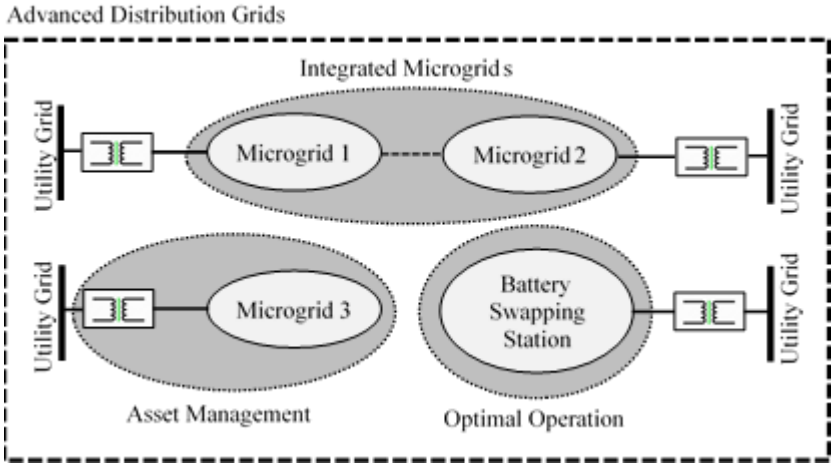

Fig. 1.1 Subject matters discussed in this dissertation under advanced distribution grids

1.1 Distribution Transformer

Asset management denotes management and engineering practices applied to valuable assets of a system in order to deliver the required level of service to the customers. Asset management has always been a critical responsibility of electric utility companies to maintain network reliability and quality of service at acceptable levels by reducing the failure probability of critical grid components. In other words, asset management extends the lifetime of equipment and decreases the risk of equipment failure and unplanned power outages. Considering that the current power grid is mainly built in 1950s and 60s and at the same time the customers' expectations of a high quality of service are at all-time high, the topic of asset management has become more important than ever [1]-[4].

Among power system equipment, distribution transformer (Fig 1.2) is one of the fundamental and pivotal elements that its maintenance and management need to be

continuously investigated by electric utility companies. Distribution transformers play a vital role in ensuring a reliable power supply as their failure will commonly result in unplanned power outages. Moreover, transformers not only are considered as a cost-intensive component in power systems, but also their maintenance and repair services are labor-intensive and time-consuming [1], [2]. Condition monitoring, online monitoring, routine diagnostic, scheduled maintenance, and condition-based maintenance (CBM) are some of the most common transformer asset management methods [2], [5], [6]. The lifetime of a transformer highly depends on its insulation condition owing to higher probability of insulation failure compared with its other components. Moreover, aging of transformer insulation is a function of insulation moisture, oxygen amount, and internal temperature specifically at the hottest spot, which is mainly governed by transformer loading and ambient temperature [7]-[9].

Fig. 1.2 Transformer maintenance service [10]

Distribution transformer, as the most critical component in the distribution grid, is selected as the component of the choice for asset management studies. In this dissertation three asset management studies are discussed. First, leveraging sensory data, an approach in estimating transformer lifetime is presented. Then, machine learning and data fusion techniques are integrated to estimate transformer loss of life. Finally, a microgrid-based distribution transformer asset management model is proposed to prolong the transformer lifetime. Nevertheless, utility companies can reap the benefits of these approaches for distribution asset management in terms of transformer lifetime and loss of life assessments.

1.2 Integrated Microgrids

The microgrid, as defined by the U.S. Department of Energy, is

> "a group of interconnected loads and Distributed Energy Resources (DERs) within clearly defined electrical boundaries that acts as a single controllable entity with respect to the grid and can connect and disconnect from the grid to enable it to operate in both grid-connected or island-mode" [11].

Microgrids provide both consumers and utility companies with significant advantages including, but not limited to, improved resiliency and reliability, reduced emission, improved power quality, and enhanced energy efficiency. Microgrids can be operated in either islanded or grid-connected mode. A microgrid in the default operation mode, i.e., grid-connected, is able to exchange power with the utility grid based on its economic objectives [12]-[14]. In case of faults and/or disturbances in the upstream network, islanded mode plays an active role in microgrid operation, where the microgrid can be intentionally disconnected from the utility grid in order to face the minimum load curtailment [15]-[17].

Integrating the microgrids can enhance the anticipated economic benefits, increase the integrated system resiliency and reliability, make full use of the installed distributed energy storages (DESs), and promote further utilization of renewable energy resources [18]-[21]. A promising type of power distribution grids, i.e., holonic distribution grids, is introduced to facilitate the microgrid integration in distribution grids [22]-[23]. The holonic distribution grid is expected to have an essential application in future distribution grids [22], [24] due to its privilege in: i) enhancing the information and power exchange among integrated holons; ii) optimizing the aggregated system performance by offering the capability of a dynamic reconfiguration; iii) fostering the diversity of energy resources, system autonomy, and the connectivity among integrated systems; and iv) improving both individual holon and aggregated system objectives.

1.3 Battery Swapping Station

It is envisioned that EVs, as major players in transportation electrification revolution, will be adopted widely, not only to lessen reliance on fossil fuels but also to help mitigate transportation-generated greenhouse gas emissions [25]. Various types of financial support are offered in the U.S. at local and state levels, and also around the world to incentivize customers to purchase EV with the objective of expanding this emerging technology [26]-[29]. Along with these incentives, and by considering emerging advances in battery technologies, it is anticipated that by 2040, 35% of the global automotive market will be taken by EVs [30].

The EV market penetration forecasts are however highly dependent on the technology advances in energy refill. Energy refill plays a pivotal role in EV adoption as

well as its operation. The battery charging is commonly based on plugging the EV into an outlet, either in a household or in a Battery Charging Station (BCS). The main shortcomings of these schemes, which are directly impacting EV adoption, include high investment cost, long charging time, and limited mobility range. The installation of residential fast chargers may need significant upgrades in the household's electrical installation, which increases the investment cost. The cost of building charging facilities and the spacious real estate required for the EVs to be parked and charged for several hours are the key monetary obstacles for deploying the BCS. This issue is more tangible in densely populated urban areas. Each of these two schemes takes much longer to fully charge the EV when compared to fueling a gasoline-powered vehicle, thus representing itself as a key barrier in EV adoption [31]. The EV charging duration depends on several key factors, including battery capacity, battery charger power, method of charging and cell balancing algorithm, supply voltage, and the category of charging levels, to name a few [32]. The study by the Society of Automotive Engineers on the required charging duration for a 25 kWh EV battery clearly demonstrates the charging duration-related barrier in EV adoption [33]. The third crucial limitation in EV adoption is the range anxiety [34]-[36], which is originated from the limited mobility range of the current EVs, currently in the order of couple of hundred miles. A major cause of this limited mobility range is the lack of extensive deployment of BCS. Nevertheless, long charging time in BCS presents itself as an obstacle to EV owners to take on long-distance trips.

An alternative to the aforementioned traditional EV charging methods is to use battery swapping through a Battery Swapping Station (BSS). The idea of battery swapping,

in which EV owners can exchange a near-empty battery with a fully-charged one, has been proposed with the objective of resolving the mentioned obstacles regarding EV charging [37]-[41]. Unlike the plug-in method, battery swapping provides the EV owners with a fully-charged battery within a few minutes, preventing waiting anxiety. An optimal BSS placement in this case could potentially mitigate the issue of travel distance, and as a result address the range anxiety to a great extent [42].

In order to reap the benefits of battery swapping, two issues should be taken into account. First, the EV battery charging technology should follow a consistent standard. In this respect, a standardized EV battery, which can include specific characteristics such as high mileage service, high energy density, high recycling ratio, high recovery ratio, and environment friendliness, should be considered [43]. This is currently doable for specific car manufacturers as they use a quite consistent technology in their battery developments. Furthermore, a proper business model for subscription service of EV battery should be defined. The company-owned battery model, in which EV owners can lease the batteries while the company is the owner of the batteries, can be perceived as a viable scheme [44]. The distinguished features of this approach are that not only EVs can be charged in a short amount of time, but also the price of the EVs will be dropped dramatically, as the battery cost is deducted from the total cost of the EV.

Although the idea of BSS suffers from a black eye due to the bankruptcy of Better Place company in 2013 [45],[46], this innovative idea is still extensively favored across the globe. China aims to achieve 12,000 centralized charging/battery swapping stations by 2020 in order to meet charging demand of 5 million EVs along with the essence of one

vehicle to one charging pile [47]. Recently, the first battery swapping and charging station for EVs in India has been launched, and it is planned to be replicated to facilitate adoption of electric mobility [48]. In Germany, by utilizing photovoltaic plants for charging swappable batteries, the idea of battery swapping system is developed for the CITY eTaxi in urban areas [49]. These ongoing projects advocate that the BSS idea is quite appealing because of the rapid proliferation of EVs in the automotive market and there should be expectations of growing deployment at a global level [50].

1.4 Dissertation Overview

The main body of this dissertation is based on the collection of articles published during the Ph.D. studies. The rest of this dissertation is organized as follows.

Chapter 2 focuses on distribution transformer, as one of the fundamental and pivotal equipment in distribution grids. First, leveraging sensory data, an approach in estimating transformer lifetime is presented. Next, machine learning and data fusion techniques are integrated to estimate transformer loss of life. Finally, a microgrid-based distribution transformer asset management model is proposed to maximize the distribution transformer lifetime.

Chapter 3 focuses on a spinning reserve based optimal scheduling model of integrated microgrids in holonic distribution grids. This model solves the common convergence issues with the existing models in the literature by moving away from a power exchange focused modeling and adopting a spinning reserve based approach. The developed model aims at identifying the optimal super-holons combinations based on minimum net spinning reserve.

Chapter 4 focuses on the Battery Swapping Station (BSS) concept as a fast and viable means in EV energy refill, in addition to many potential benefits in providing energy and ancillary services to the distribution grids. An original model for BSS optimal scheduling under uncertainties is proposed. The objective of the proposed model is to minimize the BSS operation cost which represents the aggregated costs of exchanging energy with the utility grid and battery degradation over a predefined scheduling horizon. Then, the BSS is introduced as an energy storage for mitigating solar PV variability in the distribution grids.

2 Chapter Two: Distribution Transformer Asset Management

2.1 Introduction

Transformer asset management has always been an important responsibility of utility companies to ensure system health and to prevent undesired component failures through timely upgrade and upkeep, and as a result, deliver the best service to electricity customers and reduce the power system outages as much as possible. In [4], power transformer asset management is performed using a two-stage maintenance scheduler. The effect of temperature, thermal aging factors, and electrical aging factors on transformer insulation are experimentally analyzed in [51]. In [52], an experimental thermal model for 25 kVA transformers is proposed which estimates transformer lifetime and accordingly the time of transformer maintenance or replacement.

A method for calculating transformer insulation loss of life is provided as a standard, IEEE Std. C57.91-2011 Guide for Loading Mineral-Oil-Immersed Transformers, in [53]. Authors in [54] present a sensory model framework in which transformer lifetime is estimated based on the measured values of winding hottest-spot temperature and the aforementioned IEEE standard. The study in [7] proposes a model for estimating the remaining life of transformer insulation via this IEEE standard, based on historical data of load and ambient temperature. A fuzzy modeling in [55] is applied for transformer asset management while improvement in remaining life of transformer is achieved by a fuzzy

model system. Application of different machine learning methods, such as Adaptive Network-Based Fuzzy Inference System (ANFIS), Multi-Layer Perceptron (MLP) network and Radial Basis Function (RBF) network, in estimating transformer loss of life is presented in [56], where further these methods are fused together to improve the estimation accuracy [57]. In [58], an artificial neural network is modeled to predict top oil temperature in a transformer, where ambient temperature and load current are considered as the input layer and top oil temperature as the output layer. Since transformer loading has the most significant effect on transformer insulation loss of life, its management and control can remarkably increase transformer lifetime. In [8], [59] and [60], the effect of electric vehicles on distribution net load profile and accordingly on distribution equipment such as transformers is studied, and a smart charging method is proposed to manage distribution and transmission assets, including transformers, via controlling and managing distribution net load profile. The effect of electric vehicles and rooftop solar photovoltaic on distribution transformer aging is investigated in [61] and [62]. These studies show that rooftop solar generation decreases transformer loss of life, as it reduces the power transferred from the utility grid to loads, while electric vehicles increase transformer loss of life and their charging/discharging should be controlled to prevent negative impacts on the connected transformer's lifetime. A control algorithm with the objective of controlling the electric load of plug-in electric vehicle on distribution transformer is proposed in [63]. The proposed algorithm aims at reducing distribution transformer overloading via leveraging vehicle-to-gird strategy. An electric vehicle charging algorithm is studied in [64] in order to coordinate the gird and distribution transformer. The algorithm is able to

prevent the distribution transformer from overloading and sharp ramping through smoothing the transformer load profile.

2.2 Leveraging Sensory Data in Estimating Transformer Lifetime

The primary objective of this section is to provide a sensory model framework to measure the transformer internal temperature, i.e., the winding hottest-spot temperature, plug these measured values into the IEEE Std. C57.91-2011 to calculate the transformer loss of life at each time interval, and accordingly determine a good estimate of transformer lifetime. A Cumulative Moving Average (CMA) model is applied to the data stream of the transformer loss of life for this purpose. Using the CMA value, transformer lifetime is estimated at each time interval up until it is converged. Numerical examples, to be carried out in this section, justify that the transformer lifetime can be estimated using the measured sensory data of the winding hottest-spot temperature and the proposed CMA model.

2.2.1 Model Outline and Formulation

A sensory data in line with CMA approach are employed in a dynamic manner to estimate transformer lifetime. In what follows, first, a sequence of nonlinear and exponential functions based on the IEEE Std.C57.91-2011 is presented to calculate transformer loss of life. Then, a sensory model structure for measuring transformer winding-hottest-spot temperature is introduced. Finally, CMA model is proposed in order to apply to the data stream of transformer loss of life, and consequently estimate transformer lifetime.

2.2.1.1 The IEEE Standard Model

The internal temperature of the transformer, which is a function of transformer loading and ambient temperature, is the primary factor on the aging of the transformer insulation. The IEEE Std. C57.91-2011 provides a model for calculation of the transformer loss of life based on the winding hottest-spot temperature. As the temperature does not have a uniform distribution in the transformer, the hottest- spot is considered in calculations. The Arrhenius' chemical reaction rate theory is the source of the IEEE standard experimental equations for calculation of transformer loss of life. Equation (2.1) defines the per unit life of transformers,

$$\text{Per unit life} = A \exp\left(\frac{B}{\theta_H + 273}\right), \tag{2.1}$$

where A is a modified per unit constant and B is the aging rate. A is equal to 9.8 $\times 10^{-18}$ which is calculated based on selection of 110 °C as the temperature for "one per unit life" and B is computed between 11350 and 18000 in various experiments; a value of 15000 is chosen for B in IEEE Std. C57.91-2011.

Substitution of constants A and B in (2.1), gives Aging Acceleration Factor (AAF) for a given winding hottest-spot temperature (2.2).

$$F_{AA} = \exp\left(\frac{15000}{383} - \frac{15000}{\theta_H + 273}\right). \tag{2.2}$$

The hottest-spot temperature on the winding is a critical point as in this temperature transformer insulation degrades. As (2.2) demonstrates, the insulation's lifetime and

accordingly the transformer's lifetime is exponentially related to hottest-spot winding temperature. At 110°C, AAF equals 1 which means transformer will have its normal life expectancy. While, for hottest-spot winding temperature higher/lower than 110°C the transformer lifetime decreases/extends. It is worth to mention that the phrase "loss of life" commonly means "loss of insulation life", although "insulation" is frequently omitted.

The equivalent aging of the transformer in a desired time period is obtained based on (2.2), as follows:

$$F_{EQA} = \sum_{n=1}^{N} F_{AA_n} \Delta t_n \Big/ \sum_{n=1}^{N} \Delta t_n \,, \tag{2.3}$$

where Δt_n is time interval, n is the time interval index and N is the total number of time intervals. The insulation loss of life is accordingly calculated as below:

$$LOL\ (\%) = \frac{F_{EQA} \times t \times 100}{\text{Normal insulation life}}, \tag{2.4}$$

The IEEE standard considers 180000 hours as the normal insulation lifetime for distribution transformers to be included in (2.4).

As (2.1)-(2.4) show, the first step for calculation of transformer loss of life is computing hottest-spot temperature (2.5).

$$\theta_H = \theta_A + \Delta\theta_{TO} + \Delta\theta_H \,, \tag{2.5}$$

In this equation, θ_A represents ambient temperature, $\Delta\theta_{TO}$ is top-oil rise over ambient temperature which is calculated by (2.6), and $\Delta\theta_H$ is the winding hottest-spot rise over top-oil temperature, calculated by (2.7).

$$\Delta\theta_{TO} = (\Delta\theta_{TO,U} - \Delta\theta_{TO,i})(1-\exp(-\frac{1}{\tau_{TO}})) + \Delta\theta_{TO,i}\ , \tag{2.6}$$

$$\Delta\theta_{H} = (\Delta\theta_{H,U} - \Delta\theta_{H,i})(1-\exp(-\frac{t}{\tau_{w}})) + \Delta\theta_{H,i}\ . \tag{2.7}$$

Furthermore, the initial and ultimate values of $\Delta\theta_{TO}$ and $\Delta\theta_{H}$ in (2.6) and (2.7) are calculated through (2.8)-(2.11), as follows:

$$\Delta\theta_{TO,i} = \Delta\theta_{TO,R}(\frac{K_i^2 R+1}{R+1})^n\ , \tag{2.8}$$

$$\Delta\theta_{TO,U} = \Delta\theta_{TO,R}(\frac{K_U^2 R+1}{R+1})^n\ , \tag{2.9}$$

$$\Delta\theta_{H,i} = \Delta\theta_{H,R} K_i^{2m}\ , \tag{2.10}$$

$$\Delta\theta_{H,U} = \Delta\theta_{H,R} K_U^{2m}\ . \tag{2.11}$$

Note that $\Delta\theta_{TO,R}$, $\Delta\theta_{H,R}$, R, m, n are constants and come from transformer characteristics. m and n depend on the transformer cooling system and vary between 0.8 and 1 [53, Table 4].

Considering (2.1)-(2.11), derived from the IEEE standard, it can be seen that the transformer winding hottest-spot, i.e., θ_H, is the main factor in calculating the transformer loss of life at each time interval. Moreover, the value of the winding hottest-spot temperature is governed by ambient temperature, initial value of transformer load ratio, and ultimate value of transformer load ratio at each time interval, i.e., θ_A, K_i and K_U, respectively. Nevertheless, by having a temperature sensor and measuring the transformer

winding hottest-spot temperature, the transformer loss of life could be calculated at each time interval.

2.2.1.2 Sensory Model Structure for Transformer

This section develops a sensory model structure to measure the winding hottest-spot temperature via a temperature sensor and consequently calculates the transformer loss of life based on the above-mentioned equations. This temperature sensor takes the responsibility of measuring the real temperature values of the transformer winding hottest-spot at each time interval. Next, these measured values are utilized to calculate the transformer loss of life. In other words, the value of the transformer loss of life is updated at each time interval using the sensory measured value of the winding hottest-spot temperature. As mentioned in the IEEE Standard, normal lifetime of distribution transformers is 180000 hours, i.e., 20 years. However, this value for normal lifetime is not a fixed number during transformer operational lifecycle, and could be shortened or prolonged in line with the variation of the winding hottest-spot temperature. In other words, if the winding hottest-spot temperature increases or decreases, the transformer loss of life would be increased/decreased, and consequently the normal lifetime for the transformer would be reduced/extended.

Employing the discussed equations and the measured data from the temperature sensor, the transformer loss of life is calculated at each time interval, then the transformer lifetime is estimated in a dynamic manner. Fig. 2.1 shows the overall sensory model structure to estimate the transformer lifetime. As shown in this figure, transformer lifetime, which could possess a different value from the normal lifetime of the transformer, could

be estimated using the sensory data captured from the transformer winding hottest-spot temperature.

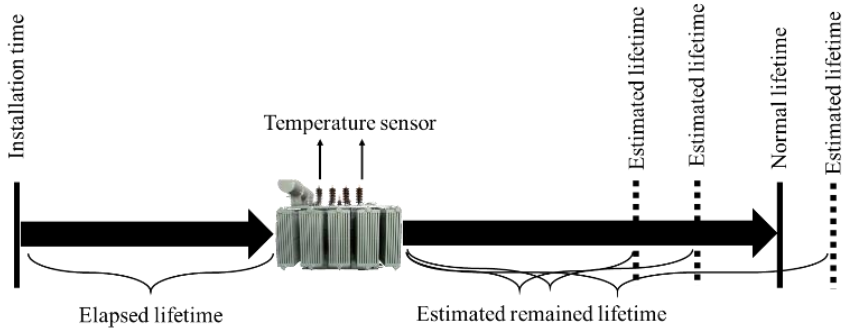

Fig. 2.1 Sensory model structure for transformer lifetime using temperature sensor

2.2.1.3 Cumulative Moving Average Model to Estimate Transformer Lifetime

In order to estimate transformer lifetime, a CMA model is applied to the recorded data stream, generated form the values of the transformer loss of life. In this regard, the calculated values for the transformer loss of life arrive in an ordered data stream, and the CMA model apply the averaging operator to all the ordered data values up until the current point. Through averaging, the model takes the advantages of all the calculated data for the loss of life to estimate the transformer lifetime. Using the CMA model, as each new data point arrives, the average value for the transformer loss of life at the time of the measuring the transformer winding hottest-spot temperature is calculated for all of the ordered values up to that current point, and the lifetime is accordingly updated. Equation (2.12) demonstrates the CMA model for the ordered data values of the transformer loss of life.

$$\mathrm{CMA_n}(\%) = \frac{(LOL_1 + LOL_2 + ... + LOL_n)}{n}, \tag{2.12}$$

where, LOL_1, LOL_2…. LOL_n represent the ordered data stream for the transformer loss of life, n is the number the data stream arrived to the model, and CMA_n represents the CMA value for the ordered data stream of the transformer loss of life. Using, (2.13) the cumulative average is dynamically updated when a new value for the transformer loss of life, i.e., LOL_{n+1}, becomes available.

$$\mathrm{CMA}_{\mathrm{n+1}}(\%) = \frac{LOL_{n+1} + n \times CMA_n}{n+1}, \tag{2.13}$$

As the CMA model is updating the value of the transformer loss of life at each time interval, the transformer lifetime is estimated at that corresponding time interval. Equation (2.14) is used to calculate the estimated transformer lifetime in a desired time interval.

$$\mathrm{Estimated\,Lifetime}_{\mathrm{n}} = \frac{\Delta t_n}{8760 \times CMA_n} + \frac{n \times \Delta t_n}{8760}. \tag{2.14}$$

The first term in (2.14) is the estimated remained lifetime using the CMA value of the transformer loss of life at that time interval. The second term represents the elapsed lifetime for the transformer during the period of feeding the temperature sensor data points into the estimating process. This estimating process is occurring dynamically up until the value for the transformer lifetime is converged. Fig. 2.2 depicts the flowchart of the proposed framework for estimating the transformer lifetime in which the sensory data of the transformer winding hottest-spot temperature, formulations of the IEEE standards, and the CMA model are coming together to aim this goal.

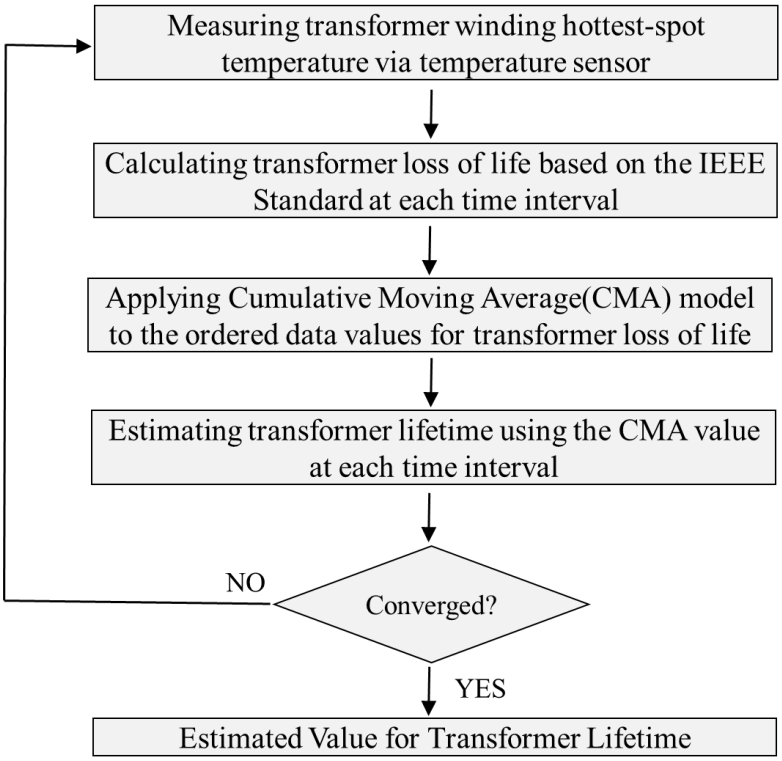

Fig. 2.2 Flowchart of the proposed framework for estimating transformer lifetime using sensory data and CMA model

2.2.2 Numerical Examples

In order to evaluate the performance of the proposed framework for estimating transformer lifetime, an hourly sequence of data for the transformer winding hottest-spot temperature is synthesized under various weather conditions and transformer's loading. In this respect, an hourly ambient temperature, and initial and ultimate values of the transformer load ratio are used. The process of the data synthesis needs some characteristics of the transformer which are borrowed from [7] and tabulated in Table 2.1. Furthermore, a time interval, i.e., Δt_n, of 1 hour is considered for data synthesis and modeling. A total number of 8760-time intervals are considered, equal to the number of hours in one year.

Table 2.1 Characteristics of the studied transformer [7]

I_{rating}	R	m,n	$\Delta\theta_{H,R}$	$\Delta\theta_{TO,R}$	$\tau_{TO,R}$
934 A	7.43	0.8	17.6 °C	53.9 °C	6.8 h

According to various weather conditions, which imply different ambient temperature, and the load ratio for the transformer, following cases are studied:

Case 1: Mild weather condition

Case 2: Warm weather condition

Case 3: Warm weather conditions along with overloading

Case 1: In this case, the transformer is considered to be in a specific place which has a mild climate. This mild weather condition causes the transformer to experience both normal ambient temperature and normal load ratio during operation. The transformer winding hottest-spot temperature is measured via the temperature sensor at each hour, then employed in the proposed framework to estimate the transformer lifetime. Fig. 2.3 compares the hourly and the CMA values of the transformer loss of life. The convergence process for estimating the value of the transformer lifetime is shown in Fig. 2.4. As shown in these two figures, due to the fact that the data in the beginning of the measurement horizon are sparse, the CMA value does not represent the transformer loss of life precisely so that the estimated lifetime for the transformer is oscillating. After measuring 8003 sample points, i.e., after 8003 hours, the CMA value is rich enough to be generalized to all the pervious measured data value, and as a result the transformer lifetime value is converged to a constant. The lifetime value for the transformer is estimated to be 37.3 years

in this case, much greater than the initially estimated lifetime of 20 years. It should be mentioned that in all the figures, logarithmic scale is considered for Y-axis.

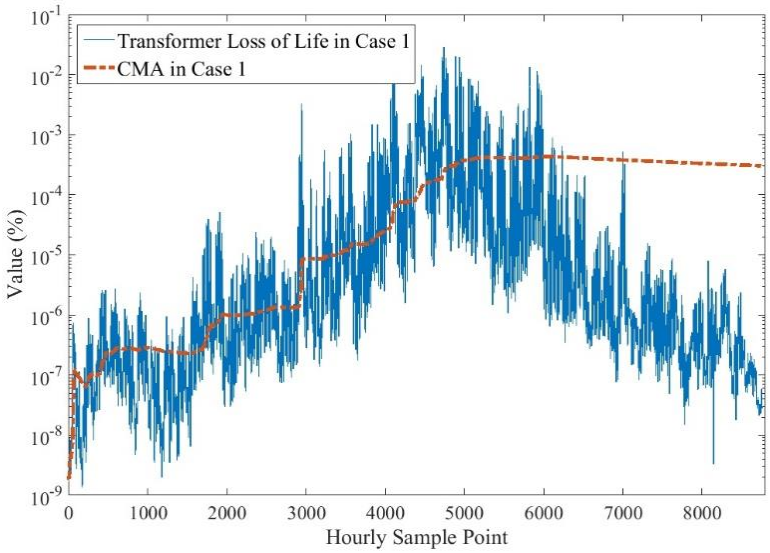

Fig. 2.3 Hourly and CMA values for transformer loss of life in Case 1

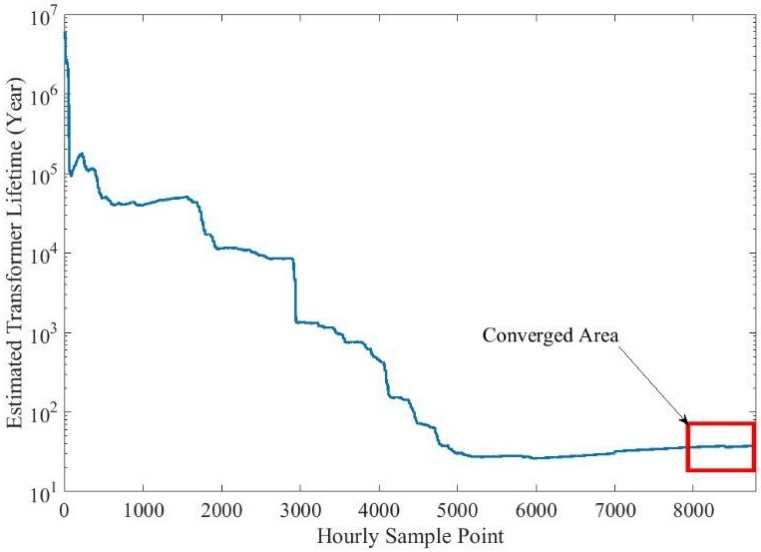

Fig. 2.4 Estimating transformer lifetime up to its convergence in Case 1

Case 2: A warm weather condition is considered for the transformer in this case. It is clear that there is a correlation between ambient temperature and the transformer load

ratio; warm ambient temperature causes higher load ratio to the transformer during operation. Accordingly, the transformer winding hottest-spot temperature will increase. Nevertheless, in order to estimate the transformer lifetime, the data for the winding hottest-spot temperature, measured hourly by the temperature sensor, are fed to the proposed model. Fig. 2.5 shows the hourly and the CMA values of the transformer loss of life, and Fig. 2.6 depicts the convergence process for estimating the value of the transformer lifetime. As shown in these figures, after 8150 samples of data stream, the transformer lifetime is converged to 23.5 years, which again is greater than the initially assumed lifetime. The transformer in this case has a shorter lifetime, compared to Case 1, conceivably due to higher temperature at the hottest-spot. Thus, transformer lifetime in the warm climate considerably declines, compared to the mild climate in Case 1, due to the double impact of warm ambient temperature and excessive transformer load ratio on its winding hottest-spot temperature.

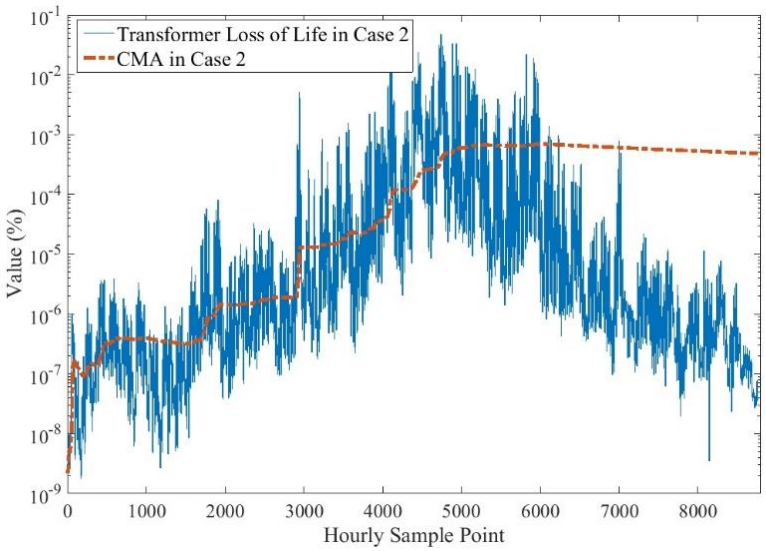

Fig. 2.5 Hourly and CMA values for transformer loss of life in Case 2

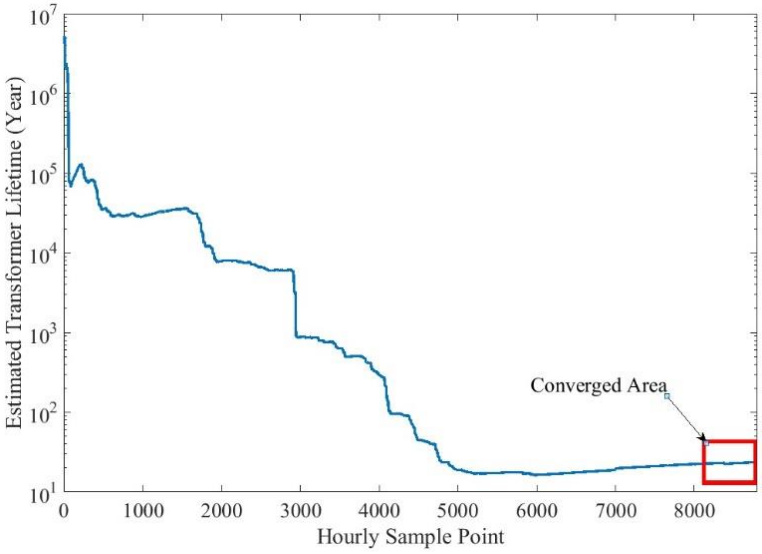

Fig. 2.6 Estimating transformer lifetime up to its convergence in Case 2

Case 3: Overloading has a negative impact on the transformer lifetime. Transformer overloading sets the stage for a sharp decline in its lifetime. The more transformer undergoes overloading conditions, the more its winding hottest-spot temperature increases, and the less its lifetime will be. This case investigates the effect of overloading on the transformer lifetime. In this regard, the transformer in Case 2 is assumed to undergo 20% overloading at 3 hours of 20 randomly selected days in a whole year. Fig. 2.7 compares the estimated transformer lifetime for all these three cases. In Case 3, the proposed framework uses 8340 hourly sample points to estimate the transformer lifetime, and the transformer lifetime is estimated to be 21.7 years, which is lower than Case 2, and advocates how overloading negatively impacts the transformer lifetime. It is interesting to see that this considerable decrease in transformer lifetime is a result of a limited overload in a limited number of hours, which shows the significant impact of overloading on transformer lifetime.

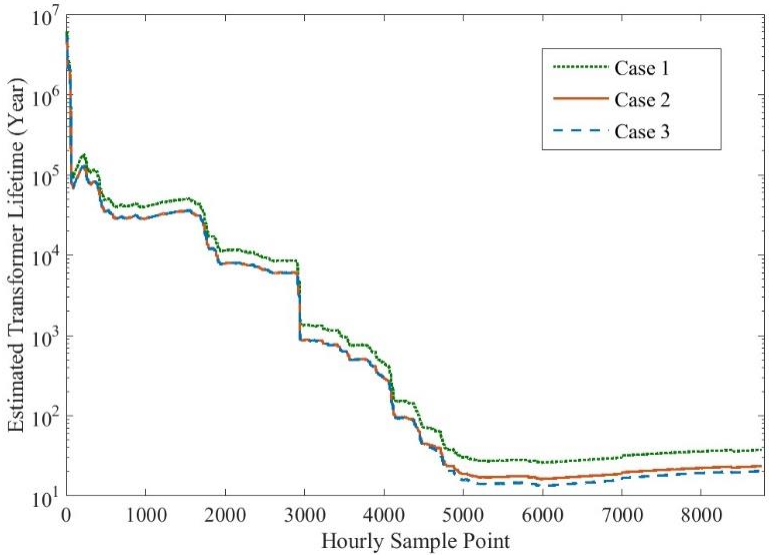

Fig. 2.7 Comparison of estimating transformer lifetime up to its convergence in all studied cases

2.2.3 Discussions

Power transformers, which are not only considered as a mainstay of providing reliable power to customers but are also expensive relative to other power system components, have always played a major role in asset management. By leveraging sensory data, an efficient approach in estimating transformer lifetime was proposed. Measuring the hourly winding hottest-spot temperature via the temperature sensor, and employing the CMA model to the data stream of the transformer loss of life, the transformer lifetime was estimated at each hour, until it was converged to a constant value. Comparing this calculated lifetime with the time that the transformer has been in service, would provide the remaining lifetime of the asset. The proposed approach was analyzed through numerical simulations under different weather conditions and transformer's loading, where it was shown that overloading could potentially lead to significant drop in the transformer lifetime. Utility companies can reap the benefits of this simple, practical, and yet intelligent

approach for transformer asset management, without the need for additional investment in the system.

2.3 Data Fusion and Machine Learning Integration for Transformer Loss of Life Estimation

Given that a significant amount of data can be collected from sensors installed in transformers, machine learning methods can be of value in estimating transformer lifetime. A machine learning-based study with the goal of estimating transformer loss of life is proposed in this dissertation. Authors in [55] utilize a fuzzy modeling system for transformer asset management. An artificial neural network model for predicting top oil temperature in transformer is used in [58]. A naïve thermal model to estimate transformer lifetime and transformer replacement time on the basis of an evolutionary algorithm, here genetic program and by using experimental data, is presented in [52].

The existing literature in this research area lacks studies on data-driven methodologies, such as machine learning and data fusion, for transformer lifetime assessment. The primary objective in this section is to integrate data fusion and machine learning techniques for providing a more accurate and reliable estimation of transformer loss of life.

Utilizing machine learning methods to estimate the transformer loss of life sets the stage for using data fusion techniques, and thus call for additional studies. In general, all tasks that demand any type of estimation from multiple sources can reap the benefit of using data fusion techniques. The following well-known definition of data fusion is

provided in [65]: “data fusion techniques combine data from multiple sensors and related information from associated databases to achieve improved accuracy and more specific inferences than could be achieved by the use of a single sensor alone.” In this section, by leveraging the historical data of transformer loading and ambient temperature, various machine learning methods, including Adaptive Network-Based Fuzzy Inference System (ANFIS), Multi-Layer Perceptron (MLP) network and Radial Basis Function (RBF) network are employed to accurately estimate the transformer loss of life. Then, two types of data fusion techniques, including Ordered Weighted Averaging (OWA) and Kalman filter are presented to improve the transformer loss of life estimation. Comparison among the proposed machine learning and data fusion techniques is further provided in this section.

2.3.1 Data Synthesis Based on the IEEE Std. C57.91-2011

Considering (2.1)-(2.11), obtained from the IEEE standard, it can be seen that the transformer loss of life is a function of both transformer loading and ambient temperature. In other words, as shown in Fig. 2.8, by plugging the hourly values of transformer loading and ambient temperature into the above-mentioned equations, the hourly transformer loss of life could be calculated. This process is called data synthesis in which the hourly value of the transformer loss of life is synthesized on the basis of this IEEE standard. The synthesized data is utilized to be employed in machine learning methods and data fusion techniques for estimating the transformer loss of life.

Fig. 2.8 Data synthesis process based on the IEEE standard

2.3.2 Machine Learning and Data Fusion

An overview of machine learning methods and data fusion techniques for estimating transformer loss of life is presented in this section. Data fusion techniques are utilized to improve the machine learning estimated values of the transformer loss of life. In fact, data fusion is used to fuse the outputs of machine learning methods in such a way that the estimated transformer loss of life becomes more accurate. In what follows, machine learning methods to estimate the transformer loss of life are provided, then two various kinds of data fusion techniques, including Ordered Weighted Averaging (OWA) and sequential Kalman filter, are introduced with the goal of integrating machine learning and data fusion.

In order to evaluate and compare the performance and the accuracy of the proposed models for transformer loss of life estimation, two performance measures are applied: Mean Square Error (MSE) and coefficient of determination (R^2) which are calculated in (2.15) and (2.16), respectively. R^2 ranges from 0 to 1, where R^2=1 means the proposed ANFIS model can estimate the actual transformer loss of life without error, and R^2=0 means the proposed ANFIS model cannot estimate the actual transform loss of life.

$$\mathrm{MSE} = \frac{1}{Q}\sum_{q=1}^{Q}\left(Y_q - \hat{Y}_q\right)^2, \tag{2.15}$$

$$R^2 = 1 - \left[\sum_{q=1}^{Q} \left(Y_q - \hat{Y}_q \right)^2 \Big/ \sum_{q=1}^{Q} \left(Y_q - \bar{Y} \right)^2 \right], \tag{2.16}$$

In above equations, Y_q is the actual output for the q^{th} test dataset, $\hat{Y}_q$ is the estimated output for the q^{th} test dataset and $\bar{Y}$ is the average of all actual outputs for test datasets. It should be considered that data pre-processing is an important step in ensuring that bad data are detected and efficiently corrected before feeding to the proposed model.

2.3.2.1 Machine Learning

Machine learning is an intelligent method to solve nonlinear estimation and classification problems [66]. Various data-driven machine learning methods, including but not limited to ANFIS, RBF and MLP, can be considered as suitable candidates for solving the estimation problems, where the transformer loss of life is estimated using these three methods, as shown in Fig. 2.9(a). Each of these machine learning methods have different performances, which are quantified by two measures: Mean Square Error (MSE) and coefficient of determination (R^2). It should be noted that these performance measures, i.e., MSE and R^2, are applicable to data fusion techniques as well. Two data fusion techniques are presented here to combine the two aforementioned machine learning methods, i.e., the ANFIS and the RBF, with the objective of improving the accuracy of the transformer loss of life estimation.

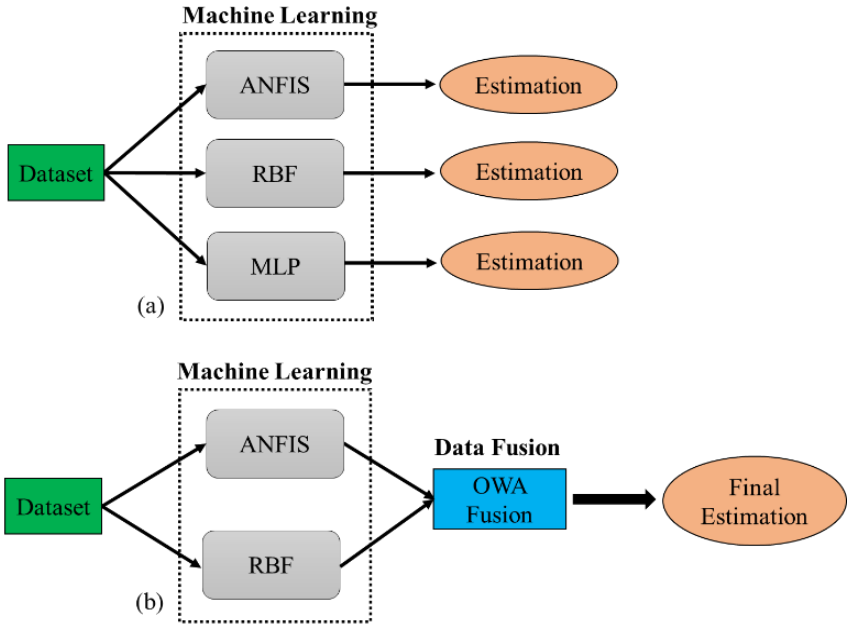

Fig. 2.9 Transformer loss of life estimation by using (a) machine learning, (b) machine learning and OWA fusion

2.3.2.2 Ordered Weighted Averaging-Based Data Fusion

OWA operator, as one of the most popular data fusion techniques, has been introduced in [67]. OWA is utilized to incorporate the output results of the estimated ANFIS and RBF methods, as shown in Fig. 2.9(b). To this end, the objective function that should be minimized is as follows:

$$\min MSE = \frac{1}{S}\sum_{s=1}^{S}\left(C_1 \times \hat{Y}_S + C_2 \times \hat{O}_S - Y_S \right)^2 , \tag{2.17}$$

$$C_1, C_2 \in [0,1] \quad and \quad C_1 + C_2 = 1 , \tag{2.18}$$

where C_1 and C_2 are weight factors corresponding to the ANFIS and RBF, respectively. Y_s is the target value for the transformer loss of life, and S is the number of training dataset.

Moreover, $\hat{Y}_s$ and $\hat{O}_s$ are respectively the ANFIS and the RBF estimated values of the transformer loss of life.

Genetic Algorithm (GA) is employed in order to obtain the optimal contribution of each machine learning method to build the OWA-based data fusion [68]. Accordingly, GA determines the optimal weight factors, i.e., C_1 and C_2, which aims at minimizing the objective function. After running GA, the optimized weight factors are acquired to be employed in the test dataset to yield the final estimation.

2.3.2.3 Kalman Filter-Based Data Fusion

The Kalman filter was developed by R. Kalman. In 1960 his well-known paper [69] was published with the goal of unknown system state estimation via filtering behavior. Generally speaking, Kalman filters encompass a number of types and topologies depending on use and application. In this section, on the basis of the Kalman filter, a sequential processing technique is developed for the purpose of data fusion. Fig. 2.10 demonstrates an overview of the sequential update architecture for data fusion using the Kalman filter.

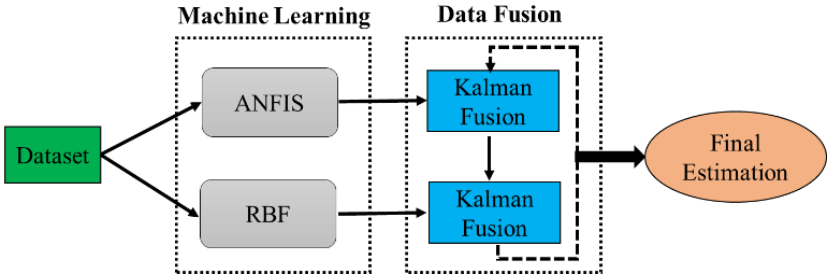

Fig. 2.10 Architecture of the sequential Kalman filter fusion

The recursive equations of the Kalman filter are shown in Fig. 2.11. At each sample point, the algorithm projects both the state estimate, i.e., x_s, and the error covariance, i.e., P_s. In the second stage, the Kalman gain, i.e., k_s, is computed. Then, by incorporating a

new value, i.e., z_s, the improved estimate is updated. Finally, the error covariance is updated. It is assumed that the process noise covariance, i.e., Q, and the measurement noise covariance, i.e., E, are not changing with each sample point, so that they both are considered as constant matrices. Noted that u_s and H are exogenous control input and observation matrix, respectively. In addition, A and B are respectively transition and control matrices. More mathematical details and explanations can be found in [70].

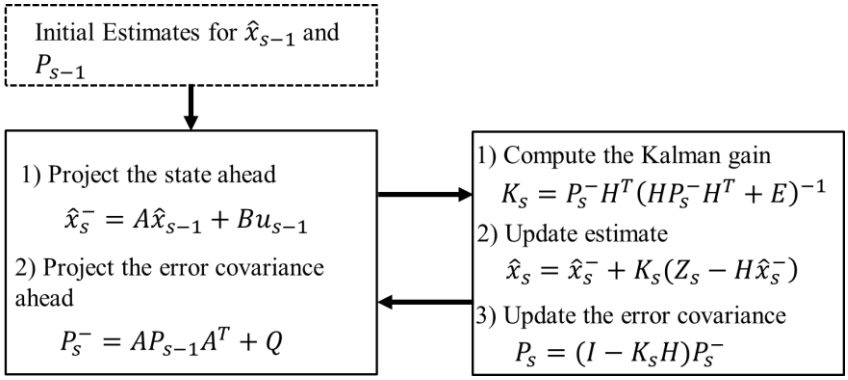

Fig. 2.11 Kalman filter algorithm

2.3.3 Numerical Simulations

The performance of the machine learning methods and the data fusion techniques for estimating the transformer loss of life is evaluated in this section. In this regard, the required data is synthesized on the basis of the mentioned IEEE standard. The following cases are studied to investigate the performance of integration of the machine learning and data fusion techniques for estimating the transformer loss of life.

Case 1: Transformer loss of life estimation using machine learning methods

Case 2: Transformer loss of life estimation using OWA-based data fusion

Case 3: Transformer loss of life estimation using Kalman filter-based data fusion

Case 1: Three machine learning methods, including ANFIS, RBF and MLP, are applied to the synthesized data to estimate the transformer loss of life. Among these three methods, two of them (ANFIS and RBF) outperform the other one (MLP) in terms of having lower MSE and higher R^2, so that these two superior methods are selected to be fused together, as will be carried out in Cases 1 and 2. The MSE and R^2 in the ANFIS method, applied in the test datasets, are respectively calculated as 2.946×10^{-10} and 0.96. For the RBF method, 4.124×10^{-10} and 0.89 are the best obtained values for the MSE and R^2, respectively.

Case 2: The OWA-based data fusion is employed in this case to combine the two selected machine learning methods of Case 1. The proposed OWA operator is modeled in MATLAB for fusing the hourly estimated values of the transformer loss of life. After running the GA, the optimized weight factors, i.e., C_1 and C_2, for fusing the output of the ANFIS and RBF are obtained as 0.9 and 0.1, respectively. The MSE and R^2 using the OWA-based data fusion are 2.832×10^{-10} and 0.97, respectively. This case advocates the fact that by leveraging the OWA-based data fusion technique, the accuracy of the results is improved. In fact, compared to each of the machine learning methods in Case 1, this data fusing technique leads to lower MSE and higher R^2 for estimating the transformer loss of life.

Case 3: The Kalman filter-based data fusion is used in this case. The estimated output results of the ANFIS and RBF are fused in a sequential manner using the Kalman filter equations to achieve better performance measures. It is worth to mention that in the proposed Kalman filter algorithm, both A and H are equal to 1, and B is 0. Moreover, z_z is

an estimated value achieved either from the ANFIS or the RBF method. After running the simulation, the values of MSE and R^2 are calculated as 2.389×10^{-10} and 0.99, respectively, which outperforms the corresponding values in Cases 0 and 1. Fig. 2.12 compares the Kalman filter-fused values of the transformer loss of life with the actual ones, obtained from the data synthesis process, as well as the error (the difference between these two values). It should be noted that Fig. 2.12 is depicted only for 50 samples of the test datasets to provide a better visual comparison.

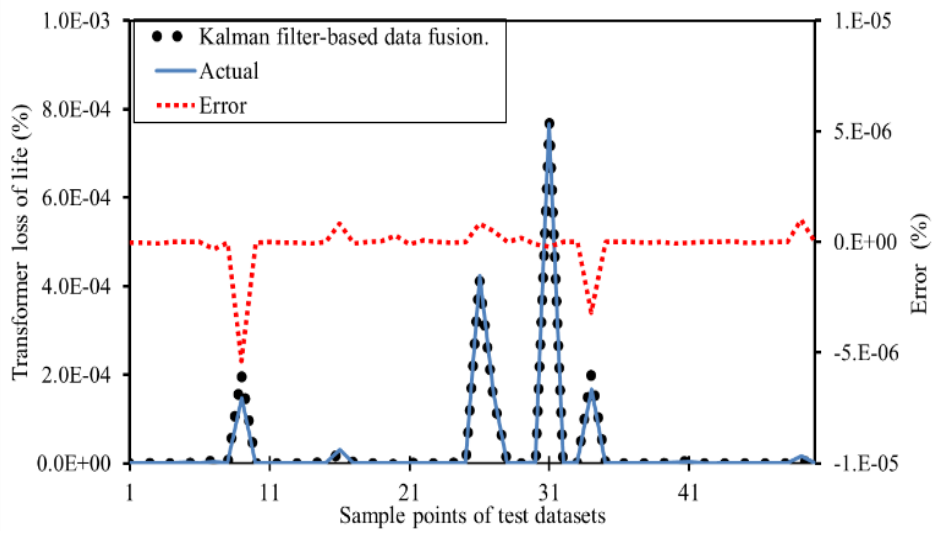

Fig. 2.12 Comparison between Kalman filter-fused values of the transformer loss of life with the actual ones

The obtained results from these three case studies are ranked based on the two performance measures (MSE and R^2), and tabulated in Table 2.2. As the table demonstrates, integrating machine learning methods and data fusion techniques enhance the accuracy of the transformer loss of life estimation. A comparison between Cases 2 and 3 advocates that the Kalman- filter-based data fusion technique surpasses the OWA-based one in terms of performance measures. It should be noted that as the simulations are carried

out offline, the computation times are of no importance, thus not listed here. Taking all the results into consideration, it is admitted that incorporating the machine learning methods and the data fusion techniques boosts the accuracy of the transformer loss of life estimation.

Table 2.2 Comparison of the machine learning methods and data fusion techniques for estimating the transformer loss of life

		MSE	R^2	Rank
Machine Learning	ANFIS	2.946×10^{-10}	0.96	3
	RBF	4.124×10^{-10}	0.89	4
Data Fusion	OWA	2.832×10^{-10}	0.97	2
	Kalman Filter	2.389×10^{-10}	0.99	1

2.3.4 Discussions

Transformer maintenance and repair service has always been one of the priorities of power system operators, as transformer failure causes unplanned outages and can negatively impact power system reliability. A methodology to obtain a low-error estimate of transformer loss of life was proposed in this section, leveraging an integrated machine learning and data fusion technique. The IEEE Std. C57.91-2011 was used to synthesize data, followed by two machine learning methods, including the ANFIS and RBF, to estimate the transformer loss of life. Then, by leveraging the OWA operator and the Kalman filter, the estimated results of these two machine learning methods were fused together to obtain a more accurate estimate. The proposed Kalman filter-based data fusion technique outperforms OWA as well as individual machine learning methods in terms of the MSE and R^2.

2.4 Distribution Transformer Asset Management through Coordinated Microgrid Scheduling

A new method for distribution transformer asset management by leveraging microgrids is proposed in this section. In recent years, microgrid deployment has been meaningfully increased and it can be expected that the growing trend is even becoming faster in the near future [71], [72], expected to reach a global revenue of $19.9 billion by 2020 [73]. This trend advocates on the growing interest in microgrids as a mainstay of future power grids. A comprehensive survey on microgrid research trends can be found in [74]. This section builds up on existing research and deployment efforts and focuses on the flexibility advantages of the utility-owned microgrids as a complementary value proposition for distribution transformer asset management. The microgrid capability in managing its adjustable loads, dispatchable Distributed Generation (DG) units, Distributed Energy Storage (DES) units, and the ability of exchanging power with the utility grid in the grid-connected mode is specifically considered in this dissertation for smoothing distribution transformer loading, and consequently decreasing transformer loss of life which leads to higher transformer lifetime. It is assumed that the studied microgrid is utility-owned, thus can be scheduled by the electric utility company or any designated entity as the operator.

By leveraging the IEEE Std. C57.91-2011, the distribution transformer loss of life is calculated in order to be integrated in the microgrid optimal scheduling model. The aforementioned standard for calculation of the distribution transformer loss of life has a set of nonlinear equations which would make the microgrid optimal scheduling a nonlinear

and hard to solve problem. To ensure that the microgrid optimal scheduling problem keeps its linear characteristics, the original problem is decomposed into a mixed integer linear programming master problem (minimizing the microgrid operation cost) and a nonlinear subproblem (determines the distribution transformer loss of life) using Benders decomposition. These two problems are further coordinated through Benders cuts in an iterative manner. Using this proposed iterative method, the master problem solves the microgrid optimal scheduling problem, as discussed in many existing research such as [15]-[17], while the added subproblem acts as a feedback on how microgrid operation would impact the transformer lifetime, and accordingly, would provide a signal (the Benders cut) on how microgrid schedule should change to increase transformer lifetime. It should be noted that although the proposed models are based on the IEEE Std. C57.91-2011, any other standard or updates to this standard can be modeled using the same approach and without loss of generality in the proposed model.

Taking (2.1)-(2.11) into account, it can be seen that the percentage value for loss of life at each time interval is a nonlinear function of initial/ultimate values of transformer load ratio, and ambient temperature, i.e., K^I, K^U and θ^A, respectively. In other words, by knowing K^I, K^U and θ^A at each time interval, the percentage value for loss of life can be calculated via the sequence of these nonlinear functions. One key point is that θ^A can be forecasted accurately for each location at each time interval so that the percentage value for loss of life, as defined in (2.19), will be a nonlinear function of initial and ultimate values of transformer load ratio, i.e., K^I and K^U, respectively:

$$LOL\,(\%) = f\,(K_{ht}^{I}, K_{ht}^{U}) \qquad \forall h, \forall t, \tag{2.19}$$

2.4.1 Transformer Asset Management via Microgrid Optimal Scheduling

The proposed extended microgrid optimal scheduling problem determines the least-cost schedule of available resources (DERs and loads) while minimizing the cost of distribution transformer loss of life (2.20), subject to prevailing operational constraints (2.21)-(2.47).

$$\min \sum_{h}\sum_{t}[\sum_{i\in G} F_i(P_{iht}) + \rho_{ht}^{M} P_{ht}^{M}] + \psi\, f(K_{ht}^{I}, K_{ht}^{U}) \tag{2.20}$$

$$\sum_{i} P_{iht} + P_{ht}^{M} = \sum_{d} D_{dht} \qquad \forall h, \forall t, \tag{2.21}$$

$$-P^{M,\max} w_{ht} \le P_{ht}^{M} \le P^{M,\max} w_{ht} \qquad \forall h, \forall t, \tag{2.22}$$

$$P_i^{\min} I_{iht} \le P_{iht} \le P_i^{\max} I_{iht} \qquad \forall i \in \mathrm{G}, \forall h, \forall t, \tag{2.23}$$

$$P_{iht} - P_{ih(t-1)} \le UR_i \qquad \forall i \in \mathrm{G}, \forall h,\ t \ne 1, \tag{2.24}$$

$$P_{ih1} - P_{i(h-1)T} \le UR_i \qquad \forall i \in \mathrm{G}, \forall h, \forall t, \tag{2.25}$$

$$P_{ih(t-1)} - P_{iht} \le DR_i \qquad \forall i \in \mathrm{G}, \forall h,\ t \ne 1, \tag{2.26}$$

$$P_{i(h-1)T} - P_{ih1} \le DR_i \qquad \forall i \in \mathrm{G}, \forall h, \forall t, \tag{2.27}$$

$$T_i^{\mathrm{on}} \ge UT_i(I_{iht} - I_{ih(t-1)}) \qquad \forall i \in \mathrm{G}, \forall h,\ t \ne 1, \tag{2.28}$$

$$T_i^{\mathrm{on}} \ge UT_i(I_{ih1} - I_{i(h-1)T}) \qquad \forall i \in \mathrm{G}, \forall h, \forall t, \tag{2.29}$$

$$T_i^{\mathrm{off}} \ge DT_i(I_{ih(t-1)} - I_{iht}) \qquad \forall i \in \mathrm{G}, \forall h, t \ne 1, \tag{2.30}$$

$$T_i^{\mathrm{off}} \ge DT_i(I_{i(h-1)T} - I_{ih1}) \qquad \forall i \in \mathrm{G}, \forall h, \forall t, \tag{2.31}$$

$$P_{iht} \le P_{iht}^{\mathrm{dch,max}} u_{iht} - P_{iht}^{\mathrm{ch,min}} v_{iht} \qquad \forall i \in \mathrm{S}, \forall h, \forall t, \tag{2.32}$$

$$P_{iht} \ge P_{iht}^{\mathrm{dch,min}} u_{iht} - P_{iht}^{\mathrm{ch,max}} v_{iht} \qquad \forall i \in \mathrm{S}, \forall h, \forall t, \tag{2.33}$$

$$u_{iht} + v_{iht} \le 1 \qquad \forall i \in \mathrm{S}, \forall h, \forall t, \tag{2.34}$$

$$C_{iht} = C_{ih(t-1)} - (P_{ith} u_{iht} \tau^{ES} / \eta_i) - P_{iht} v_{iht} \tau^{ES} \quad \forall i \in \mathrm{S}, \forall h, t \ne 1, \tag{2.35}$$

$$C_{ih1} = C_{i(h-1)T} - (P_{ih1} u_{iht} \tau^{ES} / \eta_i) - P_{ih1} v_{iht} \tau^{ES} \qquad \forall i \in \mathrm{S}, \forall h, \forall t, \tag{2.36}$$

$$C_i^{\min} \le C_{iht} \le C_i^{\max} \qquad \forall i \in \mathrm{S}, \forall h, \forall t, \tag{2.37}$$

$$T_{iht}^{\mathrm{ch}} \ge MC_i (u_{iht} - u_{ih(t-1)}) \qquad \forall i \in \mathrm{S}, \forall h, t \ne 1, \tag{2.38}$$

$$T_{ih1}^{\mathrm{ch}} \ge MC_i (u_{ih1} - u_{i(h-1)T}) \qquad \forall i \in \mathrm{S}, \forall h, \forall t, \tag{2.39}$$

$$T_{iht}^{\mathrm{dch}} \ge MD_i (v_{iht} - v_{ih(t-1)}) \qquad \forall i \in \mathrm{S}, \forall h, t \ne 1, \tag{2.40}$$

$$T_{ih1}^{\mathrm{dch}} \ge MD_i (v_{ih1} - v_{i(h-1)T}) \qquad \forall i \in \mathrm{S}, \forall h, \forall t, \tag{2.41}$$

$$D_d^{\min} z_{dht} \le D_{dht} \le D_d^{\max} z_{dht} \qquad \forall d \in \mathrm{D}, \forall h, \forall t, \tag{2.42}$$

$$T_d^{on} \ge MU_d (z_{dht} - z_{dh(t-1)}) \qquad \forall d \in \mathrm{D}, \forall h, t \ne 1, \tag{2.43}$$

$$T_d^{on} \ge MU_d (z_{dh1} - z_{d(h-1)T}) \qquad \forall d \in \mathrm{D}, \forall h, \forall t, \tag{2.44}$$

$$\sum_{[\alpha,\beta]} D_{dht} = E_d \qquad \forall d \in \mathrm{D}, \tag{2.45}$$

$$\left(\left| \hat{P}_{ht}^{M} \right| \Big/ P_{nom}^{Trans} \right) = K_{ht}^{U} \qquad \forall h, \forall t, \tag{2.46}$$

$$\left(\left| \hat{P}_{h(t-1)}^{M} \right| \Big/ P_{nom}^{Trans} \right) = K_{ht}^{I} \qquad \forall h, \forall t. \tag{2.47}$$

The first term in the objective function (2.20) minimizes the microgrid annual operation cost, including the local generation cost and the cost of energy exchange with the utility grid. The second term represents the cost of distribution transformer loss of life. This term consists of multiplication of distribution transformer loss of life, based on the IEEE Standard, and the distribution transformer investment cost (ψ). This term attempts to

minimize the distribution transformer loading in order to reduce its loss of life and consequently increase its lifetime. This investment cost is used to ensure that both terms in the objective have a similar unit (here $). It should also be noted that the maintenance cost of generation units has been already included in the first term of the objective function (2.20) as the local generation cost.

The load balance equation (2.21) ensures that the summation of power exchange with the utility grid and the local generations (including dispatchable DGs, nondispatchable DGs, and the DES) would be equal to microgrid total load at each operating hour. The DES power can be positive (discharging), negative (charging) or zero (idle). In addition, the power exchange between microgrid and the utility grid (P^M) could be positive (import), negative (export) or zero. This power is also restricted to the capacity of the line between the microgrid and the utility grid (2.22). Hourly generation of dispatchable DGs are constrained by the maximum and minimum capacity limits (2.23), where the unit commitment state variable *I* would be 1 when the unit is committed and 0 otherwise. Constraints (2.24)-(2.27) represent ramp up and ramp down constraints of dispatchable DG units, where (2.24) and (2.26) belong to intra-day intervals and (2.25) and (2.27) represent ramping constraints for inter-day intervals. Dispatchable DG units are subject to the minimum up and down time limits, represented by (2.28)-(2.31). Constraints (2.28),(2.30) and (2.29),(2.31) represent minimum up/down time for inter-day and intra-day intervals, respectively. Constraints (2.32) and (2.33) respectively define the minimum and maximum limits of the DES charging and discharging. It should be noted that in the charging/discharging mode the binary charging/discharging state variable *v/u* is 1/0 and the

binary discharging/charging state variable *u/v* is 0/1. Constraint (2.34) ensures that the DES can merely operate in one mode of charging or discharging at every time period. The amount of charged and discharged power in the DES and the available stored energy determine the stored energy in intra-day (2.35) and inter-day (2.36) intervals, where one hour is considered for time period of charging and discharging. The amount of stored energy in DES is further limited to its capacity (2.37). Constraints (2.38),(2.40) and (2.39),(2.41) represent the minimum charging/discharging times of DES for intra-day and inter-day intervals, respectively. Constraint (2.42) confines adjustable loads to minimum and maximum rated powers, and (2.43),(2.44) represent the minimum operating time of adjustable loads for intra-day and inter-day intervals. It should be noted that in (2.42)-(2.44), when load is on, binary operating variable *z* is 1, otherwise it is 0. Moreover, (2.45) considers the required energy to complete an operating cycle for adjustable loads. Note that the adjustable loads utilized in this dissertation are responsive to price changes and controlling signals from the microgrid controller so that no compensation costs are considered. It should be mentioned that $b=0$ represents the last day of the previous scheduling horizon, and T represents the last scheduling hour, i.e., T=24.

As the exchanged power between the microgrid and the utility grid (P^M) determines the distribution transformer load ratio, i.e. K^U and K^I, constraints (2.46) and (2.47) are developed to show the interdependency of these variables. Based on the direction of power exchange between the microgrid and the utility grid, the amount of P^M could be positive (exporting power) or negative (importing power), but the transformer load ratio (K^I or K^U) accepts just positive values. Thus, the absolute value of P^M should be considered in (2.46)

and (2.47), which represent the relationship between the transformer loading and the microgrid power exchange with the utility grid.

2.4.1.1 Transformer Asset Management Model Outline

Fig. 2.13 depicts the flowchart of the proposed microgrid-based distribution transformer asset management model by using Benders decomposition. The objective of the original microgrid-based distribution transformer asset management model is the summation of microgrid operation cost and the distribution transformer cost of loss of life, i.e., the summation of a linear and a nonlinear term. However, in Benders decomposition the subproblem does not need to be necessarily in a linear form [76]. In this dissertation, Benders decomposition is employed to decompose the microgrid-based distribution transformer asset management problem to a mixed integer linear programming master problem (minimizing the microgrid operation cost) and a nonlinear subproblem (determines the distribution transformer loss of life). These two problems are further coordinated through optimality cuts in an iterative manner. Using this proposed iterative method, the master problem solves the microgrid optimal scheduling problem, while the added subproblem acts as a feedback on how microgrid operation would impact the transformer lifetime, and accordingly, would provide a signal (the optimality cut) on how microgrid schedule should change to increase transformer lifetime. The procedure for microgrid-based distribution transformer asset management solution is as follows:

(i) Solve the microgrid optimal scheduling master problem by considering the commitment and dispatch of available DGs, the charging and discharging schedules of

DESs, the schedule of adjustable loads, and the exchanged power with the utility grid. Note that there is no optimality cut available in the first iteration of the master problem.

(ii) Minimize the transformer asset management subproblem by considering the exchanged power of the microgrid with the utility grid (transformer loading).

(iii) Compare the subproblem's solution, i.e., an upper bound, with the solution of the master problem, i.e., a lower bound. If the difference is larger than a predetermined threshold, form the optimality cut and send back to the master problem to consequently revise the current schedule of available resources and the exchanged power with the utility grid. Otherwise, consider the microgrid-based distribution transformer asset management solution as optimal.

The optimality of the Benders decomposition method is extensively discussed in the following references [76]-[78]. A comprehensive discussion on branch-and-bound technique for solving the microgrid-based distribution transformer asset management model is provided in Appendix.

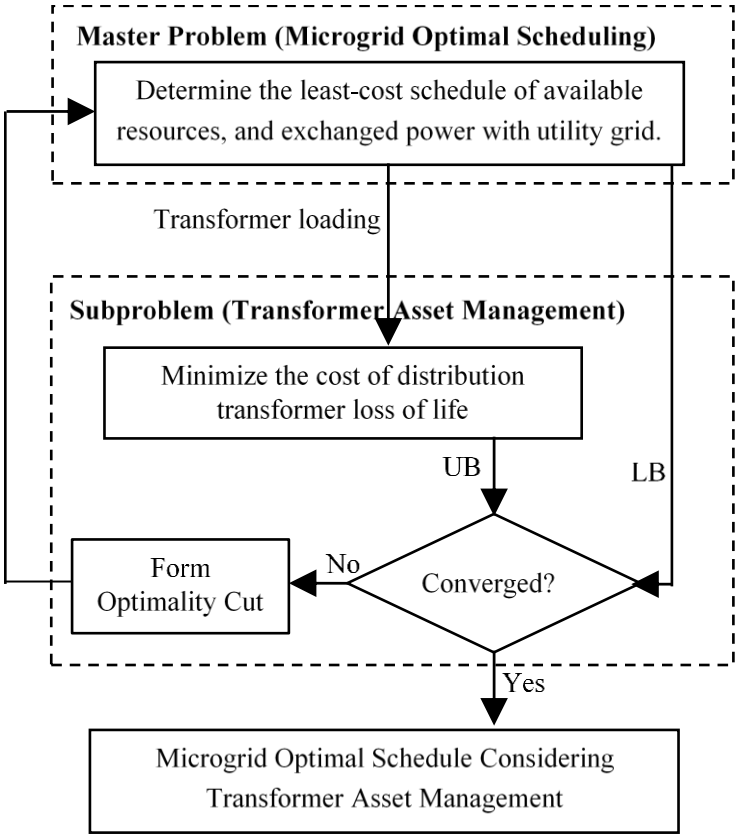

Fig. 2.13 Proposed flowchart for microgrid-based transformer asset management

2.4.1.2 Microgrid Optimal Scheduling (Master Problem)

The objective of the microgrid optimal scheduling master problem is to minimize the microgrid annual operation cost, subject to (2.21)-(2.45). The second term added to the objective function is the projected cost of the distribution transformer loss of life, which will be obtained from the optimality cuts generated in the transformer asset management subproblem. The value of this term in the first iteration will be 0. The master problem determines the optimal microgrid schedule, where the optimal values of the exchanged power between the microgrid and the utility grid will be sent to the distribution asset management subproblem with the objective of calculating the optimal value for the distribution transformer loss of life.

$$\min \sum_{h} \sum_{t} [\sum_{i \in G} F_i(P_{iht}) + \rho_{ht}^{M} P_{ht}^{M}] + \Lambda \tag{2.48}$$

Subject to (2.21)-(2.45).

2.4.1.3 Transformer Asset Management (Subproblem)

The objective of the transformer asset management subproblem is to minimize the cost of distribution transformer loss of life based on the IEEE Std. C57.91-2011, as defined in (2.49), and subject to additional limitations on the distribution transformer loading (2.50)-(2.51).

$$\min Q = \sum_{h} \sum_{t} \psi f(K_{ht}^{I}, K_{ht}^{U}) \tag{2.49}$$

$$P_{h(t-1)}^{M} = \hat{P}_{h(t-1)}^{M} \qquad \lambda_{ht} \qquad \forall h, \forall t, \tag{2.50}$$

$$P_{ht}^{M} = \hat{P}_{ht}^{M} \qquad \mu_{ht} \qquad \forall h, \forall t. \tag{2.51}$$

The exchanged power of the microgrid with the utility grid (transformer loading) is calculated in the master problem and used in the subproblem as given values in (2.50), (2.51). λ_{ht} and μ_{ht} are dual variables associated with the initial and ultimate microgrid exchanged power with the utility grid at each time interval, respectively. These dual variables are calculated thorough linearization of subproblem around the operating point in each iteration, determined in the master problem.

The solution of the original integrated problem based on the current obtained solution would provide an upper bound (2.52), while the lower bound in each iteration is the solution of the master problem, i.e., microgrid annual operation cost plus the term reflecting cost of transformer loss of life.

$$UB = \sum_{h} \sum_{t} [\sum_{i \in G} F_i(\hat{P}_{iht}) + \rho_{ht}^{M} \hat{P}_{ht}^{M}] + \psi\, f(\hat{K}_{ht}^{I}, \hat{K}_{ht}^{U}) \tag{2.52}$$

The final solution of the original problem is achieved when the difference between these two bounds is smaller than a threshold. If the convergence criterion is not satisfied, the optimality cut (2.53), is generated and added to the master problem to revise the solution in the next iteration.

$$\Lambda \geq \hat{Q} + \sum_{h} \sum_{t} \lambda_{ht} (\left|P_{h(t-1)}^{M}\right| - \left|\hat{P}_{h(t-1)}^{M}\right|) + \sum_{h} \sum_{t} \mu_{ht} (\left|P_{ht}^{M}\right| - \left|\hat{P}_{ht}^{M}\right|) \tag{2.53}$$

$\hat{Q}$ is the calculated objective value for the distribution transformer loss of life (optimal solution for the subproblem). Moreover, the optimality cut (2.53) consists of two terms associated with the initial and ultimate microgrid exchanged power with the utility grid. This cut indicates that the solution of the revised microgrid optimal scheduling could lead to a better solution for the transformer asset management subproblem, i.e., the one which causes a smaller cost for the distribution transformer loss of life. The absolute function in (2.53) makes the master problem nonlinear. In order to have a linear model in the master problem, two new nonnegative variables (P^{M1} *and* P^{M2}) are considered in a way that only one of them can be selected via binary variables x and y (2.54),(2.55). As P^{M1}, P^{M2} are both nonnegative variables and only one of them can be nonzero at every hour, in case of power export ($P^{M}>0$) $P^{M}=P^{M1}$ and $P^{M2}=0$, and similarly, in case of power import ($P^{M}<0$) $P^{M}=-P^{M2}$ and $P^{M1}=0$.

$$P_{ht}^{M} = x_{ht}\, P_{ht}^{M1} - y_{ht}\, P_{ht}^{M2} \qquad \forall h, \forall t, \tag{2.54}$$

$$x_{ht} + y_{ht} \leq 1 \qquad \forall h, \forall t. \tag{2.55}$$

Multiplication of binary variables (x and y) with continues variables (P^{M1} *and* P^{M2}) makes bilinear terms ($x_{ht}P^{M1}$ and $y_{ht}P^{M2}$) in (2.54), which are linearized via (2.56)-(2.58), with M as a large positive constant.

$$-M\,x_{ht} - M\,y_{ht} \le P_{ht}^{M} \le M\,x_{ht} + M\,y_{ht} \qquad \forall h, \forall t, \tag{2.56}$$

$$P_{ht}^{M1} - M(1-x_{ht}) \le P_{ht}^{M} \le P_{ht}^{M1} + M(1-x_{ht}) \quad \forall h, \forall t, \tag{2.57}$$

$$-P_{ht}^{M2} - M(1-y_{ht}) \le P_{ht}^{M} \le -P_{ht}^{M2} + M(1-y_{ht}) \quad \forall h, \forall t. \tag{2.58}$$

If binary variables x and y are zero, P^M would be 0 and (2.57),(2.58) would be relaxed. If binary variables x or y are 1, (2.56) would be relaxed and P^M would be equal to either P^{M1} or -P^{M2}, based on (2.57) and (2.58), respectively. In order to have a positive value for P^M in (2.53), this variable is replaced with the summation of P^{M1} and P^{M2} which leads to a revised representation of the optimality cut:

$$\Lambda \ge \hat{Q} + \sum_{h}\sum_{t} \lambda_{ht}[(P_{h(t-1)}^{M1} + P_{h(t-1)}^{M2}) - (\hat{P}_{h(t-1)}^{M1} + \hat{P}_{h(t-1)}^{M2})] + \sum_{h}\sum_{t} \mu_{ht}[(P_{ht}^{M1} + P_{ht}^{M2}) - (\hat{P}_{ht}^{M1} + \hat{P}_{ht}^{M2})] \tag{2.59}$$

The optimality cut (2.53) plays a key role for restricting the lower bound of the microgrid optimal scheduling master problem. Using the proposed Benders decomposition procedure in the iterative manner between the master problem and the subproblem, a decomposed model for the microgrid-based distribution transformer asset management will be achieved. This model reaps the benefits of reshaping microgrid exchanged power with the utility grid to maximize the distribution transformer lifetime.

2.4.2 Numerical Simulations

To investigate the performance of the proposed model, a test microgrid which consists of four dispatchable DGs, two nondispatchable DGs (G5: wind and G6: solar), one

DES, and five adjustable loads is considered and studied. The characteristics of generation units, energy storage system, and adjustable loads are tabulated in Tables 2.3–2.5, respectively. The forecasted values for microgrid hourly fixed load, nondispatchable units' generation, and market price for one sample day are provided in Tables 2.6–2.8, respectively. Note that scheduling horizon of one year is considered in this dissertation . More details on the hourly loads and market price for the considered one-year operation are available in [79]. A 10 MVA distribution transformer is considered at the Point of Common Coupling (PCC) with the characteristics borrowed from [7]. The nominal active power of the distribution transformer is considered to be 10 MW. In order to calculate the transformer loss of life, the hourly forecasted ambient temperature of a specific location in Houston, TX [80] for one year is used. Since this study does not take into account power congestion and power flow calculations, the system topology diagram is not of significance and the results are independent of the topology.

Table 2.3 Characteristics of generation units (D: Dispatchable, ND: Non-Dispatchable)

Unit	Type	Cost coefficient ($/MWh)	Min-Max capacity (MW)	Min up/down time (h)	Ramp up/down rate (MW/h)
G1	D	27.7	1 – 5	3	2.5
G2	D	39.1	1 – 5	3	2.5
G3	D	61.3	0.8 – 3	1	3
G4	D	65.6	0.8 – 3	1	3
G5	ND	0	0 – 1	-	-
G6	ND	0	0 - 1.5	-	-

Table 2.4 Characteristics of the energy storage system

Storage	Capacity (MWh)	Min-Max charging/discharging power (MW)	Min charging/dis-charging time(h)
ESS	10	0.4 - 2	5

Table 2.5 Characteristics of adjustable loads (S: Shiftable, C: Curtailable)

Load	Type	Min-Max capacity (MW)	Required energy (MWh)	Initial start-end time (h)	Min up time(h)
L1	S	0 - 0.4	1.6	11 - 15	1
L2	S	0 - 0.4	1.6	15 - 19	1
L3	S	0.02 - 0.8	2.4	16 - 18	1
L4	S	0.02 - 0.8	2.4	14 - 22	1
L5	C	1.8 - 2	47	1 - 24	24

Table 2.6 Microgrid hourly fixed load (one day as a sample)

Time (h)	1	2	3	4	5	6
Load (MW)	8.73	8.54	8.47	9.03	8.79	8.81
Time (h)	7	8	9	10	11	12
Price ($/MWh)	10.12	10.93	11.19	11.78	12.08	12.13
Time (h)	13	14	15	16	17	18
Price ($/MWh)	13.92	15.27	15.36	15.69	16.13	16.14
Time (h)	19	20	21	22	23	24
Price ($/MWh)	15.56	15.51	14.00	13.03	9.82	9.45

Table 2.7 Generation of non-dispatchable units (one day as a sample)

Time (h)	1	2	3	4	5	6
G5 (MW)	0	0	0	0	0.63	0.80
G6 (MW)	0	0	0	0	0	0
Time (h)	7	8	9	10	11	12
G5 (MW)	0.62	0.71	0.68	0.35	0.62	0.36
G6 (MW)	0	0	0	0	0	0.75
Time (h)	13	14	15	16	17	18
G5 (MW)	0.4	0.37	0	0	0.05	0.04
G6 (MW)	0.81	1.20	1.23	1.28	1.00	0.78
Time (h)	19	20	21	22	23	24
G5 (MW)	0	0	0.57	0.60	0	0
G6 (MW)	0.71	0.92	0	0	0	0

Table 2.8 Hourly electricity price (one day as a sample)

Time (h)	1	2	3	4	5	6
Price ($/MWh)	15.03	10.97	13.51	15.36	18.51	21.8
Time (h)	7	8	9	10	11	12
Price ($/MWh)	17.3	22.83	21.84	27.09	37.06	68.95
Time (h)	13	14	15	16	17	18
Price ($/MWh)	65.79	66.57	65.44	79.79	115.45	110.28
Time (h)	19	20	21	22	23	24
Price ($/MWh)	96.05	90.53	77.38	70.95	59.42	56.68

In order to investigate the effectiveness of the proposed model, the following cases are studied.

Case 0: Transformer loss of life calculation.

Case 1: Microgrid optimal scheduling ignoring transformer asset management constraints.

Case 2: Microgrid optimal scheduling considering transformer asset management constraints.

Case 3: Microgrid optimal scheduling with limited transformer overloading while ignoring asset management constraints.

Case 4: Microgrid optimal scheduling with limited transformer overloading and asset management constraints.

Case 5: Sensitivity analysis with regards to market price forecast errors, transformer loading, and adjustable loads.

Case 0: In this case, it is assumed that the microgrid loads are only supplied by the utility grid, i.e., the local generation is ignored. The transformer loading in this case is similar to the microgrid load profile, as the exchanged power with the utility grid to supply the microgrid load passes through the transformer. The annual transformer loss of life in this case is calculated as 3.1%, which represents an expected lifetime of 32 years.

Case 1: The grid-connected price-based optimal scheduling is analyzed for a one-year horizon. In the price-based scheduling the main goal is to minimize the microgrid operation cost without any commitments in supporting transformer asset management. The microgrid operation cost is calculated as $1,632,296, and the annual transformer loss of

life is calculated as 2.7% in this case. If this value is considered as the average annual loss of life, an expected lifetime of 37 years is perceived for the transformer. The primary reason of this longer lifetime (37 years) compared to the value calculated in Case 0 (32 years) is the microgrid local generation which would partially supply local loads and thus reduce the transformer loading. This situation leads to a smaller loss of life and consequently longer lifetime for the distribution transformer. In other words, even without considering asset management in microgrid scheduling, the transformer lifetime will be prolonged as the microgrid reduces transformer loading through local generation and partial load offset. It should however be noted that possible transformer overloading is ignored in this case.

Case 2**:** In this case, the microgrid controller minimizes the microgrid operation cost while considering the transformer asset management constraints. In other words, in addition to minimizing the operation cost, the microgrid controller attempts to reduce the transformer loading which leads to lowering the transformer loss of life, and consequently translates into longer lifetime. The annual transformer loss of life is reduced from 2.7% in Case 1 to 2.08%, at the expense of 0.11% increase in microgrid operation cost compared to Case 1 to reach a cost of $1,634,239. The transformer lifetime is increased in this case by an average of 11 years. Two points can be considered here: (i) this considerable increase in the transformer lifetime is achieved by the insignificant addition of less than $2,000/year to the microgrid operation cost, and (ii) transformer is not overloaded in any of the operation hours, i.e., the microgrid only reshapes the transformer loading profile without causing any overloads. The considerable impact of overloads will be further discussed in following cases.

Fig. 2.14 compares the exchanged power with utility grid in Cases 1 and 2 in one day, as a sample from the one-year optimal scheduling horizon. As the figure shows, as the mere aim of the microgrid in Case 1 is minimizing its operation cost, the power is purchased from the utility grid when the market price is low, and the extra power is sold back to the utility grid when the market price is high. In other words, the economic incentive is the only major factor in determining the optimal schedule. However, in Case 2, in addition to microgrid optimal scheduling the distribution transformer loss of life is considered, so the exchanged power is reshaped in order to reduce load variations. Explicitly power exchange is changed in hours 13, 15, and 18 as it is more economical to reduce the transformer loading rather than purchasing less expensive power from or selling extra power to the utility grid.

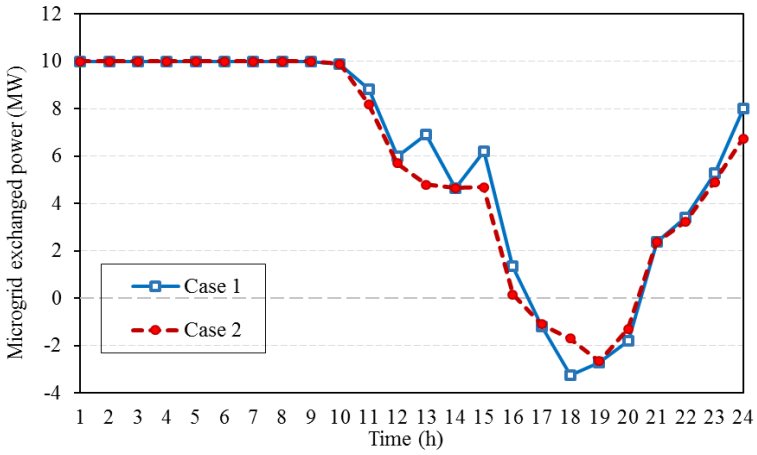

Fig. 2.14 Microgrid exchanged power with the utility grid in Cases 1 and 2 in a sample day of the studied year

Fig. 2.15 depicts the transformer loading in both cases in the same studied day, which better illustrates the effect of the transformer asset management constraints on the microgrid power exchange. The depicted transformer loading is the absolute value of

microgrid exchanged power with the utility grid shown in Fig. 2.14. As this figure shows the transformer loading is reduced in the range between 0.1 MW (at hour 17) and 2.1 MW (at hour 13). This decrease causes a reduction in the transformer loss of life in this specific day from 0.0040% to 0.00367%. This reduced rate is the effect of applying transformer asset management in the microgrid optimal scheduling during only one sample day of the studied year.

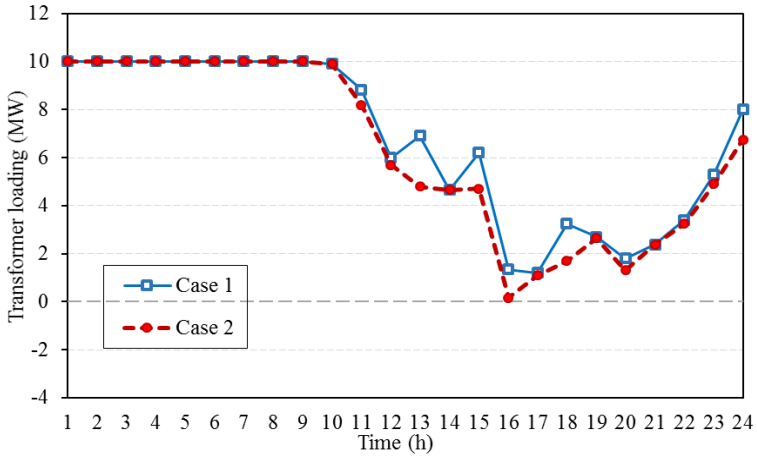

Fig. 2.15 Transformer loading in Cases 1 and 2 in a sample day of the studied year

Case 3: The transformer overloading is considered in this case, without taking the transformer asset management constraints into account. A 20% overloading at 3 hours (13, 14, and 15) of 20 random days in a year is considered, that is in only 60 hours of 8760 hours in a year. Fig. 2.16 shows the transformer loading in this case and compares it with that of Case 1 (without transformer overloading). As Fig. 2.16 shows, a 3-hour overloading in the afternoon not only leads to changes in the transformer loading pattern during the transformer overloaded hours, but also impacts the transformer loading in the remaining hours of the studied day. The transformer loss of life in this case is increased to 3.09% compared to 2.7% in the case without overloads.

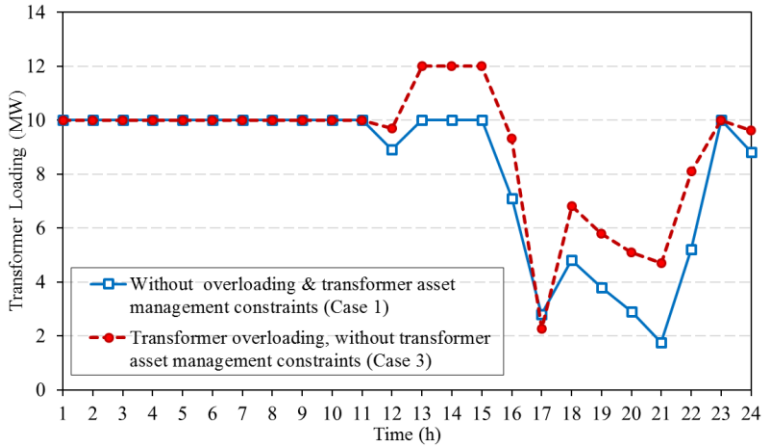

Fig. 2.16 Transformer loading in Case 3 in one of the days with transformer overloading as a sample

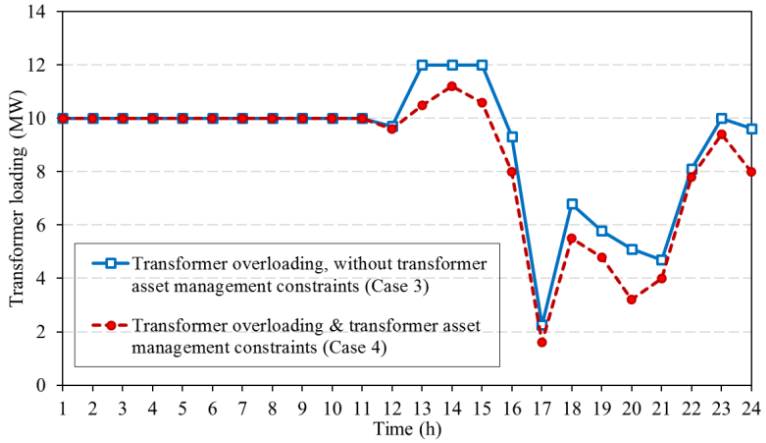

Fig. 2.17 Comparison of transformer loading in Cases 3 and 4, transformer overloading with and without transformer asset management

The results show that the initial transformer loss of life of 0.0065% is increased to 0.0264% in this sample day only due to a 3-h overload. This significant rise of the transformer loss of life (more than 4 times) shows the considerable effect of the transformer overloading on its lifetime reduction. This increase occurs due to the exponential nature of the equations used in calculating the transformer loss of life. The microgrid operation cost in this case is calculated as $1,628,345. It should be noted that the sample day in this case,

shown in Figs. 2.16 and 2.17, is selected from the twenty studied days for transformer overloading, and it is not the same as the selected day in Figs. 2.14 and 2.15.

Case 4: The parameters and conditions of this case are similar to those in Case 3, while the transformer asset management constraints are considered as well. By adding the transformer asset management constraints, as Fig. 2.17 demonstrates, the transformer loading decreases not only during the overloading hours but also at the most hours after the overloading. The changes in microgrid schedule and energy arbitrage lead to 22% decrease in the transformer loss of life (2.41% in this case compared with 3.09% in Case 3). However, this drop in the transformer loss of life and increasing its lifetime leads to a higher microgrid operation cost, calculated as $1,630,842 in this case.

The obtained results of the studied cases are tabulated in Table 2.9 As the results of Cases 0 and 1 demonstrate, utilizing a microgrid significantly decreases the annual transformer loss of life and consequently increases the expected lifetime of the transformer. A comparison between Cases 1 and 2 advocates that taking transformer asset management constraints into account leads to decreasing the annual transformer loss of life even further (48 years in Case 2, compared to 37 years in Case 1), while the annual microgrid operation cost marginally increases. A comparison between Cases 3 and 4 also highlights the impact of the transformer asset management constraints on reducing the transformer loss of life under transformer overloading conditions.

Table 2.9 Microgrid operation cost and transformer loss of life and lifetime for studied cases

	Annual Microgrid Operation Cost ($)	Annual Transformer Loss of Life (%)	Transformer Expected Lifetime (years)
Case 0	-	3.1	32
Case 1	1,632,296	2.7	37
Case 2	1,634,239	2.08	48
Case 3	1,628,345	3.09	32.3
Case 4	1,630,842	2.41	41.5

Case 5: The sensitivity of provided results with regards to market price forecast errors, transformer loading, and adjustable loads are thoroughly investigated in this case.

Case 5.a: Sensitivity analysis with regards to market price forecast errors: a sensitivity analysis is performed to study the impact of forecast errors on annual transformer loss of life, transformer expected lifetime, and annual microgrid operation cost. Forecast errors of ±10%, ±20%, and ±30% are considered for the annual hourly market price. The obtained results for this sensitivity analysis are tabulated in Table 2.10. As the obtained results show, the annual transformer loss of life drops by increasing market price forecast errors, and accordingly the transformer expected lifetime increases. When market price increases, the master controller readjusts the microgrid schedule with the objective of supplying the loads locally rather than importing power from the utility grid. Nevertheless, the microgrid exchanged power with the utility grid, i.e., transformer loading, is decreased which translates into the lower transformer loss of life and a higher transformer expected lifetime, in cases of ignoring and considering transformer asset management constraints. In addition, the results demonstrate that the annual transformer loss of life as well as the transformer expected lifetime are significantly improved by taking

the transformer asset management constraints into account. For instance, in case of “30% decrease” and “30% increase”, the transformer expected lifetime grows 6 years and 12.5 years, respectively.

It should be noted that the annual microgrid operation cost slightly raises by considering transformer asset management constraints, in expense of lowering the transformer loss of life and increasing the transformer expected lifetime.

Case 5.b: Sensitivity analysis with regards to transformer loading: the effect of transformer loading on the annual transformer loss of life as well as the transformer expected lifetime are investigated in this case. To this end, 50%, 75% 100%, and 125% of the transformer nominal power (*Pn*) are considered as the maximum limitation for the transformer loading. The obtained results for this study are listed in Table 2.11. The sensitivity results clearly depict the exponential growth of transformer loss of life by increasing the transformer loading. By keeping the transformer loading within the limit of 50%, the annual transformer loss of life is calculated respectively as 0.455% and 0.452% in cases of ignoring and considering transformer asset management constraints. On the other hand, overloading the distribution transformer will dramatically reduce its lifetime. The transformer loss of life under 125% transformer loading, i.e. 25% overload, is respectively calculated as 11.83% and 8.61% in cases of ignoring and considering transformer asset management constraints, where accordingly the transformer expected lifetime will be 8.5 and 11.6 years, respectively. Moreover, the results demonstrate that the transformer expected lifetime will be increased slightly while taking the transformer asset management constraints into account for lower transformer loading limits. It should be

noted that the cases with very low/ high limits of the transformer loading, i.e 50% or 125%, are not practical and just are considered in this study as extreme operating conditions.

Case 5.c: Sensitivity analysis with regards to adjustable loads: to demonstrate the effect of adjustable loads on the annual transformer loss of life, transformer expected lifetime, and annual microgrid operation cost, the problem is solved for various cases of adjustable loads. The required energy of the five aggregated adjustable loads is changed from 10 MWh to 50 MWh (which however can be considered as having more adjustable loads in the microgrid). The obtained results for this study are provided in Table 2.12. As the sensitivity analysis results show, by increasing the adjustable loads, the annual transformer loss of life slightly lessens, which means the transformer expected lifetime increases. By changing the total required energy of adjustable loads from 10 MWh to 50 MWh, the transformer expected lifetime increases by 1.2 years from 48.05 to 49.25 years, when taking the transformer asset management constraints into account. In addition, as the total required energy of adjustable loads increase, the annual microgrid operation cost reduces in both cases of ignoring and considering transformer asset management constraints. Nevertheless, adjustable loads play a key role in reshaping the loading of the distribution transformer at the point of interconnection in order to increase its lifetime. The cost associated with the power loss is extremely smaller than the transformer loss of life and microgrid operation costs so that its impacts will be negligible. Nevertheless, in order to ensure this assumption, a case study is performed in which 6% distribution power loss is considered in the distribution deployed microgrid. The obtained results demonstrate that cost associated with the power loss is a very small fraction of the transformer loss of life

and microgrid operation costs. Thus, if the power loss cost of the microgrid is taken into consideration, the results will be affected to a minimal extent; however, the final assessment and conclusion remain intact.

Table 2.10 Sensitivity analysis with regards to market price forecast error

Market Price	Annual Transformer Loss of Life (%)		Transformer Expected Lifetime (years)		Annual Microgrid Operation Cost ($)	
	Ignoring transformer asset management constraints	Considering transformer asset management constraints	Ignoring transformer asset management constraints	Considering transformer asset management constraints	Ignoring transformer asset management constraints	Considering transformer asset management constraints
30% decrease	3.41	2.83	29.3	35.3	1,242,627	1,245,215
20% decrease	3.077	2.41	32.5	41.5	1,396,111	1,399,733
10% decrease	2.84	2.23	35.2	44.8	1,525,675	1,528,842
Default	2.7	2.08	37.0	48.1	1,632,296	1,634,239
10% increase	2.57	2.011	38.9	49.7	1,715,356	1,717,944
20% increase	2.51	1.935	39.8	51.7	1,776,963	1,779,887
30% increase	2.456	1.88	40.7	53.2	1,821,077	1,823,412

Table 2.11 Sensitivity analysis with regards to transformer loading

Transformer loading	Annual Transformer Loss of Life (%)		Transformer Expected Lifetime (years)	
	Ignoring transformer asset management constraints	Considering transformer asset management constraints	Ignoring transformer asset management constraints	Considering transformer asset management constraints
50%	0.455	0.452	219.8	221.2
75%	1.67	1.38	59.9	72.5
100%	2.7	2.08	37	48.1
125%	11.83	8.61	8.5	11.6

Table 2.12 Sensitivity analysis with regards to adjustable load

Adjustable load	Annual Transformer Loss of Life (%)		Transformer Expected Lifetime (years)		Annual Microgrid Operation Cost ($)	
	Ignoring transformer asset management constraints	Considering transformer asset management constraints	Ignoring transformer asset management constraints	Considering transformer asset management constraints	Ignoring transformer asset management constraints	Considering transformer asset management constraints
Default	2.704	2.081	36.98	48.05	1,632,296	1,634,239

10 MWh increase	2.698	2.071	37.07	48.30	1,590,523	1,590,890
20 MWh increase	2.684	2.060	37.25	48.55	1,553,959	1,557,723
30 MWh increase	2.672	2.050	37.43	48.78	1,520,413	1,524,829
40 MWh increase	2.663	2.041	37.56	49.00	1,496,362	1,499,589
50 MWh increase	2.650	2.030	37.73	49.25	1,476,587	1,478,510

2.4.3 Discussions

A microgrid-based distribution transformer asset management model was proposed and formulated in this section. Using a Benders decomposition method, the proposed model was decomposed into a microgrid optimal scheduling master problem and a distribution transformer asset management subproblem. Based on a relevant IEEE Standard, the optimal cost of the distribution transformer loss of life was calculated in the subproblem in order to examine the optimality of the microgrid scheduling solution. This means that the distribution transformer asset management subproblem was presented to manipulate the distribution transformer loading via scheduling microgrid resources in an efficient and asset management-aware manner. Numerical simulations were carried out for various conditions of transformer loading to show the advantages and the effectiveness of the proposed model. The results showed that the utility companies can efficiently manage their resources to decrease transformer loss of life and consequently ensure a considerable increase in transformer lifetime.

2.4.4 Appendix

Branch-and-bound is a commonly-used technique for solving mixed integer linear programming problems. Two processes are employed in this technique (i) bounding

process, and (ii) branching process. In the bounding process, the solution of a relaxed mixed integer linear programming problem, i.e., converting mixed integer linear programming problem into liner programming problem via removing integrity restrictions, is calculated and then imposed as lower bound for minimization problems or upper bound for maximization problems. In the branching process, the problem is broken into two subproblems, where further are solved to obtain the solutions. If the solutions for both of these subproblems satisfy the integrity conditions, they are compared with each other, and the subproblem solution related to smaller objective function value for minimization problem or larger one for maximization problem will be selected as the optimal solution. Note that if only one of these two subproblems solution satisfies the mixed integer linear programming integrity condition, this solution is kept as an incumbent solution (i.e., the optimal solution if no better solution will be achieved further). Nevertheless, the branching process is continued to search on the other subproblem with the objective of finding a better solution that satisfied the mixed integer linear programming integrity condition [81].

Mixed integer linear programming solvers, including but not limited to CPLEX, Xpress-MP, SYMPHONEY, and CBC, reap the benefits of a combination of branch-and-bound techniques and cutting-plane techniques to accelerate the computation time associated with solving mixed integer linear programming problems, which consequently facilitate solving large mixed integer linear programming problems using personal computers.

The branch-and-bound technique for solving mixed integer nonlinear programming problems is based on the same idea as the branch-and-bound technique employed to solve

mixed integer linear programming problems. Similar to the branch-and-bound technique explained above, the technique starts by solving the problem in where the discrete conditions of the binary variables are relaxed. If the obtained solution is integral, then this solution is considered as an optimal solution for the problem. Without loss of generality, the two processes of bounding and branching are employed in order to find the optimal solution for the mixed integer nonlinear programming problem [82].

3 Chapter Three: Spinning Reserve-based Optimal Scheduling of Integrated Microgrids

3.1 Introduction

Fig. 3.1 illustrates a holonic system structure. Clustering holons in the holonic distribution grid creates distinct levels of holons, called super-holons, for enhancing individual- and aggregated- system objectives. The generated super-holons can be reconfigured or reorganized to form different super-holons based on certain optimization criteria [22]. The holonic architecture is limitedly discussed and investigated in the literature. The study in [83] proposes a generic architecture system based on the holarchy concept for smart grids, where the proposed architecture comprises multiple autonomous prosumers that are recursively interconnected at various combination layers with a bottom-up organization. A holonic multi-agent system architecture is presented in [84] for adaptive control of the distribution grids. The proposed architecture can optimize the system performance and maintain the system operation within predefined limits. The study in [24] presents an optimal scheduling model of integrated microgrids, where the proposed model identifies the optimal network topology that minimizes holon-specific and system-wide operation cost. Leveraging an illustrative example, authors in [85] overview the influence of microgrids spinning reserve in enabling the power exchange among the integrated microgrids in the holonic distribution grids.

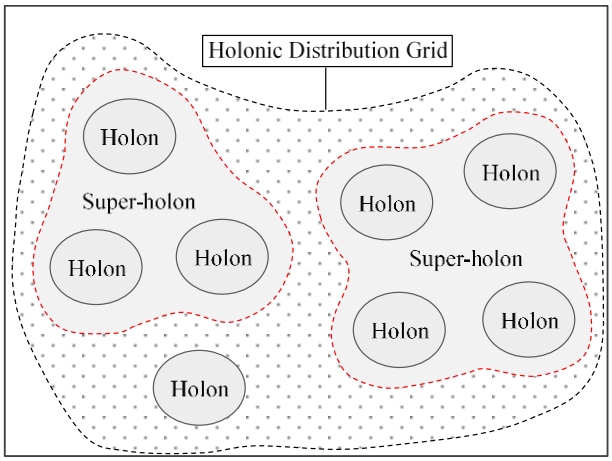

Fig. 3.1 Holonic system structure

This chapter proposes a spinning reserve based optimal scheduling model of integrated microgrids in the holonic distribution grids. This model solves the common convergence issues with the existing models in the literature by moving away from a power exchange focused modeling, and instead adopting a spinning reserve-based approach. The developed model aims at identifying the optimal super-holons combinations based on minimum net spinning reserve. Identifying optimal super-holons clusters could improve participated players (holons) economic benefits and significantly enhance the entire system reliability. Nevertheless, determining the optimal configuration of integrated microgrids and forming super-holons through a spinning reserve is proposed in this chapter.

3.2 Model Outline

Consider a holonic distribution grid in which microgrids play the role of holons. As depicted in Fig. 3.2, in the normal operation mode of the holonic distribution grid, microgrids (holons) are connected to the utility grid and operated in the grid-connected mode. In this mode, each microgrid aims at determining the least-cost commitment and dispatch of available dispatchable units, charging/discharging schedules of energy storage

systems, schedule of adjustable loads, and the exchanged power with the utility grid. Owing to economic discretion, each microgrid in the grid-connected mode prefers to exchange power with the utility grid rather than with adjacent microgrids. When it comes to the islanded operation mode, however, the microgrids in the holonic distribution grid are disconnected from the utility grid and accordingly each microgrid relies on its local resources as well as the spinning reserve provided by the adjacent microgrid to meet their load demands. In case of lacking adequate local capacity in a microgrid, i.e., power deficiency, microgrids can make connections based on the spinning reserve to form super-holons, and accordingly increase the microgrid capacity, as well as overall system reliability. Nevertheless, as the spinning reserve provision is costly, the configuration of connecting microgrids and forming super-holons are optimally determined via a spinning reserve based integrated microgrids scheduling model.

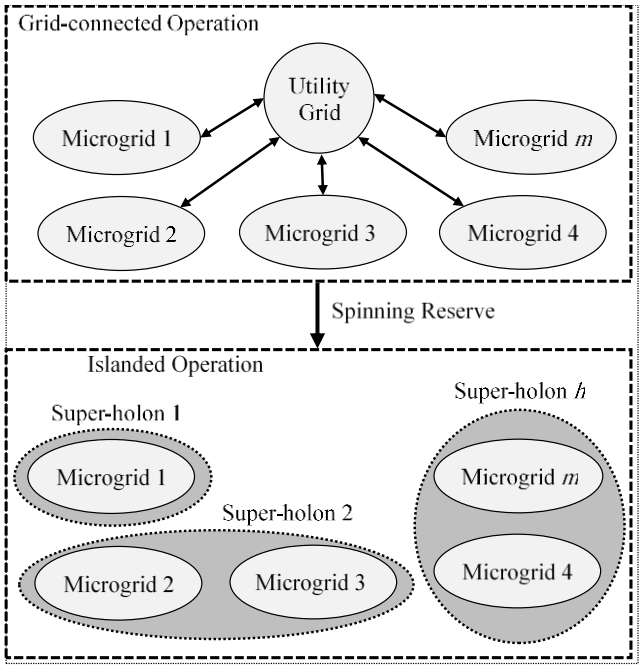

Fig. 3.2 Proposed spinning reserve-based model for integrated microgrids in a holonic distribution grid.

The proposed spinning reserved based optimal scheduling model for integrated microgrids in the holonic distribution grids is casted to minimize not only the operation cost associated with all microgrids in the grid-connected operation, but also the costs of power deficiency and spinning reserve in the islanded operation mode. Since the value of lost load (VOLL) is significantly higher than the value of net spinning reserve, it is more economical to reap the benefits of the system-aggregated spinning reserve and make the system reliable through reducing the amount of power deficiency. Thus, determining an optimal configuration of the system in the islanded operation, i.e., optimal super-holons combination, plays a key role in minimizing the system-aggregated operation cost and improving the overall system reliability.

The spinning reserve for each microgrid is characterized based on the dispatchable DGs and energy storage systems available in that microgrid. Given that each microgrid could undergo power deficiency during the islanded operation, net spinning reserve is determined for the microgrid. Each super-holon is formed in a way that the net spinning reserve of that specific super-holon is minimized. In other words, among all possible microgrids combinations to form super-holons, those combinations that provide the least net spinning reserve during the islanded operation are the desired ones that are determined through the proposed model.

3.3 Problem Formulation

The objective of the problem is to minimize the system-aggregated operation cost in the grid-connected mode, and the costs of power deficiency and spinning reserve in the

islanded mode, as formulated in (3.1):

$$\min \sum_{m\in \mathrm{M}} \sum_{t} \left(\sum_{i\in \mathrm{G}} F_{mi}\left(P_{mit\,0}\right) + \rho_{mt} P^{M}_{mt\,0} \right) + \sum_{m\in \mathrm{M}} \sum_{t} \sum_{s\in \mathrm{K}} \upsilon_{mt} PD_{mts} + \sum_{h\in \mathrm{H}} \sum_{t} \sum_{s\in \mathrm{K}} \pi_{ht} \left| SR^{Net}_{hts} \right| \qquad (3.1)$$

This objective function consists of four distinct terms, which include the generation cost of all dispatchable DGs related to each individual microgrid, the cost of exchanged power between each microgrid and the utility grid, the cost of power deficiency (which will be translated to load curtailment if additional generation is not available) as well as the cost of spinning reserve in the islanded operation. The generation cost is often formulated via a quadratic function; however, it is linearized through a piecewise linearization approach. The second term is the cost of exchanged power with the utility grid, calculated based on the market price at the point of interconnection (POI) for each individual microgrid. This term could be either positive (denoting a cost) or negative (denoting a revenue), according to power follow direction associated with each microgrid. The third term represents the cost of power deficiency for each microgrid during the islanded operation. This term is calculated as the value of lost load (VOLL) multiplied by the deficient power in each microgrid. The last term indicates the cost of net spinning reserve of each super-holon, calculated based on the multiplication of the value of net spinning reserve and the absolute value for the net spinning reserve of that super-holon. The absolute value causes nonlinearity, which is further linearized. The absolute value is assigned to an auxiliary variable ϕ_{hts}, i.e., $\phi_{hts} = \left| SR^{Net}_{hts} \right|$. Next, the objective is to minimize ϕ_{hts}, subject to an additional constraint, i.e., $-\phi_{hts} \le SR^{Net}_{hts} \le \phi_{hts}$.

In the proposed problem, two operation modes, i.e., grid-connected and islanded, are investigated. These two modes are separated from each other in the objective function and further in the constraints using scenario index *s*, where *s*=0 is used for the grid-connected mode and $s \geq 1$ for the islanded mode. This objective is subject to prevailing operational and spinning reserve constraints, listed as follows:

$$\sum_{i \in \mathrm{R}} P_{mit} + P_{mt}^{M} = D_{mt} \qquad \forall m, \forall t \tag{3.2}$$

$$-P_{m}^{M,\max} U_{ts} \leq P^{M}{}_{mts} \leq P_{m}^{M,\max} U_{ts} \qquad \forall m, \forall t, \forall s \tag{3.3}$$

$$P_{mi}^{\min} I_{mit} \leq P_{mits} \leq P_{mi}^{\max} I_{mit} \qquad \forall m, \forall i \in \mathrm{G}, \forall t, \forall s \tag{3.4}$$

$$P_{mits} - P_{mi(t-1)s} \leq UR_{mi} \qquad \forall m, \forall i \in \mathrm{G}, \forall t, \forall s \tag{3.5}$$

$$P_{mi(t-1)s} - P_{mits} \leq DR_{mi} \qquad \forall m, \forall i \in \mathrm{G}, \forall t \ \forall s \tag{3.6}$$

$$T_{mi}^{\mathrm{on}} \geq UT_{mi} (I_{mit0} - I_{mi(t-1)}) \qquad \forall m, \forall i \in \mathrm{G}, \forall t \tag{3.7}$$

$$T_{mi}^{\mathrm{off}} \geq DT_{mi} (I_{mi(t-1)} - I_{mit}) \qquad \forall m, \forall i \in \mathrm{G}, \forall t \tag{3.8}$$

$$P_{mits} \leq P_{mit}^{dch,\max} u_{mit} - P_{mit}^{\mathrm{ch},\min} v_{mit} \qquad \forall m, \forall i \in \mathrm{S}, \forall t, \forall s \tag{3.9}$$

$$P_{mits} \geq P_{mit}^{dch,\min} u_{mit} - P_{mit}^{\mathrm{ch},\max n} v_{mit} \qquad \forall m, \forall i \in \mathrm{S}, \forall t, \forall s \tag{3.10}$$

$$u_{mit} + v_{mit} \leq 1 \qquad \forall m, \forall i \in \mathrm{S}, \forall t \tag{3.11}$$

$$C_{mits} = C_{mi(t-1)s} - \frac{P_{mits} u_{mits} \tau}{\eta_{i}^{dch}} - \eta_{i}^{ch} P_{mits} v_{mits} \tau \qquad \forall m, \forall i \in \mathrm{S}, \forall t, \forall s \tag{3.12}$$

$$C_{mi}^{\min} \leq C_{mits} \leq C_{mi}^{\max} \qquad \forall m, \forall i \in \mathrm{S}, \forall t, \forall s \tag{3.13}$$

$$T_{mi}^{\mathrm{ch}} \geq MC_{mi} (u_{mit} - u_{mi(t-1)}) \qquad \forall m, \forall i \in \mathrm{S}, \forall t \tag{3.14}$$

$$T_{mi}^{\mathrm{dch}} \geq MD_{mi} (v_{mit} - v_{mi(t-1)}) \qquad \forall m, \forall i \in \mathrm{S}, \forall t \tag{3.15}$$

$$D_{mdt}^{\min} z_{mdt} \le D_{mdts} \le D_{mdt}^{\max} z_{mdt} \qquad \forall m, \forall d \in \mathrm{D_A}, \forall t, \forall s \tag{3.16}$$

$$T_{md}^{\text{on}} \ge MU_{md} (z_{mdt} - z_{md(t-1)}) \qquad \forall m, \forall d \in \mathrm{D_A}, \forall t \tag{3.17}$$

$$\sum_{[\alpha_d, \beta_d]} D_{mdts} = E_{md} \qquad \forall m, \forall d \in \mathrm{D_A}, \forall s \tag{3.18}$$

$$PD_{mts} = D_{mts} - \sum_{i \in R} P_{mits} \qquad \forall m, \forall t, \forall s \tag{3.19}$$

$$sr_{mits}^{DG} \le P_{mi}^{\max} - P_{mits} \qquad \forall m, \forall i \in \mathrm{G}, \forall t, \forall s \tag{3.20}$$

$$0 \le sr_{mits}^{DG} \le 10 MSR_{mi} I_{mit} \qquad \forall m, \forall i \in \mathrm{G}, \forall t, \forall s \tag{3.21}$$

$$0 \le sr_{mits}^{ES} \le P_{mit}^{\text{dch,max}} u_{mit} \qquad \forall m, \forall i \in \mathrm{S}, \forall t, \forall s \tag{3.22}$$

$$sr_{mits}^{ES} \le P_{mit}^{dch,\max} - P_{mits} \qquad \forall m, \forall i \in \mathrm{S}, \forall t, \forall s \tag{3.23}$$

$$sr_{mts}^{net} = \sum_{i \in \mathrm{G}} sr_{mits}^{DG} + \sum_{i \in \mathrm{S}} sr_{mits}^{ES} - PD_{mts} \qquad \forall m, \forall t, \forall s \tag{3.24}$$

$$SR_{hts}^{Net} = \sum_{m \in \mathrm{M}} (w_{mhts} sr_{mts}^{net}) \qquad \forall h \in \mathrm{H}, \forall t, \forall s \tag{3.25}$$

$$\sum_{h \in H} w_{mhts} = 1 \qquad \forall m, \forall t, \forall s \tag{3.26}$$

$$\sum_{m \in M} \sum_{h \in H} w_{mhts} = N_m \qquad \forall t, \forall s \tag{3.27}$$

The load balance equation (3.2) ensures that the sum of power generated by all DERs (i.e., dispatchable and non-dispatchable units and energy storage systems) and the exchanged power with the utility grid would match the hourly load for each microgrid. This constraint is only considered for the grid-connected mode, and as each microgrid has adequate generation during this mode (either locally generated by DERs or imported from the utility grid), the power deficiency variable is not added to the equation. The generation of non-dispatchable units is forecasted on a day-ahead basis for each microgrid, then

accordingly utilized in (3.2). The power associated with energy storage systems is either positive (discharging), negative (charging), or zero (idle). The power exchange between each microgrid and the utility grid can be positive (purchasing power), negative (selling back), or zero. This power exchange is limited by the thermal limit of the line connecting each microgrid to the utility grid (3.3). The binary islanding indicator U_{ts} ensures that the exchanged power with the utility grid is forced to be zero during the islanded operation. The dispatchable unit generation in each microgrid is restricted by the minimum and maximum generation capacity limits (3.4). The binary variable I_{mit} indicates the unit commitment state of that unit, which is one once committed and zero otherwise. Constraints (3.5) and (3.6) are respectively defined for ramp up and ramp down limits associated with dispatchable units in each microgrid. The minimum up and down time limits are formulated in (3.7) and (3.8), respectively.

The energy storage system constraints mainly include limitations associated with its power and energy, charging/discharging mode, and minimum charging/discharging time. Constraints (3.9) and (3.10) characterize the energy storage system power for each microgrid based on the maximum and minimum charging and discharging power limits and operation mode. The energy storage system can be charging, discharging, or idle at each hour (3.11). The stored energy at each hour is determined according to the stored energy at previous hour, the amount of charged/discharged power, and charging/discharging efficiency (3.12), which is also further restricted with minimum and maximum capacity limits (3.13). Constraints (3.14) and (3.15) respectively outline minimum charging and discharging time limits, denoting the minimum number of

successive hours that energy storage system must maintain charging or discharging once the operational mode is toggled. Adjustable loads associated with each individual microgrid are bounded between minimum and maximum rated power limits (3.16). The minimum operating time (3.17), as well as the required energy to wrap up the operating cycle (3.18) are also regarded for adjustable loads.

Spinning reserve is one of the key resources utilized for ensuring integrated microgrids reliability in responding to unforeseen events such as islanding. In case of islanding, each microgrid is disconnected from the utility grid, in which adequate generation capacity may not be available to fully supply local loads. The amount of deficient power for each microgrid during the islanded operation is calculated based on the difference between the microgrid load and the power generated by all DERs (3.19). The spinning reserve of a dispatchable DG cannot exceed the difference between its maximum generation capacity and current generation (3.20). This spinning reserve is also limited by the 10-minute maximum sustained rate (3.21). Similar to dispatchable DGs, energy storage systems can provide spinning reserve to protect integrated microgrids in case of islanding. An energy storage system can contribute to spinning reserve only during discharging mode, which is restricted by its maximum discharging power limit (3.22). The spinning reserve of an energy storage system cannot be greater than the difference between its maximum discharging power and existing discharged power (3.23). Net spinning reserve of a microgrid is calculated based on the aggregated spinning reserve associated with dispatchable DGs and energy storage systems, and the power deficiency (3.24).

In the proposed holonic distribution grids, it is assumed that holons are connected

based on the available net spinning reserves (i.e., sr^{net}) to form super-holon. Binary variable w_{mhts} is defined to decide whether microgrid m belongs to super-holon h or not. If w_{mhts} is one, it means that microgrid m belongs to super-holon h. The number of super-holons is set to be equal to the number of microgrids, i.e., $N_{\mathrm{m}}=N_h$. This means if a holonic distribution grid is comprised of N_{m} microgrids, N_h (which equals to N_{m}) super-holons are formed out of those microgrids; however, there could be certain super-holons formed by no microgrids (empty member). Net spinning reserve of a super-holon (i.e., SR^{net}) is determined according to the net spinning reserve of those microgrids belonging to that super-holon (3.25). Constraint (3.26) ensures that each microgrid belongs to only one super-holon. In order to assure that all microgrids are assigned to create super-holons, (3.27) is defined. Multiplication of variables w_{mhts} and sr^{net} makes (3.25) nonlinear, which is further linearized in (3.28)-(3.30). κ and B are auxiliary variable and large positive number, respectively.

$$-B\,(1-w_{mhts}) \le \kappa_{mhts} - sr_{mts}^{net} \le B\,(1-w_{mhts}) \qquad \forall m, \forall h, \forall t, \forall s \tag{3.28}$$

$$-B\,w_{mhts} \le \kappa_{mhts} \le B\,w_{mhts} \qquad \forall m, \forall h, \forall t, \forall s \tag{3.29}$$

$$SR_{hts}^{Net} = \sum_{m \in \mathrm{M}} \kappa_{mhts} \qquad \forall h \in \mathrm{H}, \forall t, \forall s \tag{3.30}$$

3.4 Numerical Simulation

An integrated microgrid test system comprised of five microgrids is employed to investigate the performance and effectiveness of the proposed spinning reserve based optimal scheduling of integrated microgrids in the holonic distribution grids. Microgrids characteristics are tabulated in Tables 3.1-3.5, which show the aggregated generation of

non-dispatchable units, hourly fixed load, adjustable load characteristics, and the dispatchable DGs and DES units characteristics. The power exchange between the utility grid and each microgrid is limited by the connecting line ampacity limit, which is set to 15 MW for all five microgrids. The proposed problem is solved for a 24-hour scheduling horizon considering one-hour time period, i.e, τ=1. A total of 25 operation scenarios are regarded in this study (scenario 0 for the grid-connected and scenarios 1-24 for the islanded operation). Note that each islanding scenario denotes the islanded operation in a specific one-hour time interval during the 24-hour scheduling horizon. The following cases are studied:

Case 0: Individual microgrid optimal scheduling.

Case 1: Spinning reserve based optimal scheduling of integrated microgrids.

Table 3.1 Aggregated generation of non-dispatchable units (MW)

Time (h)	**1**	**2**	**3**	**4**	**5**	**6**	**7**	**8**
MG 1	0	0	0	0	0.63	0.8	0.62	0.71
MG 2	0	0	0	0	0	0	0	0.02
MG 3	0.09	0.08	0.11	0.08	0.4	0.42	0.51	0.59
MG 4	0.04	0.05	0.08	0.09	0.01	0	0	0.01
MG 5	0	0	0	0	0	0	0.01	0.02
Time (h)	**9**	**10**	**11**	**12**	**13**	**14**	**15**	**16**
MG 1	0.68	0.35	0.62	1.11	1.21	1.57	1.23	1.28
MG 2	0.08	0.26	0.48	0.74	0.92	0.99	0.97	0.91
MG 3	0.69	0.87	0.91	0.93	0.90	0.94	0.92	0.95
MG 4	0.06	0.13	0.24	0.36	0.43	0.46	0.49	0.41
MG 5	0.09	0.29	0.51	0.57	0.65	0.61	0.53	0.44
Time (h)	**17**	**18**	**19**	**20**	**21**	**22**	**23**	**24**
MG 1	1.05	0.82	0.71	0.92	0.57	0.6	0	0
MG 2	0.83	0.72	0.45	0.12	0	0	0	0
MG 3	0.79	0.69	0.31	0.14	0.1	0.02	0.12	0.09
MG 4	0.32	0.19	0	0	0	0	0	0
MG 5	0.3	0.11	0.09	0.01	0	0	0	0

Table 3.2 Hourly fixed load (MW)

Time (h)	**1**	**2**	**3**	**4**	**5**	**6**	**7**	**8**
MG 1	8.73	8.54	8.47	9.03	8.79	8.81	10.12	10.93

MG 2	6.20	6.19	6.07	5.91	4.43	4.79	5.09	4.75
MG 3	17.81	18.29	18.58	18.95	19.21	19.89	19.99	19.82
MG 4	5.29	6.16	6.34	5.79	5.99	6.11	5.84	4.99
MG 5	4.17	4.51	4.82	5.29	5.19	5.74	5.86	5.85
Time (h)	**9**	**10**	**11**	**12**	**13**	**14**	**15**	**16**
MG 1	11.19	11.78	12.08	12.13	13.92	15.27	15.36	15.69
MG 2	4.93	5.69	4.91	5.79	6.92	7.81	8.09	8.08
MG 3	19.56	19.11	18.16	18.27	17.63	16.31	16.12	15.09
MG 4	4.92	4.89	4.81	4.98	4.71	4.65	4.82	4.73
MG 5	6.47	6.72	6.74	6.81	7.49	7.24	8.11	8.64
Time (h)	**17**	**18**	**19**	**20**	**21**	**22**	**23**	**24**
MG 1	16.13	16.14	15.56	15.51	14.0	13.03	9.82	9.45
MG 2	7.07	6.41	5.46	5.27	6.01	6.43	7.15	7.12
MG 3	15.14	15.31	15.46	15.75	16.87	17.34	17.93	18.21
MG 4	4.85	4.91	4.93	5.01	5.71	5.62	5.91	5.64
MG 5	9.06	9.01	9.31	8.41	8.06	7.51	7.33	6.36

Table 3.3 Adjustable load (S: Shiftable, C: Curtailable)

	Load	Type	Min.-Max. Capacity (MW)	Required Energy (MWh)	Required Start-End Time (h)	Min Up Time (h)
MG 1	L1	S	0 – 0.4	1.6	11 – 15	1
	L2	S	0 – 0.4	1.6	15 – 19	1
	L3	S	0.02 – 0.8	2.4	16 – 18	1
	L4	S	0.02 – 0.8	2.4	14 – 22	1
	L5	C	1.8 – 2	47	1 – 24	24
MG 2	L1	S	0 – 0.4	1.6	12 – 16	1
	L2	S	0.02 – 0.8	2.4	15 – 23	1
	L3	C	1.8 – 2	47	1 – 24	24
MG 4	L1	S	0 – 0.4	1.6	1 – 5	1
	L2	S	0.02 – 0.8	2.4	6 – 14	1

Table 3.4 Dispatchable units

	Unit	Cost Coefficient ($/MWh)	Min.-Max. Capacity (MW)	Min. Up/Down Time (h)	Ramp Up/ Down Rate (MW/h)
MG 1	G1	27.7	1 – 5	3	2.5
	G2	39.1	1 – 5	3	2.5
	G3	61.3	0.8 – 3	1	3
	G4	65.6	0.8 – 3	1	3
MG 2	G1	30.9	1 – 2	4	1
	G2	45.7	0.5 – 2	4	2
	G3	73.5	0.5 – 1	2	1
	G4	78.4	1 – 3	3	1.5
MG 3	G1	25.6	1.5 – 3	6	1
	G2	28.3	1.5 – 4	6	2.5

	G3	63.9	0.5 – 3	4	2
	G4	67.1	0.5 – 3	4	2.5
	G5	89.2	1 – 6	3	3
MG 4	G1	23.3	0.5 – 1	2	1
	G2	51.6	0.5 – 3	4	2
	G3	69.2	1 – 3	5	1.5
MG 5	G1	23.6	0.5 – 1	4	1
	G2	35.4	1 – 2	3	2
	G3	45.7	0.5 – 2	4	2
	G4	63.1	1 – 3	3	1.5

Table 3.5 Distributed energy storages

	Storage	Capacity (MWh)	Min.-Max. Charging/Discharging Power (MW)	Min. Charging/Discharging Time (h)
MG 1	DES	10	0.4 – 2	5
MG 2	DES	5	0.2 – 1	4
MG 3	DES	6	1 – 2	3
MG 4	DES	8	0.5 – 2	4
MG 5	DES	4	0.5 – 1	4

Case 0: Each of the five microgrids in this case is individually scheduled for both the grid-connected and islanded operation modes. In the grid-connected scenario, each microgrid determines the optimal schedule of its local resources as well as the exchanged power with the utility grid. In the islanded scenarios, each microgrid only relies on its local resources which means no spinning reserve is scheduled by the adjacent microgrids to support the whole system. The results show that total load shedding of all five microgrids is calculated as 10.08MWh, in this case.

Case 1: In this case, the microgrids are not only responsible for minimizing their own operation cost, but also they provide spinning reserve to the adjacent microgrids which have power deficiency. The five microgrids aim at supplying their own local loads, while providing spinning reserve to offer to the adjacent microgrids with the objective of

minimizing the system-aggregated operation cost. Each super-holon is formed in a way that the net spinning reserve of that specific super-holon is minimized. In other words, among all possible microgrids combinations to form super-holons, those combinations that provide the least net spinning reserve during the islanded operation are the desired ones.

Table 3.6 illustrates how the super-holons are formed in a 24-hour horizon with the objective of minimizing the system-aggregated operation cost in the grid-connected mode, and the costs of power deficiency and spinning reserve in the islanded mode. The numbers utilized in Table 3.6 represent each microgrid belongs to which super-holon in each hour. For instance, at t=1, two super-holons are formed; microgrids 1, 3 and 5 are in one super-holon and microgrids 2 and 4 are formed another super-holon. In hours such as hour 4, the microgrids do not have spinning reserve to offer to adjacent microgrids so that each microgrid is considered as one super-holon.

Table 3.6 Super-holon formation in a 24-hour scheduling horizon

	Hours (1-24)																							
MG1	1	1	1	1	1	1	1	1	1	1	1	1	1	1	1	1	1	1	1	1	1	1	1	1
MG2	2	2	2	2	2	2	1	2	2	2	2	2	2	2	2	1	2	2	2	2	2	2	1	2
MG3	1	3	3	3	2	2	1	3	3	3	2	3	3	1	3	1	1	3	3	3	1	3	2	3
MG4	2	1	2	4	3	2	1	3	3	3	3	1	4	3	4	2	1	3	3	2	1	3	3	3
MG5	1	2	3	5	4	3	5	1	4	3	4	2	5	1	2	1	2	2	3	2	1	1	4	1

Spinning reserve and power deficiency of microgrids at hours 17-20 are tabulated in Table 3.7, as a sample. At t=17, two super-holons are formed in a way that the net spinning reserve of whole system would be zero. In this hour, microgrids 1 and 4 have respectively 0.32MW and 0.30MW of spinning reserve, which together cover 0.62MW

power deficiency of microgrid 3. In addition, 1.48MW power deficiency of microgrid 5 is supplied by 1.48MW spinning reserve of microgrid 2. At t=18, microgrids 3 and 4 form a super-holon, however, the spinning reserve of microgrid 4 is not adequate to supply the power deficiency of microgrid 3, and this super-holon experiences 0.3MW load curtailment. The other formed super-holon in this hour does not experience any load curtailment as spinning reserve of microgrid 2 supports power deficiency of microgrid 5.

Table 3.7 Spinning reserve and power deficiency of microgrids in four hours (MW)

Time (h)	**17**	**18**	**19**	**20**
MG 1	0.32	0	0	0
MG 2	1.48	1.60	0	1.50
MG 3	-0.62	-0.74	0.42	0
MG 4	0.30	0.44	0.93	0.13
MG 5	-1.48	-1.60	-1.35	-1.63

Fig. 3.3 demonstrates the load curtailment of integrated microgrids, before and after the formation of super-holons. As this figure shows, before the formation of super-holons, the system has load curtailment between hours 14-21, while after the formation of super-holons, the system undergoes load curtailment only at hour 18. The total load curtailment before the formation of super-holons is calculated as 10.08 MWh, whereas after the super-holons formation, this number reduces to 0.3 MWh. This significant decrease in load curtailment after the supper-holon formation, which improves the system reliability, clearly proves the effectiveness of the proposed model.

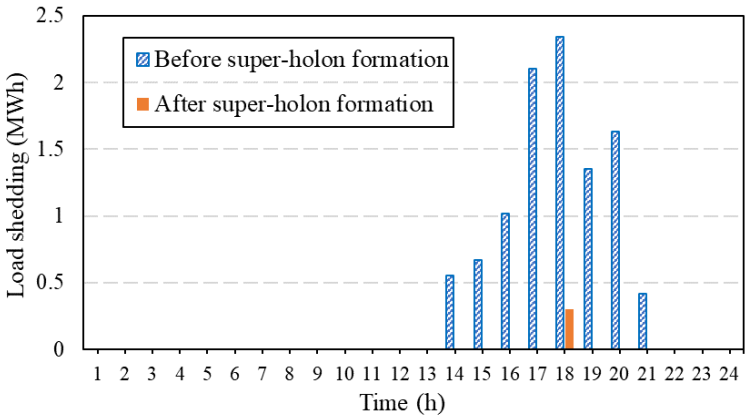

Fig. 3.3 Load curtailment of integrated microgrids, before and after super-holon formation.

4 Chapter Four: Optimal Operation of a Battery Swapping Station

4.1 Introduction

In line with the rapid deployment of BSS across the world, the concept of BSS has been studied from a variety of aspects in the literature. Ongoing research on the BSS can be generally categorized into four groups of studies: renewable-based BSS, BSS as an energy storage, BSS investment and planning, and BSS operation. The studies on renewable-based battery swapping/switching station aim at reducing carbon emission (by utilizing clean energy) and maximizing economic benefits by providing required energy of swapping/switching stations by renewable energy sources [86]-[90]. The BSS as an energy storage benefits from the fact that BSS can potentially be a relatively large and highly flexible battery with the capability of selling electricity to the utility grid and also participating in electricity markets [91]-[93]. The studies on BSS planning investigate a system-level perspective of BSS deployment and required investment strategies. A model for BSS optimal planning, taking into account locations, sizes, and charging strategies of the BSS in the distribution network, is proposed in [94]. In [95], the optimal planning problem is formulated based on a linear integer programming model considering customer satisfaction related to EV owner anxieties. A detailed techno-economic evaluation process, required for calculating the business startup cost of a BSS, is conducted in [96]. In [97] a subscription service concept for BSS is introduced, followed by an analysis to determine

whether and how such a subscription service might be economically viable based on the gasoline and electricity prices, the capital costs of batteries, and battery swapping stations. Authors in [98] present a study for simultaneous placement of distributed generation and BSS in distribution grid, while taking into account the energy loss and voltage stability associated with the distribution grid. Major studies in this area, however, investigate how a BSS operator can operate the station in an optimal manner, as discussed in the following.

A multi-objective optimization model to maximize the BSS's battery stock level, and to minimize the average charging damage due to the use of chargers with different charging rates is proposed in [99]. Various algorithms, including varied population genetic algorithm, varied population differential evolution, and three types of particle swarm optimization, are utilized to solve the problem. The study in [100] proposes an effective charging strategy under a BSS scenario on the basis of charging priority and charging location. By utilizing hybrid particle swarm optimization and genetic algorithm, the proposed strategy aims at minimizing the total charging cost, power loss, and voltage deviation in power system. In [101], an optimal scheduling model for BSS based on time-of-use pricing is studied. An optimization-based charging model to identify the effect of an EV owner's behaviour on power grid, and in particular on the system generation, is proposed in [102]. The paper concludes that utilizing the proposed optimal charging model generates profit to both power grid and generation companies. Authors in [103] provide a smart energy management system for BSS economic operation. The proposed system consists of two modules; battery swapping demand forecasting and BSS optimal charging schedule. The multi-objective BSS optimal charging schedule model takes into account

both charging cost and load variation. The load variation, which is originally formulated as a quadratic optimization problem, is further linearized by using a piecewise linearization approach. The proposed model aims at scheduling the battery charging in an optimal manner over a 24-h horizon based on the obtained information from the battery swapping demand forecasting module. The paper concludes that the proposed multi-objective model can significantly decrease the load variation and charging cost. The companion references [104]-[106] propose a framework for optimal charging operation of battery swapping and charging stations based on queueing network model, while taking Quality of Service (QoS) into account. The problem is formulated as a constrained Markov decision process in which the standard Lagrangian method and dynamic programming are employed to derive the optimal operation policy.

A BSS optimal scheduling model is proposed in [107] with a threefold objective: meeting BSS demand, reducing possible damage caused by high-rate chargers, and minimizing the electricity cost. An integrated algorithm based on genetic algorithm, differential evolution, and particle swarm optimization is presented, where a series of simulation studies are performed to achieve the feasible solution. Authors in [108] investigate an optimal BCS schedule model to offer battery swapping service to EVs, aiming at scheduling charging bays to minimize the charging cost. The problem is formulated using mixed-integer programming with quadratic battery degradation cost, and decomposed using a Benders decomposition method. The study in [109] introduces the idea of mobile battery swapping van to offer battery swapping service to EVs. The battery swapping van is able to carry a large number of fully-charged batteries and drive up to EVs

for rapid battery swapping process. A scheduling strategy, based on minimum waiting time, priority and satisfaction, is proposed to evaluate the efficiency of the method. Although this idea needs to be investigated thoroughly from the practical and implementation perspectives, it could be considered as a starting point for the future mobile battery swapping systems. To improve the energy-saving and emission-reduction effect of EVs, authors in [110] propose a real-time battery swap pricing and charging strategy for electric taxis in China. The proposed model consists of five modules including power grid load monitoring, generator set dispatch, BSS operation, electric taxi driver response, and stakeholders' benefits. Nevertheless, the model utilizes the real-time generator set dispatch module for monitoring carbon emission reduction and accordingly determining the cost of power generation for electric taxis.

4.2 Optimal Operation of a Battery Swapping Station

The proposed model builds up on existing research and deployment efforts on BSS operation and develops an optimal scheduling model based on mixed-integer linear programming. The proposed model has not been investigated by the aforementioned studies, and can be considered as an original contribution to this body of knowledge. In the proposed model, the BSS owner exchanges electricity with the utility grid considering battery degradation. The BSS owner purchases power to charge the batteries for either delivering the fully-charged ones to EV owners through the swapping process or exporting power and making benefits through battery energy arbitrage. Given the fact that the hourly electricity price and demand are forecasted day-ahead, and by treating the batteries as shiftable loads and potential resources for energy arbitrage, the BSS owner could minimize

the operation cost (the cost of power exchange with the utility grid and the battery degradation cost) by scheduling the battery charging/discharging process in an optimal manner, while taking prevailing operational constraints into account. A robust optimization approach is adopted to capture forecast errors in demand and electricity price as further explained in the following section.

4.2.1 Players in the BSS

The primary objective of introducing a BSS into the EV market is to provide EV owners with the opportunity of swapping an empty battery with a fully-charged one within a few minutes. As shown in Fig. 4.1, various players, including the EV owner, the BSS owner, and the power system would be involved either explicitly or implicitly to make this idea happen. Each player has its own priorities and considerations. The EV owner benefits from a reduced sticker price, as the battery is owned by the BSS instead of the EV owner, and experiences a fast charging, can plan for longer distance trips, would not suffer from the range anxiety, and does not need to worry about household infrastructure upgrade or battery replacement costs. The BSS owner could minimize its operation cost for battery charging/discharging by operating at a least-cost schedule, and further make a profit via participating in electricity market and offering ancillary services. In terms of the cost of real estate, as the BSS owner does not need access to spacious parking lots, substantial cost savings would be guaranteed. Power system operators will also benefit from this scheme as the BSS can be potentially used as a large and flexible resource for network congestion and peak load reduction. Moreover, the BSS approach could potentially change the

unpredictable behaviour of EV charging in the plug-in mode into an opportunity by providing a scheduled charging/discharging strategy.

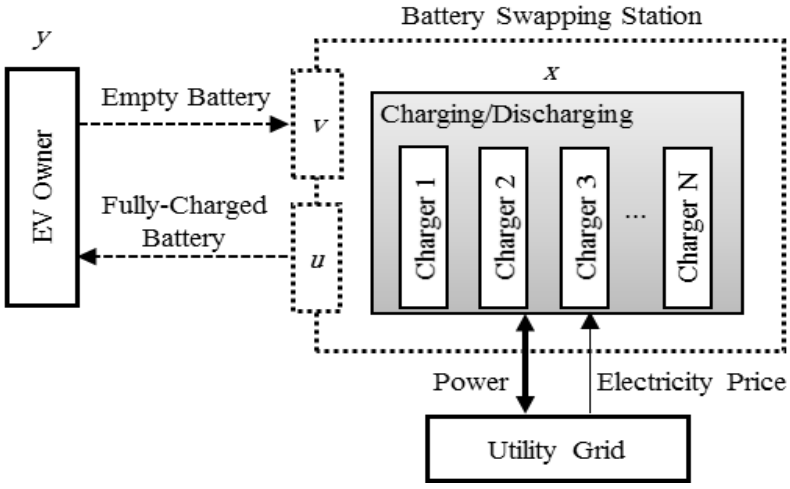

Fig. 4.1BSS architecture

4.2.2 BSS Components and Optimal Scheduling Model

The BSS model consists of sub-models for batteries, chargers, charging/discharging mode, charging/discharging time, battery degradation, and swapping actions. Batteries owned by the BSS are classified into two states of inside-station and outside-station in this dissertation. Inside-station batteries are available in the BSS and can be charged/discharged by considering minimum charging/discharging time. Outside-station batteries are outside of the BSS, used by EVs. When the outside-station batteries deplete, EV owners stop by the BSS and request to swap their empty batteries with the fully-charged inside-station ones. As these two types of batteries are swapped with each other based on the swapping demand, the total number of either inside-station or outside-station batteries will remain constant. Frequent charging/discharging cycles make batteries to be degraded, so that the battery degradation associated with the total number of cycles

must be considered. The battery charging/discharging process is controlled by the BSS master controller which considers a set of prevailing financial and technical constraints.

Each battery is assigned a state variable to show whether it is inside-station (i.e., x=1) or outside-station (i.e., y=1). The complicated part of the battery swapping process is that when a fully-charged battery is swapped with an empty one, two various actions will simultaneously occur from the BSS perspective; one fully-charged battery will go out, and in turn, one near-empty battery will come into the BSS. Two binary variables, i.e., u and v, are defined to model the swapping states of outgoing and incoming batteries, respectively. These two binary variables interact with x and y in a logical fashion, which will be formulated in the following section. Moreover, each inside-station battery could be charged (i.e., z^{ch}=1), discharged (i.e., z^{dch}=1), or idle (i.e., z^{ch}=z^{dch}=0). In order to formulate the optimal BSS operation, the following assumptions are made.

- The number of batteries owned by the BSS is constant.
- As inside-station batteries are exchanged with outside-station ones through swapping, the total number of either inside-station or outside-station batteries does not change.
- An index, as a unique identifier, is assigned to each battery, where that index does not change.
- Each battery needs several hours to be fully charged and to reach capacity. This number is varied based on battery capacity and maximum charge rate.
- The state-of-charge of outside-station batteries that enter the BSS is completely random.

- Total number of battery chargers/dischargers in the BSS is constant and equals the number of inside-station batteries.
- Battery chargers'/dischargers' efficiency is 100%, but charging/discharging efficiency (i.e., η^{ch}/η^{dch}) is less than 100%, based on battery characteristics.
- The BSS owner is able to perform swapping process for several batteries simultaneously.

4.2.3 BSS Optimal Scheduling Formulation

The BSS optimal scheduling model under uncertainty is proposed as in (4.1)-(4.19).

$$\max_{U} \min_{P} \sum_{t}\sum_{b} \left(P_{bt}^{ch} - P_{bt}^{dch}\right)\rho_t \tau + \sum_{t}\sum_{b} CD_{bt} \tag{4.1}$$

$$P_{M,t} = \sum_{b}(P_{bt}^{ch} - P_{bt}^{dch}) \qquad \forall t \tag{4.2}$$

$$-P_M^{max} \le P_{M,t} \le P_M^{max} \qquad \forall t \tag{4.3}$$

$$x_{bt} + y_{bt} = 1 \qquad \forall t, \forall b \tag{4.4}$$

$$u_{bt} \le \left(\alpha C_{bt} - \beta\right) \qquad \forall t, \forall b \tag{4.5}$$

$$\frac{1}{2}(x_{b(t-1)} + y_{bt} - 1) \le u_{bt} \le \frac{1}{2}(x_{b(t-1)} + y_{bt}) \qquad \forall t, \forall b \tag{4.6}$$

$$\frac{1}{2}(x_{bt} + y_{b(t-1)} - 1) \le v_{bt} \le \frac{1}{2}(x_{bt} + y_{b(t-1)}) \qquad \forall t, \forall b \tag{4.7}$$

$$\sum_{b} u_{bt} = D_t \qquad \forall t \tag{4.8}$$

$$\sum_{b} v_{bt} = D_t \qquad \forall t \tag{4.9}$$

$$P_b^{\text{ch, min}} z_{bt}^{\text{ch}} \le P_{bt}^{\text{ch}} \le P_b^{\text{ch, max}} z_{bt}^{\text{ch}} \qquad \forall t, \forall b \qquad (4.10)$$

$$P_b^{\text{dch, min}} z_{bt}^{\text{dch}} \le P_{bt}^{\text{dch}} \le P_b^{\text{dch, max}} z_{bt}^{\text{dch}} \qquad \forall t, \forall b \qquad (4.11)$$

$$z_{bt}^{\text{ch}} + z_{bt}^{\text{dch}} \le x_{bt} \qquad \forall t, \forall b \qquad (4.12)$$

$$T_b^{\text{ch}} \le MC_b (z_{bt}^{\text{dch}} - z_{b(t-1)}^{\text{dch}}) \qquad \forall t, \forall b \qquad (4.13)$$

$$T_b^{\text{dch}} \le MD_b (z_{bt}^{\text{ch}} - z_{b(t-1)}^{\text{ch}}) \qquad \forall t, \forall b \qquad (4.14)$$

$$C_b^{\min} \le C_{bt} \le C_b^{\max} \qquad \forall t, \forall b \qquad (4.15)$$

$$-M(1-v_{bt}) \le C_{bt} - C_{bt}^{ini} - \eta^{\text{ch}} P_{bt}^{\text{ch}} \tau + \eta^{\text{dch}} P_{bt}^{\text{dch}} \tau \le M(1-v_{bt}) \qquad \forall t, \forall b \qquad (4.16)$$

$$-M(v_{bt} + y_{bt}) \le C_{bt} - C_{b(t-1)} - \eta^{\text{ch}} P_{bt}^{\text{ch}} \tau + \eta^{\text{dch}} P_{bt}^{\text{dch}} \tau \le M(v_{bt} + y_{bt}) \qquad \forall t, \forall b \qquad (4.17)$$

$$CD_{bt} = \frac{k_b}{100} \left(\frac{P_{bt}^{\text{ch}} \tau}{C_b^{\max}} CB_b \right) \qquad \forall t, \forall b \qquad (4.18)$$

$$-Mz_{bt}^{\text{ch}} \le CD_{bt} \le Mz_{bt}^{\text{ch}} \qquad \forall t, \forall b \qquad (4.19)$$

The BSS objective (4.1) is to minimize the operation cost, which includes the cost of purchasing power from the utility grid and battery degradation cost over the scheduling horizon. The objective is maximized over uncertainty sets to achieve the worst-case solution. This cost is calculated based on the forecasted electricity price ρ, which is predicted for every time period in the scheduling horizon. τ represents time period, which can be adjusted based on the BSS owner's discretion. The forecasted electricity price and demand are considered as uncertainties. This objective is subject to constraints associated

with the BSS and the individual batteries. The difference between aggregated charged and discharged power determines the amount of power purchase form the grid in each time period (4.2), which can be either positive (power import) or negative (power export). This power exchange is limited by the thermal limit of the line connecting the BSS to the utility grid as in (4.3).

The BSS constraints represent the dynamics of the station in terms of exchanging batteries, as in (4.4)-(4.9). Each battery could be either inside or outside the station as imposed by (4.4). To determine whether the battery is ready to be swapped or not, (4.5) is defined, in which α is $1/(C_b^{max} - C_b^{min})$ and β is $C_b^{min}/(C_b^{max} - C_b^{min})$. If the stored energy in a battery is less than its capacity, that battery is not ready to be swapped as the right-hand-side in (4.5) is less than one and the binary variable u is forced to be 0. Otherwise, if the stored energy is equal to its capacity, that battery is ready to be swapped as $u_{bt} \leq 1$. Note that u_{bt} can be 1, but is not forced to be 1 unless there is an incoming battery ready to be swapped. All the defined binary variables related to the batteries' statuses are linked together in a logical fashion; $u_{bt} = x_{b(t-1)} y_{bt}$ and $v_{bt} = x_{bt}\, y_{b(t-1)}$, which are linearized in (4.6) and (4.7). As a battery is going out of the BSS, the swap state for outgoing battery u_{bt}, and the battery outside-station state y_{bt} will be set to 1 by (4.6). In a similar fashion, as a battery is coming into the BSS, the swap state for incoming battery v_{bt}, and the battery inside-station state x_{bt} will be set to 1 (4.7). The supply-demand balance (4.8) ensures that the sum of the outgoing batteries would match the hourly demand. Similarly, this is the case for incoming batteries (4.9).

The battery constraints consist of limitations associated with its power and energy, charging/discharging mode, and minimum charging/discharging time. The battery power is subject to minimum and maximum charging and discharging limits based on its mode (3.10), (4.11). When charging, the charging state z_{bt}^{ch} is 1 and the discharging state z_{bt}^{dch} is zero so that minimum and maximum charging limits are imposed. In a similar way, when discharging, the discharging state z_{bt}^{dch} is 1 and charging state z_{bt}^{ch} is zero so that minimum and maximum discharging limits are imposed. Each inside-station battery can be charging, discharging, or idle in each time period (4.12). Constraints (4.13) and (4.14) respectively define minimum charging and discharging time limits, which represent the minimum number of successive time periods that battery must maintain charging or discharging once the operational mode is toggled. The battery stored energy is restricted with minimum and maximum capacity limits (4.15). The battery stored energy is calculated based on the amount of charged/discharged power and charging/discharging efficiency (4.16), (4.17). When a battery enters the BSS, i.e., its swapping state v_{bt} is one, it is charged/discharged based on (4.16), considering the initial amount of stored energy. On the other hand, when a battery has been available inside the BSS for more than one time period, i.e., both its swapping state v_{bt} and outside-station state y_{bt} are zero, it is charged/discharged based on (4.17).

As charging/discharging cycles cause batteries to be degraded, battery degradation cost related to the number of cycles is considered in the BSS operation. Constraint (4.18) is utilized to calculate the battery degradation cost, where k_b is the linear approximation slope of battery life as a function of number of cycles, C_b^{max} is the maximum battery

capacity, and CB_b is the battery cost. Battery degradation is calculated for the round-trip cycles, which means discharging and then charging to the same value. As the battery discharging, either inside or outside the station, will eventually be occurred at some point in the future, only charging power P_{bt}^{ch} is utilized in (4.18). On the other hand, when inside-station battery is discharging, the charging state z_{bt}^{ch} is zero, so that battery degradation cost CD_{bt} is imposed to be zero (4.19).

The proposed robust model is solved through a Benders Decomposition, in which the master problem determines the binary variables and the subproblem finds the BSS's worst-case minimum operation cost over the uncertainty sets based on the fixed schedules from the master problem.

4.2.4 Numerical Simulations

A BSS with 30 similar batteries, 12 inside the BSS and the rest outside, is used to analyze the proposed BSS optimal operation model. Each battery has a capacity of 100 kWh. Twelve AC level 2 battery chargers with the maximum charging/discharging power of 17.2 kW are installed in the BSS [111]. The battery capital cost is set to 200 $/kWh [112]. There is no limit on the power exchange with the utility grid, also no limits on the required spaces for swapping batteries. The time period is considered to be 1 h, i.e, τ=1 h and the minimum charging/discharging time is also assumed to be 1 h.

The problem is solved in a computer with Intel Core i5 2.3 GHz processor and 4 GB RAM using CPLEX 11.0 [113]. Electricity price forecast error is considered to be ±20%. Given the fact that the BSS peak demand (i.e., the number of required battery swaps) could occur either in the morning, afternoon or evening, three associated scenarios are

considered (Fig. 4.2). BSS demand of ±1 is regarded as the forecast error. The following cases are studied:

Case 0: BSS operation with forecasted average values ignoring optimality objective and power export.

Case 1: BSS optimal operation with forecasted average values.

Case 2: BSS optimal operation under uncertainty parameters.

Case 3: Analysis on the number of batteries inside the BSS.

Case 4: Analysis on inclusion of various battery types.

Case 0: The BSS with forecasted average values for hourly electricity price and demand is studied under the three demand scenarios while ignoring optimal scheduling and discharging capability. If the optimal scheduling model and the capability of battery discharging are ignored, the batteries will be charged similar to the BCS approach; that is once each battery enters the station, the station owner starts the battery charging process without considering the hourly electricity price. The total 24-h operation cost in this case for scenarios 1, 2, and 3 are calculated as $124.31, $162.96, and $166.11, respectively.

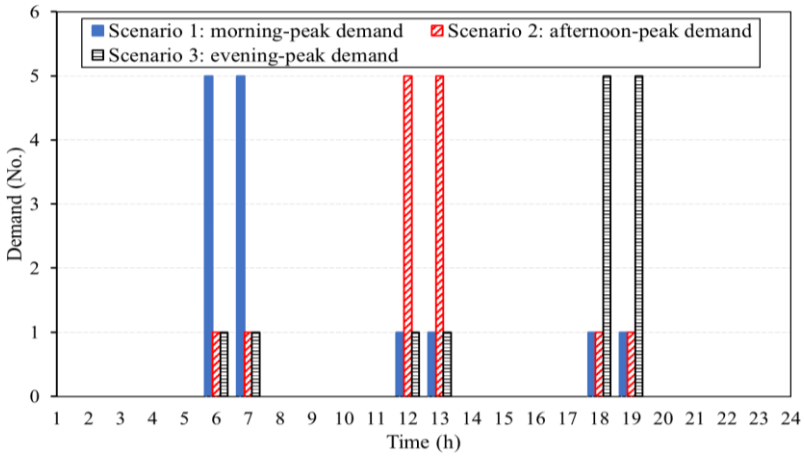

Fig. 4.2 BSS demand under the three scenarios

Case 1: The BSS optimal scheduling with forecasted average values for hourly electricity price and demand scenarios is solved for two cases. In the first case, the BSS battery discharging capability and accordingly power export are ignored, while this capability is considered in the second case. It is assumed that 5 fully-charged batteries are available inside the BSS from the previous day, and at the end of the day, 5 fully-charged batteries must be ready for the next day. The computation time for each scenario is less than 75 min.

Case 1-a: The BSS optimal scheduling with forecasted average values ignoring power export capability is solved. Compared to Case 0, the operation cost for scenarios 1, 2, and 3 is reduced to \$65.32 (-47.45%), \$83.2 (-48.95%), and \$86.85 (-47.72%), respectively. These considerable reductions affirm that leveraging the proposed optimal battery scheduling model provides the BSS owner with significant savings. Fig. 4.3 depicts the purchased power from the utility grid with respect to forecasted average values for hourly electricity price and demand.

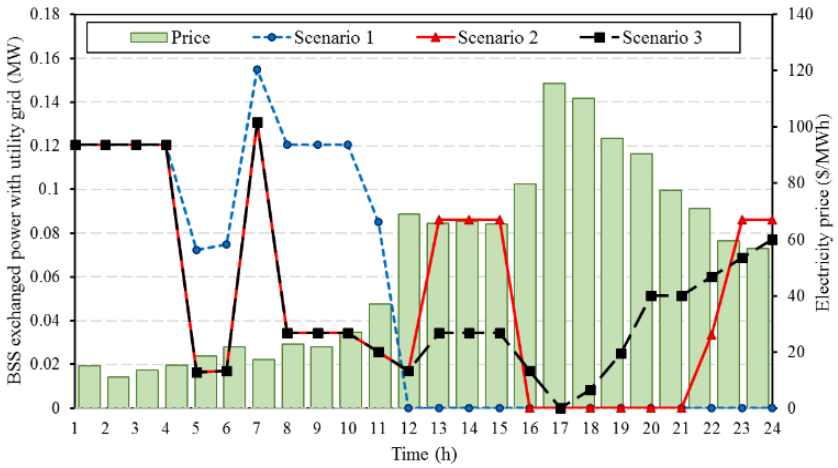

Fig. 4.3 BSS exchanged power with the utility grid in Case 1-a

Considering the lower price for the first four hours of the studied day, the purchased power from the utility grid to perform battery charging is the same for the three scenarios. As in hour 5 the electricity price slightly increases, the purchased power is reduced for all scenarios. As empty batteries enter the BSS at hours 6 and 7, the rate of purchased power grows for all scenarios. This increase is higher in scenario 1 compared to scenarios 2 and 3 due to availability of more empty batteries to be charged. Although there is demand for scenario 1 at hours 12-13 and 18-19, scenario 1 performs the task of battery charging in advance at low-price hours, i.e., from hour 1 to 11, to minimize the operation cost. As the afternoon-peak demand is at hours 12 and 13, the purchased power sharply increases in scenario 2 to charge incoming batteries and to avoid facing the peak price. In scenario 3, empty batteries are charged inside the BSS in advance to meet the evening-peak demand. Based on the evening-peak demand, ten EV owners deliver their empty batteries at hours 18 and 19, so the purchased power rises from hour 19 to 24 to ensure preparing five fully-charged batteries for the next day.

To demonstrate the performance of the proposed model, the hourly battery state in scenario 1 is studied for a 24-h horizon and provided in Table 4.1. Each battery can have one of these four states at every hour: charging (C), fully-charged (F), empty (E), and outside-station (-).

Table 4.1 Hourly battery state in scenario 1

	Hours (1-24)																							
B1	F	F	F	F	F	F	-	-	-	-	-	-	-	-	-	-	-	-	-	-	-	-	-	-
B2	F	F	F	F	F	F	-	-	-	-	-	-	-	-	-	-	-	-	-	-	-	-	-	-
B3	F	F	F	F	F	F	-	-	-	-	-	-	-	-	-	-	-	-	-	-	-	-	-	-
B4	F	F	F	F	F	F	-	-	-	-	-	-	-	-	-	-	-	-	-	-	-	-	-	-
B5	F	F	F	F	F	-	-	-	-	-	-	-	-	-	-	-	-	-	-	-	-	-	-	-

B6	C	C	C	C	C	-	-	-	-	-	-	-	-	-	-	-	-	-	-	-	-	-	-	-
B7	C	C	C	C	C	-	-	-	-	-	-	-	-	-	-	-	-	-	-	-	-	-	-	-
B8	C	C	C	C	C	-	-	-	-	-	-	-	-	-	-	-	-	-	-	-	-	-	-	-
B9	C	C	C	C	C	-	-	-	-	-	-	-	-	-	-	-	-	-	-	-	-	-	-	-
B10	C	C	C	C	C	C	C	F	F	F	F	-	-	-	-	-	-	-	-	-	-	-	-	-
B11	C	C	C	C	C	C	C	F	F	F	F	F	F	F	F	F	F	F	F	F	F	F	F	F
B12	C	C	C	C	C	F	-	-	-	-	-	-	-	-	-	-	-	-	-	-	-	-	-	-
B13	-	-	-	-	-	-	E	E	E	E	E	E	E	E	E	E	E	E	E	E	E	E	E	E
B14	-	-	-	-	-	-	C	C	C	C	C	F	F	F	F	F	F	F	-	-	-	-	-	-
B15	-	-	-	-	-	-	E	E	E	E	E	E	E	E	E	E	E	E	E	E	E	E	E	E
B16	-	-	-	-	-	-	C	C	C	C	C	F	F	F	F	F	F	-	-	-	-	-	-	-
B17	-	-	-	-	-	-	C	C	C	C	C	F	F	F	F	F	F	F	F	F	F	F	F	F
B18	-	-	-	-	-	-	-	-	-	-	-	-	-	-	-	-	-	-	E	E	E	E	E	E
B19	-	-	-	-	-	-	-	-	-	-	-	-	E	E	E	E	E	E	E	E	E	E	E	E
B20	-	-	-	-	-	-	-	-	-	-	-	-	-	-	-	-	-	E	E	E	E	E	E	E
B21	-	-	-	-	-	-	-	-	-	-	-	-	-	-	-	-	-	-	-	-	-	-	-	-
B22	-	-	-	-	-	-	-	-	-	-	-	E	E	E	E	E	E	E	E	E	E	E	E	E
B23	-	-	-	-	-	-	-	-	-	-	-	-	-	-	-	-	-	-	-	-	-	-	-	-
B24	-	-	-	-	-	-	-	-	-	-	-	-	-	-	-	-	-	-	-	-	-	-	-	-
B25	-	-	-	-	-	-	-	-	-	-	-	-	-	-	-	-	-	-	-	-	-	-	-	-
B26	-	-	-	-	-	E	E	E	E	E	E	E	E	E	E	E	E	E	E	E	E	E	E	E
B27	-	-	-	-	-	C	C	C	C	C	C	F	F	F	F	F	F	F	F	F	F	F	F	F
B28	-	-	-	-	-	C	C	C	C	C	C	F	F	F	F	F	F	F	F	F	F	F	F	F
B29	-	-	-	-	-	C	C	C	C	C	C	F	F	F	F	F	F	F	F	F	F	F	F	F
B30	-	-	-	-	-	C	C	C	C	C	C	F	-	-	-	-	-	-	-	-	-	-	-	-

At hour 1, batteries B1-B12 are available inside the BSS, while B13-B30 are outside. B1-B5 are fully-charged from the previous day and ready to be swapped based on the demand. On the other hand, B6-B12 start to be charged at hour 1 to be fully charged by hour 7. In line with the morning-peak demand at hour 6, five EV owners who carry B26-B30 arrive to the BSS and deliver these empty batteries and receive the fully-charged B5-B9. Four of these incoming empty batteries (B27-B30) start to be charged upon entering the BSS at hour 6, while the five outgoing batteries will not come back to the BSS during the 24-h studied horizon. Similar to hour 6, the five fully-charged B1-B4, and B12

are switched with B13-B17 at hour 7. At hour 12, B10 is swapped with B22. At hour 13, B30 is delivered to an EV owner and B19 is received. At hours 18 and 19, B16 and B14 which have been fully-charged for several hours, are swapped with B20 and B18, respectively.

An interesting observation here is that the battery charging process is preponed or postponed with the objective of minimizing the operation cost. In this respect, none of the batteries inside the BSS require to be charged after hour 11. This means that the battery charging process has been completely performed from hour 1 to 11. By employing this strategy, the BSS owner not only meets the demand for the remaining hours of the studied day and provides five fully-charged batteries (B11, B17, and B27-29) for the next day, but also minimizes the total cost by preponing the charging process to the low-cost morning hours. On the other hand, the charging process for some of the batteries, such as B13 and B15, will be postponed to the next day, as the price is expected to be cheaper for the early morning hours of the next day.

Case 1-b: In this case, inside-station batteries can be scheduled to be discharged, and accordingly the BSS owner can gain benefit through energy arbitrage revenue. Compared to Case 1-a, the operation cost for scenarios 1, 2, and 3 is reduced to $45.56 (-30.3%), $75.79 (-8.9%), and $81.3 (-6.4%), respectively. These reduced operation costs advocate that adding battery discharging capability is profitable for the BSS owner. Fig. 4.4 shows the exchanged power between the BSS and the utility grid with respect to forecasted average values for hourly electricity price and demand. The general trend of power exchange is the same for all scenarios, that is, making energy arbitrage revenue by

purchasing electricity at low price hours for charging batteries and selling back electricity through discharging at high price hours. The difference in scenarios' exchanged power curves are due their associated peak demands.

The obtained results for Case 1-a and Case 1-b illustrate how the BSS owner can schedule battery charging in a way that (a) the operation cost is minimized, (b) constraints associated with the proposed model are closely followed, (c) there is a certain number of fully-charged batteries inside the BSS, so as to be used in the next day, and (d) each battery is closely tracked, so its degradation is accurately determined.

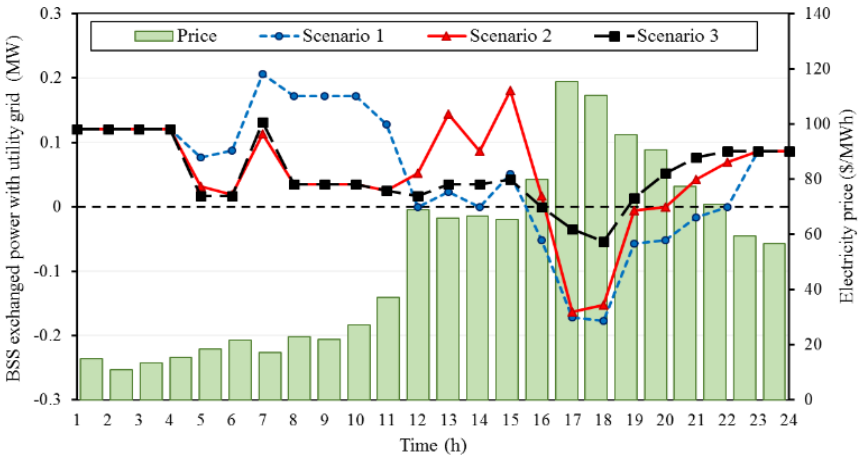

Fig. 4.4 BSS Exchanged power with the utility grid in Case 1-b

Case 2: Considering the constant number of total daily demand (i.e., 14), the BSS demand forecast error of ±1, and a limit on uncertainty option of 6 hours/day, the BSS optimal scheduling with the capability of power export is solved, where the operation cost is increased from Case 1-b to $52.89 (+16.1%), $86.32 (+13.9%), and $94.1 (+15.6%) for scenarios 1, 2, and 3, respectively. This increase represents the cost of robustness which are paid to make the BSS operation more robust against demand uncertainty. This study suggests that an optimal scheduling of BSS is achievable at higher cost when the data are

not totally predictable. At extreme points of uncertainty, the demand scenarios are at their higher bounds at the last hours of the studied day, which offer the worst-case economic solutions, i.e., reduced demand at the morning hours and increased demand in the evening.

To evaluate the impact of uncertainty in the electricity price, the electricity price forecast error of ±20 with a limit on uncertainty option of 12 hours/day is considered. A robust solution is obtained when the electricity price is at its lower/higher bound at high/low priced hours. At these extreme points, the BSS not only would make less benefit from selling back electricity, but also would spend more on purchasing. The operation cost is increased from Case 1-b to $59.25 (+30.05%), $81.48 (+7.5%), and $87.18 (+7.23%) for scenarios 1, 2, and 3, respectively. This increase is the cost of robustness against electricity price uncertainty.

Case 3: A sensitivity analysis is performed to study the effect of the number of inside-station batteries on the BSS operation results. The number of batteries inside the BSS is increased from 12 to 26 with a step size of 1, and the BSS operation is solved for the three demand scenarios. Cost comparison is provided in Fig. 4.5. When the number of batteries inside the BSS is increased, the operation cost is linearly decreased. It is interesting to note that after 26 batteries inside the BSS, the operation cost will become negative for all scenarios (i.e., the BSS owner makes profit). Compared to Case 1-b, the operation cost considering 26 batteries inside the BSS is reduced by 170.41% ($-32.08), 109.75% ($-7.39), and 104.11% ($-3.34) for scenarios 1, 2, and 3, respectively, in expense of 116.6% increase in the number of batteries inside the BSS, which translates into a higher BSS capital cost.

This study advocates the fact that the BSS owner could decrease the operation cost by procuring more batteries inside the BSS. However, procuring more batteries leads to a higher investment cost for the BSS owner. In other words, the optimal number for inside-station batteries should be determined through a cost-benefit analysis under a planning paradigm considering both investment and operation costs.

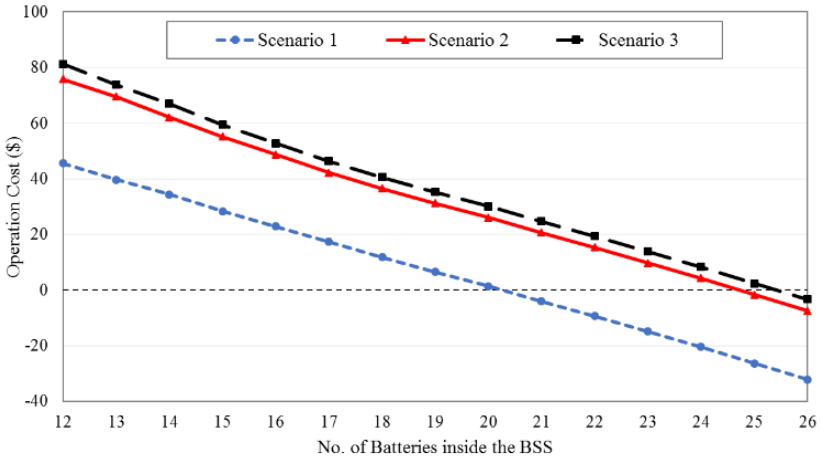

Fig. 4.5 Operation cost with various number of batteries inside the BSS

Case 4: To demonstrate the effectiveness of the proposed model in solving the optimal battery scheduling problem for a relatively larger BSS, the problem is solved for three EV models from Tesla which are powered with different battery capacities: Model X powered by a 100-kWh battery, Model S powered by a 75-kWh battery, and Model S powered by a 60-kWh battery. In this regard, the BSS is equipped with AC level 2 battery chargers with the maximum charging/discharging power of 17.2 kW, 11.5 kW, and 9.6 kW, respectively [114],[115]. For each type, the BSS owns 30 batteries (total of 90 batteries), 12 from each type being available inside the BSS. Using the proposed model, the optimal battery schedule is solved under the three mentioned demand scenarios. The operation cost in this case for scenarios 1, 2, and 3 are calculated as $106.03, $173.81, and

$187.98, respectively. Regarding the computation time, each solution is obtained in less than 120 min.

Fig. 4.6 shows the disaggregated exchanged power to perform the charging/discharging process of the three Tesla EV models in scenario 1. As it was expected, the general pattern of exchanged power in this case is similar to Case 1-b under scenario 1. Nevertheless, based on the capacity of batteries and their configured battery chargers, hourly electricity price, and the morning-peak demand, the operation cost is minimized via the proposed model. Without the loss of generality, this is also the case for scenarios 2 and 3.

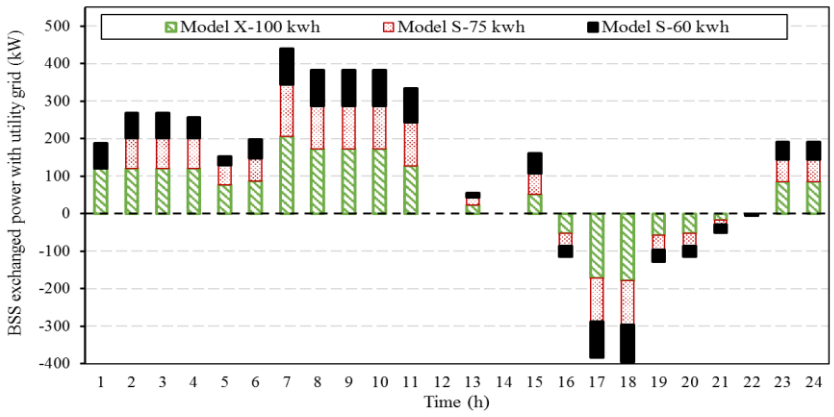

Fig. 4.6 Disaggregated BSS exchanged power with the utility grid for various Tesla EV models in Case 4 under scenario 1

4.2.5 Discussions

In the transition to transportation electrification, the BSS has been initially proposed as a viable method to pave the way for EVs fast energy refill. The BSS, however, further sets the stage for the BSS owner to export power to the utility grid and consequently benefit from an optimal battery charging schedule. In this section, a model for BSS optimal operation was proposed with the aim of minimizing the BSS daily operation cost while

taking into account the prevailing operational constraints. A robust optimization approach was also employed to find the worst-case solution of the BSS optimal schedule when considering demand and electricity price uncertainties. From model implementation and obtained numerical results, it is concluded that the BSS owners can in fact obtain a charging schedule that not only minimizes the operation cost but also follows a set of pre-defined operation limits and tracks degradation of each battery. The number of inside-station batteries further emerged as an important factor in the BSS operation, where it was shown that an optimal number of inside-station batteries needs to be determined through a cost-benefit analysis under a planning paradigm considering both investment and operation costs. The proposed model supports an optimized BSS operation, thus potentially supporting a greater adoption of EVs as environmentally-friendly modes of transportation through removing some of the existing burdens in fast battery charging.

4.3 BSS as an Energy Storage for Capturing Distribution-Integrated Solar Variability

The global environmental concern regarding the use of fossil fuels in electricity generation has motivated many countries in deploying higher levels of renewable energy resources. Among renewable energy resources, solar photovoltaic (PV) is envisioned to be a major player in future power systems and a viable enabler of sustainable power generation. Solar energy is clean, widely available, and relatively low maintenance. Moreover, unlike traditional power generation resources, which are installed in a centralized manner, solar energy resources can be easily deployed as a distributed generation resource [116]-[118]. Solar energy resources have attracted consumers who are

willing to make up part of their electricity consumption or even economically benefit from a local power generation [119],[120]. The dropping cost of solar technology and the state and governmental incentives have made the path for a rapid growth of solar generation. More than 7 GW of solar PV was installed in the U.S. in 2016, where residential PV with over 2 GW represented the biggest segment [121]. All in all, the solar generation is making fast inroads in power systems [122]-[124].

Although various methods are carried out in the literature for solar forecasting problem [125]-[127], they mainly suffer from a degree of inaccuracy due to inherent variability (i.e., intermittency and volatility) and uncertainty in solar generation. The intermittency indicates that the solar generation is not always available, while the volatility denotes the fluctuations of solar generation in different time scales such as seconds, minutes, and hours. Uncertainty indicates the failure of accurate forecast in the time and the magnitude of solar generation variability. These characteristics negatively impact the solar generation and necessitate the deployment of flexible energy resources to facilitate the integration of solar generation into power systems [128]-[130]. To this end, coordinating solar generation with battery energy storage systems is a common approach, where the coordinated scheme can pick up the variability of solar generation to achieve a smooth and controllable output power [131]-[133].

A novel and viable method for addressing the aforementioned challenges is to reap the benefit of available energy storage system in a Battery Swapping Station (BSS). The concept of the BSS as an energy storage has been studied in the literature. Authors in [41] study a BSS-enabled power system with high penetration of renewable-based energy

resources, where the BSS is utilized to provide fully-charged battery to EVs as well as to help with energy management. The optimal storage capacity of the BSS is obtained by analyzing the behavior of the power system with a high penetration of renewable energy resources. In [93], a study for evaluating the economic value of battery energy storage inside the BSS is proposed. The paper concludes that leveraging the batteries inside the BSS is more beneficial than pumped storage for managing surplus electricity generated by solar PV. The potential of providing regulation services by energy storage in BSS is investigated in [134] and [135]. Based on an interaction framework, called Station-to-Grid (S2G), the integration of BSS into power systems is presented. This framework is developed in a way that the BSS not only is in charge of battery swapping service for EVs, but also can offer regulation reserves. The simulation results carried out in the dissertation demonstrate that the BSS can mitigate frequency deviation as well as tie-line power fluctuations.

The primary objective of this section is to provide a BSS-based framework to capture distribution grid-integrated solar variability. To this end, the BSS exchanged power with the utility grid is reshaped with the objective of mitigating distributed solar generation variability. A mixed-integer programming formulation is used for problem modeling.

4.3.1 Optimal Scheduling Model

Consider a distribution network in which a BSS and several consumers with the ability of electricity generation, i.e., prosumers, are connected to a distribution feeder. The prosumers own distributed rooftop solar PV, where accordingly bring variability to the power required to be supplied by the utility grid. In addition, the behavior of prosumers for

buying/selling electricity to/from the utility grid is uncontrolled, as they aim at maximizing benefits subject to their financial objectives (i.e., the minimum electricity payment). The BSS which is deployed at the distribution network not only aims at providing fully-charged batteries to EV owners, but also can capture the variability in solar PV generation associated with the prosumers. By doing this, the power needed to be injected to the feeder by the utility grid can be controlled to some extent. Fig. 4.7 shows the BSS-based model architecture for capturing distribution grid-integrated solar variability, where the power of $P_t^u = P_t^M + \sum_{j \in N} P_{jt}^c$ is provided by the utility grid to this distribution feeder. Nevertheless, the BSS is expected to receive incentive from the utility grid to capture the variability of solar generation.

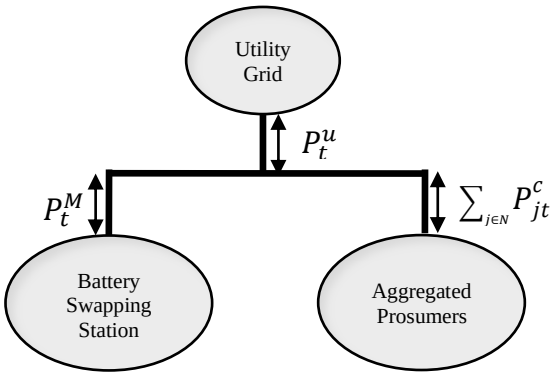

Fig. 4.7 BSS-based architecture for capturing distribution grid-integrated solar variability

A model for the BSS optimal scheduling problem is proposed from the BSS owner's perspective. The objective of the proposed model is to minimize the BSS total operation cost, which represents the accumulated cost of exchanging energy with the utility grid, while taking into account the output power adjustment for capturing solar generation variability. The proposed model is subject to four sets of constraints associated with the

utility grid, the BSS, individual batteries, and solar mitigation. A mixed-integer programing method is utilized to formulate the BSS optimal scheduling model from the BSS owner's view.

4.3.2 Problem Formulation

The BSS owner's objective is to minimize its operation cost, i.e., the cost of exchanging power with the utility grid, as in (4.20). The quantity of power exchange with the utility grid is determined by subtracting the accumulated battery charging power from the discharging power as in (4.21). This quantity can be positive or negative as for power import or export, respectively.

$$\min \sum_{t} [P_t^M \rho_t \tau] \tag{4.20}$$

$$P_t^M = \sum_{b} (P_{bt}^{\mathrm{ch}} - P_{bt}^{\mathrm{dch}}) \qquad \forall t \tag{4.21}$$

Based on the forecasted hourly electricity price ρ, the operation cost is calculated. As the power exchange with the utility grid can be positive or negative, the objective function can be positive or negative which means the BSS owner not only is able to minimize its cost, but can also make revenue through exporting power to the utility grid. τ denotes time period, which can be set according to the BSS owner's discretion. By considering shorter time periods, the BSS can more accurately capture the rapid variability of solar generation. However, the proper choice of the time period is a tradeoff between the accuracy and the computation time. The objective function of the proposed model is subject to the following constraints.

4.3.2.1 Grid Constraints

The sum of transferred power for charging/discharging batteries in each time period is limited by the flow limits of the line connecting the BSS to the utility grid, as represented in (4.22).

$$-P^{M,\max} \le P_t^M \le P^{M,\max} \qquad \forall t \tag{4.22}$$

4.3.2.2 BSS System Constraints

The BSS constraints are employed to model available fully-charged batteries in order to meet the battery swapping demand in each time period, as formulated in (4.23)-(4.24).

$$1+M(C_{bt}-C^{\max}) \le x_{bt}^F \le 1+\varepsilon(C_{bt}-C^{\max}) \quad \forall t, \forall b \tag{4.23}$$

$$D_t = \sum_b x_{b(t-1)}^F \qquad \forall t \tag{4.24}$$

To determine whether the battery is fully-charged or not, (4.23) is proposed. If C_{bt} is equal to C_b^{max}, battery b is fully-charged and binary variable x_{bt}^F is set to one, which indicates battery b is ready to be swapped in the next time period. Otherwise, if C_{bt} less than C_b^{max}, the battery is not fully-charged and the binary variable x_{bt}^F is forced to be 0, which means battery b is not ready for swapping. The balance equation (4.24) ensures that the number of the fully-charged batteries in the previous time period is equal to the current swapping demand. In other words, once a battery is fully-charged, it will be swapped in the subsequent time period.

4.3.2.3 Individual Battery and Charger Constraints

The battery and charger constraints are directly resulted from their technologies and include limitations associated with power rating and stored energy. These constraints are defined to ensure that the batteries and chargers do not exceed their associated operational limits.

$$0 \le P_{bt}^{\text{ch}} \le P_b^{\text{ch, max}} \qquad \forall t, \forall b \qquad (4.25)$$

$$0 \le P_{bt}^{\text{dch}} \le P_b^{\text{dch, max}} \qquad \forall t, \forall b \qquad (4.26)$$

$$C^{\min} \le C_{bt} \le C^{\max} \qquad \forall t, \forall b \qquad (4.27)$$

$$-M\left(1-x_{b(t-1)}^{F}\right) \le C_{bt} - C_{bt}^{ini} - \eta^{\text{ch}} P_{bt}^{\text{ch}} \tau + \eta^{\text{dch}} P_{bt}^{\text{dch}} \tau \le M\left(1-x_{b(t-1)}^{F}\right) \qquad \forall t, \forall b \qquad (4.28)$$

$$-M\left(x_{b(t-1)}^{F}\right) \le C_{bt} - C_{b(t-1)} - \eta^{\text{ch}} P_{bt}^{\text{ch}} \tau + \eta^{\text{dch}} P_{bt}^{\text{dch}} \tau \le M\left(x_{b(t-1)}^{F}\right) \qquad \forall t, \forall b \qquad (4.29)$$

Charging/discharging power rating of each battery is limited by the maximum charging/discharging power which are assumed to be positive (4.25)-(4.26). Equation (4.27) ensures that the batteries are operating within their associated capacity limits. Based on (4.27), the battery stored energy is limited by its maximum and minimum limits. Equations (4.28)-(4.29) are defined to calculate the battery stored energy according to the value of charged/discharged power and charging/discharging efficiency. When a battery is fully-charged in the previous time period (i.e., $x^F_{b(t-1)}$=1), it will be swapped with an empty battery in the next time period, and consequently this empty battery with the initial stored energy of C^{ini}_{bt} is charged/discharged based on (4.28). Without the loss of generality, when a battery is not fully-charged in the previous time period (i.e., $x^F_{b(t-1)}$=0), it is charged/discharged based on (4.29).

4.3.2.4 Solar Variability Constraints

The solar variability constraints are introduced to capture the variability caused by solar generation. The BSS exchanged power with the utility grid is utilized for mitigating PV output fluctuations.

$$-\Delta^u - \Delta_t \le P_t^M - P_{(t-1)}^M \le \Delta^u - \Delta_t \qquad \forall t \qquad (4.30)$$

$$\Delta_t = \sum_j P_{jt}^c - \sum_j P_{j(t-1)}^c \qquad \forall ta \qquad (4.31)$$

Equation (4.30) is defined to capture the aggregated prosumers net loads variability, where Δ^u denotes the amount of variability being captured by the utility grid, and the rest is picked up by the BSS. The aggregated prosumers net loads variability between two successive time periods (i.e., Δ_t) is formulated in (4.31). Nevertheless, leveraging (4.30) and (4.31), the aggregated prosumers net load variability is entirely captured by the BSS through exchanged power with the utility grid.

4.3.2.5 Uncertainty Consideration

To capture variability of solar generation, the proposed model uses hourly forecasted values of solar generation. As the solar generation is affected by weather conditions which are uncontrollable, the forecasting errors are inevitable. To deal with the solar generation uncertainty, a robust optimization method will be utilized. By maximizing the minimum value of the objective (4.20) over a defined uncertainty set, i.e., solar generation uncertainty, the worst-case solution will be determined. The uncertain parameter, i.e., solar generation, is assumed to be within an interval around the forecasted value, i.e., a polyhedral uncertainty set. By increasing maximum number of instances that

this uncertain parameter can differ from its forecasted value, which is called the budget of uncertainty, the robustness of the solution will increase, while reducing the solution optimality.

4.3.3 Numerical Simulations

The performance of the proposed model is analyzed with a BSS consisting of 300 batteries with the individual capacity of 100 kWh. The BSS is equipped with 300 AC-level-2 battery chargers with the maximum power of 17.2 kW for a 100-kWh configured battery [111]. It is assumed that there is no power transfer limit between the BSS and the utility grid. The time period is set to be 1 h, i.e, τ=1 h, where the proposed model for BSS optimal scheduling model is solved for a 24-h horizon. The maximum value of variability desired to be captured by the utility grid, i.e., Δ^u, is assumed to be 1 MW/h. It means that the BSS is used to capture the aggregated prosumers net loads variability above this value.

The day-ahead forecasted values of electricity price over the 24-h horizon are given in Table 4.2. The aggregated load data, solar generation, and consequently the net load for a sample distribution feeder are listed in Table 4.3. The BSS demand over the 24-h horizon is tabulated in Table 4.4. The proposed BSS optimal scheduling problem is solved using CPLEX 11.0 by a personal computer with Intel Core i5, 2.3 GHz processor, and 4 GB RAM. The computation time for each of the following cases is less than 10 min, which advocates the computational efficiency of the proposed model. The following cases are studied:

Case 1: BSS optimal scheduling ignoring solar variability constraints.

Case 2: BSS optimal scheduling with solar variability constraints.

Case 3: BSS optimal scheduling under solar generation uncertainty.

Table 4.2 Hourly electricity price

Time (h)	**1**	**2**	**3**	**4**	**5**	**6**
Price ($/MWh)	15.03	10.97	13.51	15.36	18.51	21.8
Time (h)	**7**	**8**	**9**	**10**	**11**	**12**
Price ($/MWh)	17.3	22.83	21.84	27.09	37.06	68.95
Time (h)	**13**	**14**	**15**	**16**	**17**	**18**
Price ($/MWh)	65.79	66.57	65.44	79.79	115.45	110.28
Time (h)	**19**	**20**	**21**	**22**	**23**	**24**
Price ($/MWh)	96.05	90.53	77.38	70.95	59.42	56.68

Table 4.3 Hourly BSS demand

Time (h)	**1**	**2**	**3**	**4**	**5**	**6**
Demand (No.)	2	1	1	2	4	6
Time (h)	**7**	**8**	**9**	**10**	**11**	**12**
Demand (No.)	8	7	6	5	5	4
Time (h)	**13**	**14**	**15**	**16**	**17**	**18**
Demand (No.)	6	7	8	10	12	12
Time (h)	**19**	**20**	**21**	**22**	**23**	**24**
Demand (No.)	9	8	6	5	2	1

Table 4.4 Hourly aggregated prosumers solar generation, load, and net load in a distribution feeder

Time (h)	**1**	**2**	**3**	**4**	**5**	**6**
Solar (MW)	0	0	0	0	0	0
Load (MW)	6.75	6.25	5.90	5.85	6.05	6.25
Net Load (MW)	6.75	6.25	5.90	5.85	6.05	6.25
Time (h)	**7**	**8**	**9**	**10**	**11**	**12**
Solar (MW)	0	0	0.50	2.00	4.00	5.75
Load (MW)	6.40	7.00	7.30	7.60	8.00	8.50
Net Load (MW)	6.40	7.00	6.80	5.60	4.00	2.75
Time (h)	**13**	**14**	**15**	**16**	**17**	**18**
Solar (MW)	7.00	7.10	7.00	6.20	5.50	3.00
Load (MW)	9.25	9.00	8.50	8.35	8.50	9.00
Net Load (MW)	2.25	1.90	1.50	2.15	3.00	6.00
Time (h)	**19**	**20**	**21**	**22**	**23**	**24**
Solar (MW)	1.35	0.40	0	0	0	0
Load (MW)	10.15	10.35	9.50	8.50	7.25	6.90
Net Load (MW)	8.80	9.95	9.50	8.50	7.25	6.90

Case 1: The BSS optimal scheduling is studied while ignoring the solar variability constraints. It means that the BSS in the distribution feeder does not participate in capturing the aggregated prosumers net load variability. As the BSS optimal schedule in this case

aims at minimizing its operation cost, i.e., focusing on the BSS price-based scheduling, it is expected that the utility grid experiences a severe net load variability. The BSS operation cost is calculated as $-1555.72 in this case. This negative value for the operation cost means that the BSS owner makes money through energy arbitrage. Fig. 4.8 shows the distribution feeder net load ($P_{u,t}$) and the BSS exchanged power with the utility grid ($P_{M,t}$).

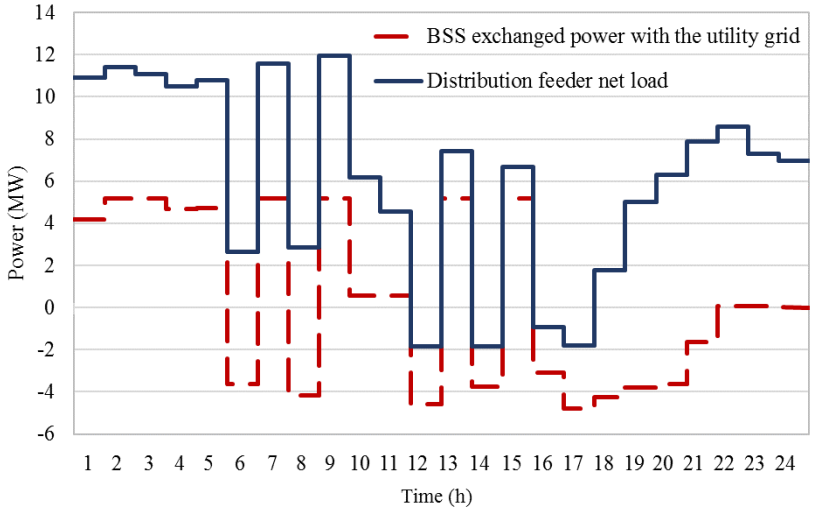

Fig. 4.8 BSS exchanged power with the utility grid and distribution feeder net load in Case 1

The trend of power exchange with the utility grid in this case is based on energy arbitrage revenue, which is purchasing electricity at low price hours for charging batteries and selling back electricity through discharging at high price hours. Moreover, since the solar variability constraints are ignored, the BSS price-based schedule is targeted to minimize its operation cost, so that the utility grid undergoes a severe net load variability in the distribution feeder. For instance, there are the severe net load changes of 9.11 MW/h and 9.24 MW/h between hours 9-10 and 13-14, respectively, which must be captured by the utility grid.

Case 2: The BSS optimal scheduling is studied considering the solar variability constraints. In this case, the BSS exchanged power with the utility grid contributes in capturing the aggregated prosumers net load variability. As the utility grid is to capture the aggregated prosumers net loads variability of less than 1 MW/h, any variability larger than this value is captured by the BSS based on the proposed model. Compared to Case 1, the BSS operation cost is increased by 21.8% to $-1216.14, which translates into less benefits for the BSS owner. Nevertheless, the BSS exchanged power with the utility grid is reshaped in such a way that the distributed solar generation variability is captured at the expense of increased operation cost for the BSS.

As the BSS operation cost is increased, the grid operator not only should pay to the BSS owner to compensate this increase, but also should incentivize the BSS owner to contribute in mitigating the solar generation variability as well as helping the power systems for hosting a higher penetration of solar generation. Fig. 4.9 compares the distribution feeder net load with and without variability constraints.

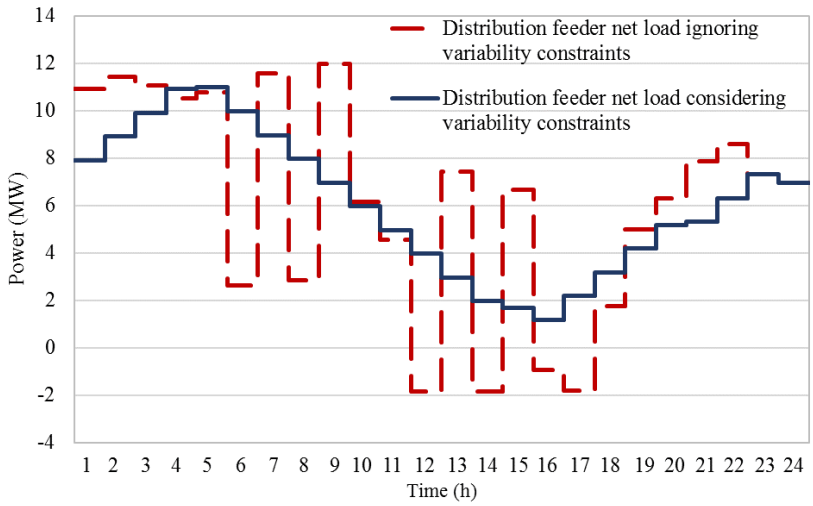

Fig. 4.9 Comparison of distribution feeder net load in Case 1 and 2

As shown in Fig. 4.9, the maximum changes in distribution feeder net load supplied by the utility grid is bounded to be less than 1 MW/h, which makes the distribution feeder net load smoother.

Case 3: In this case, the BSS optimal scheduling problem with solar variability constraints is studied under solar generation uncertainty. Accordingly, the BSS owner's objective (1) is maximized over solar generation uncertainty to achieve the worst-case solution using a robust optimization approach. Solar generation forecast error is considered to be ±20%. The sensitivity of the BSS operation cost with respect to the uncertainty budget is carried out, where the obtained results are listed in Table 4.5.

Table 4.5 BSS operation cost with respect to uncertainty budget

	Uncertainty Budget (hours/day)				
	0	**3**	**6**	**9**	**12**
BSS Operation Cost ($)	-1216.14	-1108.35	-967.1	-921.07	-910.49

The obtained results advocate the fact that by increasing the uncertainty budget, the BSS operation cost increases, which translates into a reduction in the BSS owner's benefits. This increase in the BSS operation cost indicates the cost of robustness which are paid to make the BSS operation more robust against solar generation uncertainty. Nevertheless, this study demonstrates that the BSS owner achieves an optimal scheduling at higher cost when the forecasted data are uncertain.

4.3.4 Discussions

This section introduced the BSS as an energy storage to address solar generation variability in distribution networks. A BSS optimal scheduling model was proposed from the BSS owner's perspective with the objective of capturing distribution grid-integrated solar variability. To this end, the BSS exchanged power with the utility grid was reshaped in such a way that the distributed solar generation variability was captured. Using mixed-integer linear programming, the proposed model was formulated to minimize the BSS operation cost, while taking into account the prevailing constraints associated with the utility grid power exchange, the BSS system, individual batteries, and solar variability. The proposed model was investigated through numerical simulations, where it was demonstrated that the BSS provides a viable approach in capturing the solar generation variability as well as helping the utility grids for hosting a higher penetration of solar generation.

References

[1]X. Zhang and E. Gockenbach, "Asset-management of transformers based on condition monitoring and standard diagnosis," IEEE Elect. Insul. Mag., vol. 24, no. 4, pp. 26-40, Jul./Aug. 2008.

[2]A. E. B. Abu-Elanien and M. M. A. Salama, "Asset management techniques for transformers," Elect. Power Syst. Res., vol. 80, no. 4, pp. 456-464, 2010.

[3]Ma, T. K. Saha, C. Ekanayake and D. Martin, "Smart transformer for smart grid intelligent framework and techniques for power transformer asset management," IEEE Trans. Smart Grid, vol. 6, no. 2, pp. 1026-1034, Mar. 2015.

[4]A. Abiri-Jahromi, M. Parvania, F. Bouffard, and M. Fotuhi-Firuzabad, "A two-stage framework for power transformer asset maintenance management—Part I: Models and formulations," IEEE Trans. Power Syst., vol. 28, no. 2, pp. 1395–1403, 2013.

[5]M. Arshad, S. M. Islam and A. Khaliq, "Power transformer asset management," in Proc. Int'l. Conf. Power System Technology (PowerCon), Nov. 2004, pp. 1395-1398.

[6]M. Žarković, Z. Stojković, "Analysis of artificial intelligence expert systems for power transformer condition monitoring and diagnostics," Elect. Power Syst. Res., vol. 149, pp. 125-136, 2017.

[7]K. T. Muthanna, A. Sarkar, K. Das and K. Waldner, "Transformer insulation life assessment," IEEE Trans. Power Del., vol. 21, no. 1, pp. 150–156, Jan. 2006.

[8]A. Hilshey, P. Hines, P. Rezaei and J. Dowds, "Estimating the impact of electric vehicle smart charging on distribution transformer aging," IEEE Trans. Smart Grid, vol. 4, no. 2, pp. 905-913, Jun. 2013.

[9]V. Sarfi, S. Mohajeryami and A. Majzoobi, "Estimation of water content in a power transformer using moisture dynamic measurement of its oil," IET High Voltage, In press, 2017.

[10]http://www.industrialelectricalmaintenance.in

[11]Department of Energy Office of Electricity Delivery and Energy Reliability. (2012). Summary Report: 2012 DOE Microgrid Workshop. [Online]. Available: http://energy.gov/sites/prod/files/2012%20Microgrid%20Workshop%20Report%2009102012.pdf.

[12]A. Majzoobi and A. Khodaei, "Application of microgrids in supporting grid flexibility," IEEE Trans. Power Systems, In press, 2016.

[13]L. Shi, Y. Luo and G. Y. Tu, "Bidding strategy of microgrid with consideration of uncertainty for participating in power market," Electr. Power Energy Syst., vol. 59, pp. 1–13, 2014.

[14]A. Majzoobi and A. Khodaei, "Application of microgrids in providing ancillary services to the utility grid," Energy, vol. 123, pp. 555-563, Mar. 2017.

[15]A. Khodaei, S. Bahramirad and M. Shahidehpour, "Microgrid planning under uncertainty," IEEE Trans. Power Syst., vol. 30, no. 5, pp. 2417-2425, Sep. 2015.

[16]A. Khodaei, "Microgrid optimal scheduling with multi-period islanding constraints," IEEE Trans. Power Syst., vol. 29, pp. 1383-1392, May 2014.

[17]A. Khodaei, "Resiliency-oriented microgrid optimal scheduling," IEEE Trans. Power Syst., vol. 5, pp. 1584-1591, July 2014.

[18]A. Albaker and A. Khodaei, “Valuation of microgrid unused capacity in islanded operation,” in Proc. IEEE North American Power Symposium (NAPS), Morgantown, WV, USA, 2017.

[19]L. Che, X. Zhang, M. Shahidehpour, A. Alabdulwahab, and A. Abusorrah, “Optimal interconnection planning of community microgrids with renewable energy sources,” IEEE Trans. on Smart Grid, vol. 8, no. 3, May 2017.

[20]Md. Asaduz-Zaman and A. H. Chowdhury, “Optimum economic dispatch of interconnected microgrid with energy storage system,” Int. Conf. Electrical Engineering and Information Communication Technology (ICEEICT), Dhaka, Bangladesh, May 2015, pp. 1-6.

[21]W. Xi, Q. Xiaoyan, J. Runzhou, L. Dan, W. Gang, and L. Qian, “Economic operation of multi-microgrids containing energy storage system,” Int. Conf.

Power System Technology (POWERCON), Chengdu, China, Oct. 2014, pp. 1712-1716.

[22]S. Howell, Y. Rezgui, J. L. Hippolyte, B. Jayan, and H. Li, "Towards the next generation of smart grids: Semantic and holonic multi-agent management of distributed energy resources," Renewable and Sustainable Energy Reviews, vol. 77, pp. 193-214, 2017.

[23]A. Ferreira, A. Ferreira, O. Cardin, and P. Leitão, "Extension of holonic paradigm to smart grids," IFAC-PapersOnLine, vol. 48, no. 3, pp. 1099-1104, 2015.

[24]A. Albaker and A. Khodaei, "Optimal scheduling of integrated microgrids in holonic distribution grids," in Proc. IEEE North American Power Symposium (NAPS), Fargo, ND, USA, 2018.

[25]Sh. Yang, J. Yao, T. Kang, and X. Zhu, "Dynamic operation model of the battery swapping station for EV (Electric Vehicle) in electricity market," Energy, vol. 65, pp. 544–549, Feb. 2014.

[26]Electric vehicles: Tax credits and other incentives [Online]. Available: https://energy.gov/eere/electricvehicles/electric-vehicles-tax-credits-and-other-incentives

[27]Electric vehicle charging incentive program. [Online]. Available: http://www.mto.gov.on.ca/english/vehicles/electric/charging-incentive-program.shtml

[28]G. Masiero, M. H. Ogasavara, A. C. Jussani, and M. L. Risso, "Electric vehicles in China: BYD strategies and government subsidies," RAI Revista de Administração e Inovação, vol. 13, no. 1, pp. 3-11, Jan.–Mar. 2016.

[29]National eclectic mobility mission plan. [Online]. Available: http://dhi.nic.in/UserView/index?mid=1347

[30]S. Hiti and K. Rahman, "Trends in EV propulsion components and systems," IEEE Electrification Magazine, vol. 5, no. 1, pp. 2-3, 2017.

[31]M. Mahoor, Z. S. Hosseini, A. Khodaei, and D. Kushner, "Electric vehicle battery swap station," CIGRE Grid of the Future Symposium, Cleveland, OH, Oct. 2017.

[32]S. M. Salamati, S. A. Salamati, M. Mahoor, and F. R. Salmasi, “Leveraging adaptive model predictive controller for active cell balancing in Li-ion battery,” North American Power Symposium (NAPS), Morgantown, WV, 2017.

[33]SAE Hybrid Committee, “SAE charging configuration and ratings terminology.” SAE international, 2011.

[34]O. Worley, D. Klabjan, “Optimization of battery charging and purchasing at electric vehicle battery swap stations,” IEEE Vehicle Power and Propulsion Conference (VPPC), Chicago, IL, Sept. 2011.

[35]M. Nilsson, “Electric vehicles: The phenomenon of range anxiety,” ELVIRE, Gif-sur-Yvette Cedex, France, ELVIRE Consortium FP7CICT- 2009C4-249105, 2011, pp.1-14.

[36]T. Franke, I. Neumann, F. Buhler, P. Cocron, and J. Krems, “Experiencing range in an electric vehicle: Understanding psychological barriers,” Appl. Psychol. vol. 61, pp.368-391, 2012.

[37]J. J. Jamian, M. W. Mustafa, H. Mokhlis, and M. A. Baharudin, “Simulation study on optimal placement and sizing of Battery Switching Station units using Artificial Bee Colony algorithm,” International Journal of Electrical Power & Energy Systems, vol. 55, pp. 592-601, 2014.

[38]T. H. Wu, G. H. Pang, K. L. Choy, and H. Y. Lam, “An optimization model for a battery swapping station in Hong Kong,” Proceeding of IEEE Transportation Electrification Conference and Expo (ITEC), Dearborn, MI, June 2015.

[39]F. Q. Zhou, Z. W. Lian, X. L.Wan, X. H. Yang, and Y. S. Xu, “Discussion on operation mode to the electric vehicle charging station,” Power Syst. Protection and Control, vol. 1, no. 1, pp. 65–72, Jun. 2010.

[40]Y. X. Liu, F. H. Hui, R. L. Xu, T. Chen, X. Xu, and J. Li, “Investigation on the construction mode of charging and battery-exchange station,” Power and Energy Engineering Conference (APPEEC), Wuhan, China, Mar. 2011.

[41]P. Lombardi, M. Heuer, and Z. Styczynski, “Battery switch station as storage system in an autonomous power system: optimization issue,” IEEE PES General Meeting, Providence, RI Jul. 2010.

[42]Y. Jun, H. Sun, “Battery Swap Station Location-Routing Problem with Capacitated Electric Vehicles,” Computers & Operations Research, vol. 55, pp. 217–232, March 2015.

[43]S. Wirasingha, N. Schofield, and A. Emadi, “Plug-in hybrid electric vehicle developments in the US: Trends, barriers, economic feasibility,” Proceeding of IEEE Vehicle Power and Propulsion Conference (VPPC), Harbin, China, 2008.

[44]Y. Zheng, Z. Y. Dong, Y. Xu, K. Meng, J. H. Zhao, and J. Qiu, “Electric vehicle battery charging/swap stations in distribution systems: comparison study and optimal planning,” IEEE Transactions on Power Systems, vol. 29, no. 1, pp. 221–229, Jan. 2014.

[45]A broken place: the spectacular failure of the startup that was going to change the world. [Online]. Available: https://www.fastcompany.com/3028159/a-broken-place-better-place

[46]Better Place’s failure is blow to Renault, Wall Street Journal [Online]. Available: https://www.wsj.com/articles/SB10001424127887323855804578507263247107312

[47]“China electric vehicle charging station market report, 2017-2020,” March 2017, Research in China.

[48]India’s 1st battery swapping & charging station for electric vehicles. [Online]. Available: http://india.smartcitiescouncil.com/article/india%E2%80%99s-1st-battery-swapping-charging-station-electric-vehicles

[49]Battery swapping system. [Online]. Available: http://adaptive-city-mobility.com/battery-swapping-system/

[50]R. S. Widrick, S. G. Nurre, and M. J. Robbins. “Optimal policies for the management of an electric vehicle battery swap station,” Transportation Science, Oct.2016.

[51]J. Singh, Y. R. Sood and P. Verma, "Experimental investigation using accelerated aging factors on dielectric properties of transformer insulating oil," Electric Power Components and Systems, vol. 39, pp. 1045-1059, Jan. 2011.

[52]A. Seier, P. D. H. Hines and J. Frolik, "Data-driven thermal modeling of residential service transformers," IEEE Trans. Smart Grid, vol. 6, no. 2, pp.1019-1025, Mar. 2015.

[53]IEEE guide for loading mineral-oil-immersed transformers and step-voltage regulators, IEEE Std. C57.91-2011 (Revision of IEEE Std. C57.91-1995), Mar. 2012.

[54]M. Mahoor, A. Majzoobi, Zohreh S. Hosseini and A. Khodaei, "Leveraging sensory data in estimating transformer lifetime," North American Power Symposium (NAPS), Morgantown, WV, Sep. 2017.

[55]M. Arshad and S. Islam, "A novel Fuzzy logic technique for power asset management," in proc. Industry Applications Conference, Oct. 2006, pp. 276-286.

[56]A. Majzoobi, M. Mahoor and A. Khodaei, "Machine learning applications in estimating transformer loss of life," IEEE PES General Meeting, Chicago, IL, July 2017.

[57]M. Mahoor and A. Khodaei, "Data fusion and machine learning integration for transformer loss of life estimation," IEEE PES Transmission and Distribution Conference and Exposition (T&D), Denver, CO, April 2018.

[58]J.L. Velasquez-Contreras, M.A. Sanz-Bobi, and S. Galceran Arellano, "General asset management model in the context of an electric utility: Application to power transformers," Elect. Power Syst. Res., vol. 81, no. 11 pp. 2015-2037, Nov. 2011.

[59]V. Aravinthan and W. Jewell, "Controlled electric vehicle charging for mitigating impacts on distribution assets," IEEE Trans. Smart Grid, vol. 6, no. 2, pp. 999-1009, Mar. 2015.

[60]C. Roe, F. Evangelos, J. Meisel, A. P. Meliopoulos and T. Overbye, "Power system level impacts of PHEVs," in Proc. 42nd Hawaii Int. Conf. Syst. Sci., Jan. 2009, pp. 1-10.

[61]M. K. Gray, W. G. Morsi, "On the impact of single-phase plug-in electric vehicles charging and rooftop solar photovoltaic on distribution transformer aging," Elect. Power Syst. Res., vol. 148, pp. 202-209, 2017.

[62]M. K. Gray, W. G. Morsi, "On the role of prosumers owning rooftop solar photovoltaic in reducing the impact on transformer's aging due to plug-in electric vehicles charging," Elect. Power Syst. Res., vol. 143, pp. 563-572, 2017.

[63]S. Shokrzadeh, H. Ribberink, I. Rishmawi and E. Entchev, "A simplified control algorithm for utilities to utilize plug-in electric vehicles to reduce distribution transformer overloading," Energy, vol. 133, pp. 1121-1131, 2017.

[64]E. Ramos Munoz, G. Razeghi, L. Zhang and F. Jabbari, "Electric vehicle charging algorithms for coordination of the grid and distribution transformer levels," Energy, vol. 113, pp. 930-942, 2016.

[65]D. L. Hall and J. Llinas, "An introduction to multi-sensor data fusion," Proceedings of the IEEE, vol. 85, no. 1, pp. 6–23, 1997.

[66]M. Doostan, B.H. Chowdhury, "Power distribution system equipment failure identification using machine learning algorithms," IEEE PES General Meeting, Chicago, IL, July 2017.

[67]R. R. Yager, "On ordered weighted averaging aggregation operators in multicriteria decision making," IEEE Trans. Systems, Man and Cybernetics, vol. 18, no. 1, pp.183-190, Jan./Feb. 1988.

[68]D. Nettleton, V. Torra, "A comparison of active set method and genetic algorithm approaches for learning weighting vectors in some aggregation operators," International Journal of Intelligent Systems. vol. 16, no. 9, pp. 1069–1083, Sep. 2001.

[69]R. E. Kalman, "A new approach to linear filtering and prediction problems," Trans. ASME, J. Basic Eng., vol. 82, pp. 35–45, 1960.

[70]G. Bishop, G. Welch, "An introduction to the Kalman filter," NC, Chapel Hill:Univ. North Carolina, 2001.

[71]S. Bahramirad, W. Reder and A. Khodaei, "Reliability-constrained optimal sizing of energy storage system in a microgrid," IEEE Trans. Smart Grid, Special Issue on Microgrids, vol. 3, pp. 2056-2062, Dec. 2012.

[72]M. Shahidehpour and J. Clair, "A functional microgrid for enhancing reliability, sustainability, and energy efficiency," Electricity Journal, vol. 25, PP. 21-28, Oct. 2012.

[73]Microgrid Exchange Group, DOE Microgrid Workshop Report, August 2011. [Online]. Available: http://energy.gov/oe/downloads/microgrid-workshop-report-august-2011.

[74]Navigant Research, Microgrid Deployment Tracker 4Q16, "Commercial and Industrial, Community, Utility Distribution, Institutional/Campus, Military, Remote, and DC Microgrids: Projects by Region, Segment, and Top 10 Countries and States" 2016.

[75]S. Parhizi, H. Lotfi, A. Khodaei and S. Bahramirad, "State of the art in research on microgrids: A review," IEEE Access, vol. 3, pp. 890-925, July 2015.

[76]A. M. Geoffrion, "Generalized benders decomposition", J. Optim. Theory Appl., vol. 10, no. 4, pp. 237-260, 1972.

[77]M. Shahidehpour and Y. Fu, "Benders decomposition,':IEEE Power and Energy Mag., vol. 3, no. 2, pp. 20–21, Mar. 2005.

[78]A. J. Conejo, E. Castillo, R. Minguez, and R. Garcia-Bertrand, "Decomposition techniques in mathematical programming engineering and science applications," Springer Science & Business Media, 2006.

[79]‘PEAK Lab, https://portfolio.du.edu/peaklab/page/63877, accessed 02 April 2018.

[80]‘Weather history & data archive,’ https://www.wunderground.com/history/airport, accessed 02 April 2018.

[81]J. C. Smith and Z. C. Taskin, "A tutorial guide to mixed-integer programming models and solution techniques," Optim. Med. Biol., pp. 521–548, 2008.

[82]O. K. Gupta, and A. Ravindran "Branch and bound experiments in convex nonlinear integer programming," Management science, vol 31, no.12, pp.1533-1546, 1985.

[83]E. Negeri, N. Baken, and M. Popov, "Holonic architecture of the smart grid," Smart Grid and Renewable Energy, vol. 4, no. 2, p.p 202, 2013.

[84]A. Pahwa, S. A. DeLoach, S. Das, B. Natarajan, X. Ou, D. Andresen, N. Schulz, and G. Singh, "Holonic multi-agent control of power distribution systems of the future," Grid of the Future Symposium (CIGRE), 2012.

[85]A. Albaker and A. Khodaei, "Spinning reserve based topology control in holonic distribution grids," CIGRE Grid of the Future Symposium, Reston, VA, USA, 2018.

[86]Y.J. Gao, K.X. Zhao, and C. Wang, "Economic dispatch containing wind power and electric vehicle battery swap station," IEEE PES T&D, Orlando, FL, 2012.

[87]Z. Chen, N. Liu, X. Xiao, X. Lu, and J. Zhang, "Energy exchange model of PV-based battery switch stations based on battery swap service and power distribution," IEEE Energytech, Cleveland, OH, 2013.

[88]N. Liu, Q. Chen, X. Lu, J. Liu, and J. Zhang, "A charging strategy for PV-based battery switch stations considering service availability and self-consumption of PV energy," IEEE Transactions on Industrial Electronics, vol. 62, no. 8, pp. 4878-4889, 2015.

[89]S. Wu, Q. Xu, Q. Li, X. Yuan, and B. Chen, "An optimal charging strategy for PV-Based battery swapping stations in a DC distribution system," International Journal of Photoenergy, 2017.

[90]N. Liu, Z. Chen, J. Liu, X. Tang, X. Xiao, and J. Zhang, "Multi-objective optimization for component capacity of the photovoltaic-based battery switch stations: towards benefits of economy and environment," Energy, vol. 64, pp.779-792, 2014.

[91]M. R. Sarker, H. Pandzic, and M. A. O. Vazques, “Electric vehicle battery swapping station: business case and optimization model,” IEEE International Conference on Connected Vehicles and Expo (ICCVE), Las Vegas, NV, 2013.

[92]P. Lombardi, M. Heuer, and Z. Styczynski. “Battery switch station as storage system in an autonomous power system: Optimization issue,” IEEE PES General Meeting, Providence, RI, Jul. 2010.

[93]M. Takagi, Y. Iwafune, H. Yamamoto, K. Yamaji, K. Okano, R. Hiwatari, and T. Ikeya, “Energy storage of PV using batteries of battery-switch stations,” IEEE International Symposium on Industrial Electronics (ISIE), Bari, Italy, Jul. 2010.

[94]Y. Zheng, Z. Y. Dong, Y. Xu, K. Meng, J. H. Zhao, and J. Qiu, “Electric vehicle battery charging/swap stations in distribution systems: comparison study and optimal planning,” IEEE Trans. Power Syst., vol. 29, no. 1, pp. 221-229, 2014.

[95]J. Yang, F. Guo, and M. Zhang “Optimal planning of swapping/charging station network with customer satisfaction,” Transportation Research Part E: Logistics and Transportation Review, vol. 103, pp. 174-197, 2017.

[96]J. S. Neubauer, A. Pesaran, “A techno-economic analysis of bev service providers offering battery swapping services,” No. 2013-01-0500. SAE Technical Paper, 2013.

[97]J. Lidicker, T. Lipman, and B. Williams, “Business model for subscription service for electric vehicles including battery swapping for San Francisco bay area, California,” Transp. Res. Record: Journal of Transp. Res Board, vol. 2252, pp. 83–90, 2011.

[98]U. Sultana, A. B. Khairuddin, B. Sultana, N. Rasheed, S. Hussain Qazi, N. Riaz Malik, “Placement and sizing of multiple distributed generation and battery swapping stations using grasshopper optimizer algorithm,” Energy, In press, 2018, doi: 10.1016/j.energy.2018.09.083

[99]H. Wu, G. K. Pang, K. L. Choy, and H. Y. Lam, “A charging-scheme decision model for electric vehicle battery swapping station using varied population evolutionary algorithms,” Applied Soft Computing, In Press.

[100]Q. Kang, J. B. Wang, M. C. Zhou, and A. C. Ammari, “Centralized charging strategy and scheduling algorithm for electric vehicles under a battery swapping scenario,” IEEE Transactions on Intelligent Transportation Systems, vol. 17, no. 3, pp. 659-669, 2016.

[101]L. Zhang, S. Lou, Y. Wu, L. Yi, and B. HU, “Optimal scheduling of electric vehicle battery swap station based on time-of-use pricing,” IEEE PES Asia-Pacific, Hong Kong, China, 2014.

[102]R. Rao, X. Zhang, J. Xie, and L. Ju, “Optimizing electric vehicle users’ charging behavior in battery swapping mode,” Applied Energy, vol. 155, pp. 547-559, 2015.

[103]Q. Dai, T. Cai, S. Duan, W. Zhang, and J. Zhao, “A smart energy management system for electric city bus battery swap station,” IEEE Transportation Electrification Conference and Expo Asia-Pacific (ITEC Asia-Pacific). Beijing, China, 2014.

[104]B. Sun, X. Tan, and D. Tsang, “Optimal charging operation of battery swapping and charging stations with QoS guarantee,” IEEE Transactions on Smart Grid, In press.

[105]X. Tan, B. Sun, and D. H. K. Tsang, “Queueing network models for EV charging station with battery swapping,” IEEE Conference Smart Grid Communications, Venice, Nov. 2014.

[106]B. Sun, X. Tan, and D. H. K. Tsang, “Optimal operation of battery swapping stations with QoS guarantee,” IEEE Conference Smart Grid Communications, Venice, Nov. 2014.

[107]H. Wu, G. K. H. Pang, K. L. Choy, and H. Y. Lam, “An optimization model for electric vehicle battery charging at a Battery swapping station,” IEEE Transactions on Vehicular Technology, In press.

[108]X. Tan, G. Qu, B. Sun, N. Li, and D. H. K. Tsang, “Optimal scheduling of battery charging station serving electric vehicles based on battery swapping,” IEEE Transactions on Smart Grid, In press.

[109]S. Shao, S. Guo, and X. Qiu. “A mobile battery swapping service for electric vehicles based on a battery swapping van,” Energies, vol. 10, no.10, pp. 1-21, Oct. 2017.

[110]Y. Liang and X. Zhang, “Battery swap pricing and charging strategy for electric taxis in China,” Energy, vol. 147, pp. 561-577, 2018.

[111]Charging. [Online]. Available: https://www.tesla.com/charging

[112]Electric vehicle battery cost dropped 80% in 6 years down to $227/kWh-tesla claims to be below $190/kWh. [Online]. Available: https://electrek.co/2017/01/30/electric-vehicle-battery-cost-dropped-80-6-years-227kwh-tesla-190kwh/

[113]ILOG CPLEX, ILOG CPLEX homepage. [Online]. Available: http://www.ilog.com

[114]Model X. [Online]. Available: https://www.tesla.com/modelx

[115]Model S. [Online]. Available: https://www.tesla.com/models

[116]M. R. Patel, “Wind and solar power systems: design, analysis, and operation,” CRC press, 2005.

[117]R. Chedid, S. Rahman, "Unit sizing and control of hybrid wind-solar power systems," IEEE Trans. Energy Conversion, vol. 12, pp.79-85, 1997.

[118]A. Majzoobi, A. Khodaei, and S. Bahramirad, “Capturing distribution grid-integrated solar variability and uncertainty using microgrids,” IEEE PES General Meeting, Chicago, IL, 2017.

[119]P. M. Corrigan and G. T. Heydt, "Optimized dispatch of a residential solar energy system," in North American Power Symposium (NAPS), Las Cruces, NM, Sep. 2007.

[120]A. J. Black, "Financial payback on California residential solar electric systems," Solar energy, vol. 77, no. 4, pp. 381-388, Oct. 2004.

[121]Solar Market Insight 2015 Q4, Solar Energy Industries Association research report, [Online]. Available: http://www.seia.org/research-resources/solar-market-insight-2015-q4

[122]H. Sadeghian, M. H. Athari, and Z. Wang, "Optimized Solar Photovoltaic Generation in a Real Local Distribution Network," IEEE Power & Energy Society Innovative Smart Grid Technologies Conference (ISGT), Washington, DC, 2017.

[123]S. H. Elyas, H. Sadeghian, H. O Alwan, and Z. Wang, "Optimized Household Demand Management with Local Solar PV Generation," North American Power Symposium (NAPS), Morgantown, WV, 2017.

[124]H. Sadeghian and Z. Wang, " Decentralized Demand Side Management with Rooftop PV in Residential Distribution Network," IEEE Power & Energy Society Innovative Smart Grid Technologies Conference (ISGT), Washington, DC, 2017.

[125]M. Alanazi, M. Mahoor, and A. Khodaei, "Two-stage hybrid day-ahead solar forecasting," North American Power Symposium (NAPS), Morgantown, WV, 2017.

[126]M. Alanazi, M. Mahoor, and A. Khodaei, "Day-Ahead Solar Forecasting Based on Multi-level Solar Measurements," IEEE PES Transmission and Distribution Conference and Exposition (T&D), Denver, CO, 2018.

[127]H. Sangrody, M. Sarailoo, N. Zhou, A. Shokrollahi, and E. Foruzan, "On the performance of forecasting models in the presence of input uncertainty," North American Power Symposium (NAPS), Morgantown, WV, 2017.

[128]H. Sangrody, M. Sarailoo, N. Zhou, N. Tran, M. Motalleb, and E. Foruzan, "Weather forecasting error in solar energy forecasting," IET Renewable Power Generation, vol. 11, no. 10, pp. 1274-1280, 2017.

[129]S. Eftekharnejad, V. Vittal, G. T. Heydt, B. Keel, and J. Loehr, "Impact of increased penetration of photovoltaic generation on power systems", IEEE Trans. Power Syst., vol. 28, no. 2, pp. 893-901, May 2013.

[130]J. Paatero and P. Lund, "Effects of large-scale photovoltaic power integration on electricity distribution networks", Renew. Energy J., vol. 32, no. 2, pp. 216-234, Feb. 2007.

[131]A. Sangwongwanich, Y. Yang, F. Blaabjerg, and H. Wang, "Benchmarking of constant power generation strategies for single-phase grid-connected photovoltaic systems", IEEE Transactions on Industry Applications, vol.54, no.1, pp. 447-457, 2017.

[132]R. M. Dell and D. Rand, "Energy storage—a key technology for global energy sustainability," Journal of Power Sources, vol. 100, pp. 2-17, Nov. 2001.

[133]H. Nazaripouya, Y. Wang, P. Chu, H. R. Pota, and R. Gadh, "Optimal sizing and placement of battery energy storage in distribution system based on solar size for voltage regulation", IEEE PES General Meeting, Denver, CO, 26-30 July 2015.

[134]P. Xie, B. Qian, D. Shi, J. Chen, and L. Zhu, "Supplementary automatic generation control using electric vehicle battery swapping stations," IEEE PES General Meeting, Vancouver, BC, 2013.

[135]P. Xie, D. Shi, and Y. Li, "Provision of Two-area Automatic Generation Control by Demand-side Electric Vehicle Battery Swapping Stations." J. Electr. Eng. Technol., Vol 10, no.1 pp. 300-308, 2016.

Appendix: List of Publications

- **Journal papers:**

1. **M. Mahoor**, A. Majzoobi and A. Khodaei, "Distribution Asset Management through Coordinated Microgrid Scheduling," IET Smart Grid, 2018.
2. **M. Mahoor**, Z. S. Hosseini, and A. Khodaei, "Least-Cost Operation of a Battery Swapping Station with Random Customer Requests" Energy, 2019.
3. **M. Mahoor**, Z. S. Hosseini, A. Khodaei, A. Paaso, and D. Kushner, "State-Of-The-Art in Smart Streetlight Systems: A Review," IET Smart Cities, 2019.
4. M. Alanazi**, M. Mahoor**, and Amin Khodaei, "Co-Optimization Generation and Transmission Planning for Maximizing Large-Scale Solar PV Integration," International Journal of Electrical Power and Energy Systems, 2019.
5. Z. S. Hosseini, **Mohsen Mahoor**, and A. Khodaei, "AMI-Enabled Distribution Network Line Outage Identification via ML-SVM," IEEE Transactions on Smart Grid, 2018.
6. **M. Mahoor**, A. Albaker, A. Majzoobi and A. Khodaei, "Spinning Reserve Based Scheduling of Integrated Microgrids in Holonic Distribution Grids," Under review.

- **Conference papers:**

1. **M. Mahoor** and A. Khodaei, "Data Fusion and Machine Learning Integration for Transformer Loss of Life Estimation," IEEE PES Transmission and Distribution Conference, Denver, CO, 2018.
2. **M. Mahoor**, A. Majzoobi, Z. S. Hosseini and A. Khodaei, "Leveraging Sensory Data in Estimating Transformer Lifetime," IEEE North American Power Symposium (NAPS), Morgantown, WV, Sep. 2017.
3. A. Majzoobi, **M. Mahoor** and A. Khodaei, "Machine Learning Applications in Estimating Transformer Loss of Life", IEEE PES General Meeting, Chicago, IL, July 2017.
4. Z. S. Hosseini, **M. Mahoor**, and A. Khodaei, "Battery Swapping Station as an Energy Storage for Capturing Distribution-Integrated Solar Variability," IEEE North American Power Symposium (NAPS), Fargo, ND, 2018.
5. **M. Mahoor**, Z. S. Hosseini, A. Khodaei, and D. Kushner, "Electric Vehicle Battery Swap Station," CIGRE Grid of the Future Symposium, Cleveland, OH, Oct. 2017.

6. M. Alanazi, **M. Mahoor** and Amin Khodaei, "Two-Stage Hybrid Day-Ahead Solar Forecasting," IEEE North American Power Symposium (NAPS), Morgantown, WV, Sep. 2017.
7. M. Alanazi, **M. Mahoor** and A. Khodaei, "Day-Ahead Solar Forecasting Based on Multi-level Solar Measurements," IEEE PES Transmission and Distribution Conference, Denver, CO, 2018.
8. A. Majzoobi, **M. Mahoor** and A. Khodaei, "Distribution Market as a Ramping Aggregator for Grid Flexibility Support," IEEE PES Transmission and Distribution Conference, Denver, CO, 2018.
9. A. Majzoobi, **M. Mahoor** and A. Khodaei, "Microgrid Value of Ramping," IEEE International Conference on Smart Grid Communications, Dresden, Germany, Oct. 2017.